Contributions to the design of broadband antennas and arrays for base stations for the new generation of mobile communication systems

Autor:
Sergio Martín Antón

Tesis depositada en cumplimiento parcial de los requisitos para el grado de Doctor en Multimedia y Comunicaciones

Universidad Carlos III de Madrid

Director y Tutor:
Daniel Segovia Vargas

Diciembre 2021

A la ciencia,
todo te lo da,
todo te lo quita.

"Un gran paso para un hombre,
un pequeño paso para la humanidad".

S. Martín Antón,
adaptación sobre N. Armstrong (1969)

AGRADECIMIENTOS / ACKNOWLEDGEMENTS

Aprovecho estas líneas para agradecer a todos aquellos que han contribuido al desarrollo de esta tesis.

Primeramente se antoja obligatorio el agradecimiento al Ministerio de Educación y Ciencia, en sus diferentes nombres a lo largo de los años que ha durado la tesis, por la financiación en régimen de investigador predoctoral gracias a la consecución de un contrato competitivo FPU.

A la Universidad Carlos III de Madrid por acogerme, y a mi tutor, por motivarme inicialmente a comenzar esta tesis, y apostar por mí. A las empresas con las que he participado en proyectos o colaboraciones, Telefónica, Centum, Telnet, Huawei.

A mi familia, mis padres Inma y Carlos, que cada uno a su manera que me han hecho como soy. A mi hermana Laura, que siempre ha estado ahí. Y a Nerea, mi segunda hermana. A mi gato Polan, por dejarme escribir estas líneas con no demasiados arañazos y mordiscos.

A mis amigos de siempre, que sé que estos años os he tenido más abandonados pero aún así ahí estabais como apoyo cuando hacía falta. Diego, Oscar, Sergio, Carlos ... cuando esto termine os debo una cerveza. Y a los amigos y compañeros que hice en Cáceres y que tanto me han acompañado después, Cristian, Jorge, Pedro, Tuky y los demás, también tenemos pendiente una celebración.

Tampoco quiero olvidarme de agradecer a la educación pública y a mis profesores, que desde pequeño me han ido enseñando tantas cosas y me han mostrado de lo que soy capaz, empezando por las etapas de más juventud en el colegio e instituto, sin saltarme a los buenos profesores que tuve durante mis estudios de Ingeniería en la Universidad de Extremadura, y finalmente en la Universidad Carlos III de Madrid donde algunos se convirtieron en compañeros.

A los compañeros que he tenido durante esta etapa, que estaban en los duros momentos y aún así sacando una sonrisa. Desde los primeros años de los que tanto aprendí con Fernando Albarracín, Alejandro Rivera y Adrian Amor, las risas con Gabriel Galindo y Jose Martinez, o los años que más he compartido con Ana Lopez, Kerlos Atia, y Gabriel Santamaría. Las estancias largas o intermitentes de compañeros como Alberto, Álvaro o Ebert. O las últimas etapas con Mónica, Paula, Iván, Alfonso, Elisa, Victor, Michal, Enderson, Nasser y Ahmed. Y sin duda a alguien me dejo en el tintero, pero a ningún compañero que ha pasado por la sala se olvida.

En los últimos meses de este trabajo tengo que agradecer a mis compañeros y amigos con los que he estado tocando. Jelena, Pato y Nacho(lino). Juntarse a tocar canciones con vosotros ha sido una gran válvula de escape que me ha ayudado a afrontar esta última cuesta arriba.

Y en general a todas esas personas que pasan por nuestra vida dejando una huella en mayor o menor medida, que hace que seamos como somos en este preciso instante.

PUBLISHED CONTENT AND CONTRIBUTIONS

The work developed in this Ph.D. dissertation has led to several journal and conference contributions. The complete list is detailed below.

Publications and Conferences

Related to chapter 2:

- S. Martin-Anton and D. Segovia-Vargas, "Fully planar dual-polarized broadband antenna for 3g, 4g and sub 6-ghz 5g base stations," *IEEE Access*, vol. 8, pp. 91 940–91 947, 2020

Related to chapter 3:

- S. Martin-Anton, P. Fernandez-Martinez, D. Segovia-Vargas, and V. Gonzalez-Posadas, "Effect of different reflector shapes on sub 6-ghz 5g dipole-based antennas," in *2020 IEEE International Symposium on Antennas and Propagation and North American Radio Science Meeting*. Montreal, QC, Canada: IEEE, jul 2020, pp. 111–112

Related to chapter 2:

- S. Martin-Anton and D. Segovia-Vargas, "Dual-polarized broadband antenna for new mobile communication base stations," in *13th European Conference on Antennas and Propagation (EuCAP 2019)*. Krakow, Poland: IEEE, 2019, pp. 1–3

Related to chapter 2, 3 and 4:

- S. Martin-Anton and D. Segovia-Vargas, "Broadband antenna design for new mobile communication systems," in *12th European Conference on Antennas and Propagation (EuCAP 2018)*. London, UK: IET, 2018, pp. 1–5

Related to chapter 2, 3 and 4:

- S. Martin-Anton and D. Segovia-Vargas, "Design of broadband antenna for new mobile communication base stations," in *URSI 2018 UGR - XXXIII Simposium Nacional de la Unión Científica Internacional de Radio.*, 2018

Related to chapter 2, 3 and 4:

- S. Martin-Anton and D. Segovia-Vargas, "Diseño de antena de banda ancha para nuevos sistemas de comunicaciones móviles," in *URSI 2017 UPCT - XXXII Simposium Nacional de la Unión Científica Internacional de Radio.*, 2017

Other Contributions non included in the Thesis

- P. Fernandez-Martinez, S. Martin-Anton, and D. Segovia-Vargas, "Dual-band array of cross-polarized vivaldi antennas for 5g applications," in *2020 14th European Conference on Antennas and Propagation (EuCAP)*. Copenhagen, Denmark: IEEE, mar 2020, pp. 1–5

- P. Fernandez-Martinez, S. Martin-Anton, and D. Segovia-Vargas, "Design of a wideband vivaldi antenna for 5g base stations," in *2019 IEEE International Symposium on Antennas and Propagation and USNC-URSI Radio Science Meeting*. Atlanta, GA, USA: IEEE, jul 2019, pp. 149–150

- S. Martin-Anton, D. Segovia-Vargas, L. E. García-Muñoz, and V. González-Posadas, "Amplificador diferencial híbrido de bajo ruido con ecualización resistiva para instrumentación en radioastronomía," in *URSI 2016 UAM - XXXI Simposium Nacional de la Unión Científica Internacional de Radio.*, 2016

Además de las mencionadas publicaciones, este trabajo ha contribuido a varios proyectos de investigación desarrollados en el GREMA (Grupo de Radiofrecuencia, Electromagnetismo, Microondas y Antenas) de la Universidad Carlos III de Madrid. Por una parte en iniciar la linea de trabajo, y consecución de proyectos de I+D+i, y por otra en el desarrollo y consecución de objetivos. Entre ellos podemos destacar proyectos ligados al tema de antenas de estaciones base para telefonía 5G con importantes empresas del sector como Telnet o Huawei.

In addition to the mentioned publications, this work has contributed to different research projects developed at GREMA (Radiofrequency, Electromagnetics, Microwaves and Antennas Group) in Universidad Carlos III de Madrid. On the one hand in starting the research line of work, and achieving R&D&i projects, and on the other in the development and achievement of objectives. Among them we can highlight projects related to the base station antennas for 5G mobile communication topic with important companies such as Telnet or Huawei.

CONTENTS

RESUMEN

El objetivo de esta tesis es el diseño de antenas y arrays de banda ancha para estaciones base en las nuevas generaciones de comunicaciones móviles. Los nuevos retos en los sistemas de comunicación tales como el aumento de dispositivos conectados y el Internet de las cosas (IoT), conlleva la aparición de nuevas generaciones de telefonía. Para hacer frente a ese desafío se necesitan nuevas estrategias para optimizar el espectro, aumentar el ancho de banda y las velocidades de transmisión. Aunque algunas técnicas son aumentar la frecuencia de trabajo desarrollando celdas más pequeñas y rápidas, esta tesis se centra en el otro enfoque, extender las bandas de frecuencia utilizadas en la actualidad. Este enfoque tiene algunas ventajas como una mayor penetración ofreciendo mejor cobertura en zonas aisladas, así como la coexistencia de las futuras redes 5G con los estándares 3G y 4G actuales.

En una primera parte, se presentan diseños de elementos de antenas planares cumpliendo con los nuevos requisitos. La antena está diseñada y fabricada de una forma rentable y asequible, presentando una topología compacta y completamente plana. La idea principal para la consecución de los objetivos es la inclusión de dipolos acoplados incluidos dentro de la propia antena de forma antipodal para conseguir un diseño compacto y un patrón de radiación estable en toda la banda de funcionamiento. El diseño compacto y de doble polarización se logra en un elemento que trabaja en todo el ancho de banda frecuencial entre 1.427 y 2.69 GHz, la banda que aquí se presenta como Banda Ultra Ancha Extendida (ExtUWB).

En segundo lugar, se desarrolla un estudio de diferentes formas de planos de masa o reflectores en el campo cercano del elemento. La inclusión de un plano de masa es necesaria para eliminar la radiación trasera y dar forma al haz de radiación para obtener una antena directiva con el ancho de haz deseado que permanezca estable dentro de toda la banda de trabajo. El punto clave a tratar es que el plano de masa o reflector al ser colocado en el campo cercano del elemento produce perturbaciones en el mismo, tanto en la adaptación como en su diagrama de radiación.

A continuación, se propone la combinación de dos elementos para cubrir las dos bandas requeridas. El elemento ExtUWB para la banda 1,42 a 2,69 GHz se integra con nuevos elementos para la banda 690 a 960 MHz. Se estudia la integración de los elementos de ambas bandas en un mismo espacio físico para desarrollar una antena de estación base que proporcione cobertura en las dos bandas de forma conjunta.

Finalmente, se propone la combinación de elementos en configuraciones de array para las nuevas bandas de 5G con el propósito de ser utilizados como estaciones base. La inclusión en array permite lograr diferentes propósitos: aumentar la directividad, cumplir con los requisitos generales de las estaciones base y obtener flexibilidad para diferentes configuraciones de arrays. Se proponen distintos arrays con diferentes objetivos, estos arrays son configurables para ser utilizados como estaciones base clásicas, pero también formando un nuevo sistema innovador de Massive MIMO con propiedades de haz orientable que no se ha presentado para la banda L hasta ahora.

ABSTRACT

The objective of this thesis is the design of broadband antennas and arrays for base stations for the new generations of mobile communications. The new challenges in the communication systems such as the increase of connected devices, the amount of smart products, and the Internet of Things (IoT), has brought the arrival of new 5G systems. To deal with that challenge, new mobile communication systems need new strategies for optimizing the spectrum, increase the bandwidth and the data rates as it is required. Although some techniques are to increase the working frequency and develop faster and smaller cells, this thesis is focused on the other coliving approach, which is to extend the nowadays mobile communication operating bands. That approach has some advantages as higher penetration with deeper coverage, and the coexistence of future 5G networks with the existing standards.

Firstly, some designs of planar antenna element following the new requirements are presented. The antenna is designed and manufactured in a cost-effective and affordable way presenting a compact and fully planar topology. The main idea to obtain the objectives is the inclusion of active embedded dipoles in the antipodal part of the antenna itself to achieve a compact design and a stable radiation pattern within the wide frequency band of operation. Compactness and dual polarized performance is achieved for working in the whole frequency bandwidth between 1.427 and 2.69 GHz, the band that is presented here as the Extended Ultrawideband (ExtUWB).

Secondly, a study of different ground plane shapes or reflectors in the element near field is developed. A ground plane is needed to remove the back radiation and shape the radiation beam to obtain a directive antenna with the desired beamwidth that remains stable within the broadband frequency band. The key point to deal with is that the ground plane or reflector placed in the element near field disturbs both the matching and the radiation.

Thirdly, the combination of two elements to cover both required bands is proposed. The ExtUWB element for the band 1.42 to 2.69 GHz is integrated with new elements for the band 690 to 960 MHz. Integration of both band elements in the same physical space for developing the base station antenna providing dual band coverage is studied.

Finally, the combination of elements in array configurations is proposed for the new 5G bands with the purpose of been used as base stations. It allows to accomplish different goals: increasing the directivity, fulfilling the overall base station requirements, and obtaining flexibility for different array configurations. Different arrays are proposed with different objectives, those arrays are configurable for being used as classical base stations, but also as a new innovative system of Massive MIMO with beamsteering properties that has not been presented for the L-band till now.

LIST OF FIGURES

LIST OF TABLES

CHAPTER 1

INTRODUCTION

Mobile communications have suffered an extraordinary progress through the years. Starting from the beginning of radio transmission with spark-gap devices as a primitive wireless telegraphy, or the radio broadcasting as the beginning of mobile communication. Nowadays, with the huge increase of connected devices, the amount of smart products, and the Internet of Things (IoT), the world is evolving towards a hyper-connected scenario. Consequently, the mobile network needs to support this growth.

To deal with that challenge, new mobile communication systems need new strategies for optimizing the spectrum, increase the bandwidth and the data rates as it is required. Although some techniques are to increase the working frequency and develop faster and smaller cells, this thesis is focused on the other coliving approach, which is to extend the nowadays mobile communication operating bands. That approach has some advantages as higher penetration with deeper coverage, and the coexistence of future 5G networks with the existing standards. The design of broadband element antennas and array for developing those new base stations is the main goal of the presented document.

1.1 Telecommunication Background

Antennas can be widely found in communication applications. Most of their uses are in telecommunications, which means distant communications, which is a world with Greek roots ("tele" meaning at a distance). [1]

Original communications carried by telegraph used two wire lines between the distanced stations forming a loop or a complete electrical circuit. Nevertheless, in 1837, Carl August von Steinheil of Munich, Germany, discover that if one leg of the device was connected to buried metal in the ground at each station, one wire could be removed. In that way he started the one wire communications.

Thomas Edison, at the end of XIX century, patented the "grasshopper telegraphy", an on-board telegraph system using electromagnetic induction for allowing telegraphic signal to jump between a moving train and the telegraph wires running parallel to the tracks. The invention was technically successful, but due to little interest by train travellers it was economically futile. [2]

James Clerk Maxwell, in 1865 published his proposal about electromagnetic theories. He described in his paper the theory of the propagation of electromagnetic waves. His set of "Maxwell's equations" demonstrated that electricity, magnetism and light are, all of them, the same phenomenon in different forms, the electromagnetic field. [3]

David E. Hughes in 1878 noticed that sparks could be heard in a telephone receiver when he was developing some experiment with a carbon microphone.

Heinrich Rudolf Hertz was looking for a subject for his doctoral dissertation in physics in 1879, when his instructor Hermann von Helmholtz suggested him to prove Maxwell's electromagnetic theory. After several scientific validation experiments, Hertz published his results between 1887 and 1890. This was the first time that electromagnetic radio waves were proved to have been transmitted by a spark-gap device, and detected over a short distance. [4] [5]

The first radio transmitter was the spark-gap transmitters, which were the most important kind used in wireless telegraphy during the first three decades of the radio until the First World War (WWI), the so-called spark era.

Guglielmo Marconi converted what was a laboratory experiment into a useful communication system. He patented the radio device in 1897, a portable system for long distances. His experimental device is proved to be the first commercially successful radio transmission system. Furthermore, Marconi's apparatus is credited for saving the 700 people who survived the Titanic episode. [6]

The mobile communication equipment was so huge at first, that only large vehicles as trains or ships could handle them. As an example, the toploaded T-shaped monopole used on the Royal Mail Ship Titanic. The wires were spanned most of the ship length, and were 62 meters high over the water. The ship radio was able to send a signal asking for help before sinking in 1912.

Radiotelegraphy was the first medium for radio communication. Marconi's devices used radiotelegraphy, and it was the only way for radio transmission for the first decades of radio. But, the development of radiotelephony with amplitude modulation (AM), allowed audio to be transmitted by radio waves. The prior spark gap transmitters used to send damped waves with very wide bandwidth that interfere with other transmissions. Spark gap emissions were banned in 1930. The invention of the vacuum tube (or valve) and their use as transmitters from 1920 allowed transmitting pulses and sinusoidal carrier waves in continuous waves(CW), overcoming the previous technology.

In the 1920 decade, radiotelephony and the transmission of sound started the displacement of the radiotelegraphy for many applications, which made possible the radio broadcasting. [7]

The antenna implementations at the beginning of the XX century were limited by the time technology, specifically by the lack of signal generators, and the ones available were operating in the low MHz range and below frequency. Antennas as half-wavelength dipole were physically large and provided low directivity. The search of secure communications

in the WWI motivated the research for directive antennas, more realizable at higher frequencies.

Commercial radio broadcasting started in 1920 in Pittsburgh with music and speech programming was launched for the public by Wetinghouse Company. The introduction of directional antennas for broadcasting was in 1932 in the United States. In 1940 the FM broadcasting began to operate in the 42 to 50 MHz band. Their popularity was reduced in the 50s due to the expansion of broadcast television. In 1939 in England regular black and white television broadcasting began, with its biggest growth in the next decade. Later, colour TV broadcasting started to appear using the three colour system.

The mobile telephone device was invented by Bell Telephone Company and in 1924 was introduced in the New York City police cars.

Bose and Lodge investigated microwave antennas for low GHz frequency before XX century, but the application was found after signal generators for those frequencies appeared in the 30s. In 1934 the first microwave radio telephone was used between England and France at 1.8 GHz. The microwave sources as magnetron and reflex klystron were developed in the late 30s, which stimulated new applications as horn antennas, reflector antennas, radar, etc.

After the WWII, some wireless applications have been highly developed. The full mechanical scanning with reflector antennas used in early radar applications has been gradually replaced by feed-only mechanical scan and phased arrays with no mechanical moving parts. Satellite communications started in the 60s and nowadays provide broadband connections for voice, video or data for nodes as well as mobile satellite phones and broadcast radio. The cellular terrestrial mobile communications started in the 80s and brought a lot of innovations in smaller antennas for handset devices. [1]

1.2 Mobile Communication Evolution and New Generations

Cell phone mobile communication, as it is known nowadays, began in the first half of the 20th century, with big and heavy machines that were

installed in ships and trains, and later in car trunks. However, it was in the 70s when Martin Cooper developed the handy wireless cellphone, making the first wireless phone call with one of his inventions [8]. With that background scenario, it could be possible to talk about a radio generation, or Zero Generation, in which, transmissions were made in simple modulations as AM or FM as in the radio broadcasting, making use of frequencies of dozens of MHz in the so-called HF and VHF bands, what it is nowadays considered as low frequency bands.

The protocols for multiplexing and dividing signals in the medium were developing different access media techniques, with the purpose of sharing the common resources by several users. At first by frequency division (FDMA) in first generation, to time division (TDMA) in second one. Third generation included the code division multiplex access (CDMA), where signals were differenciated by coding with interference immunity. The fourth generation included the Orthogonal Frequency Division (OFDMA) where the channel was divided into subcarriers that were distributed by the user needs. [9]

New generations of mobile communication are working in the study of different technologies and protocols. One of them is the Spatial Division Multiplex Access (SDMA), where it is possible to reuse the same frequency in the cell for several users if they are physically separated from each other. Smart antennas are being developed for including this technique mainly in millimeter-wave frequency, in that way the information is directed to the user, avoiding redundant information in areas with inactive users. Another new technique that is being developed for the new generations is Carrier Aggregation, in which several subcarriers can be used together to establish the communication, even in different operation bands, with the purpose of more flexible, and faster communications in an optimized style of using the spectrum.

The new (5G) generation will converge with different approaches in several frequency bands. While higher frequencies in the mm-wave region and dozens of GHz will be used generating smaller cells and more data speed and capacity, it will be combined with the lower classical frequency bands (hundreds and thousands of MHz), in which more range and penetration can be obtained for outside cities, rural areas, or obstacles environments.

The better coverage and deeper penetration of 5G will open some opportunities in the rural areas. For example, the possibility of working from home in the "Empty Spain", by using 5G modems where 4G modems or fast wired networks are not an available solution. This can be an important step, as has been evidenced in relation to the recent pandemic of COVID-19, which has open some new ideas and opportunities to new ways of lifestyle, working from home and living in healthier remote rural areas, where nowadays there is low coverage of mobile communications and the fiber optic service has not been deployed. [10]

The explosion of applications and products growing smarter and more connected leads to an increase of the connectivity demand. Smart homes, self-driving cars, smart grids, health care provisioning, remote surgery, connectivity for IoT (Internet of Things), an ever growing amount of connected devices, and a multitude of new and exciting capabilities, all of them will require new types of improved performance. For instance, low latency will provide real time interactivity, or low power consumption will allow connected products to operate for long periods without any supervision or assistance. [11]

In terms of power efficiency, in 5G it is expected to achieve ten times better values than the ones obtained with 4G. Near the place we are located, in Talavera de la Reina (Toledo, Spain), real measurements recently developed by Ericsson and Telefonica in early tests, have demonstrated 5G consuming 10% the power for an equivalent 4G scenario, meaning 5G is 10 times more efficient.

Nowadays, the new challenges in the communication systems such as the biggest number of connected devices ever known with an extremely low latency and highest data rates ever used has brought the arrival of new 5G systems. These demands imply that users will require higher bandwidths for mobile connections. In addition, the explosion of connected devices as in the new IoT (Internet of Things) technology makes that more than 20 billions of connected devices will be available in 2020 [12]. The challenge to satisfy the new technological demands implies huge efforts to increase the bandwidth and obtain high bit rates (i.e. 10 Gbits/s or higher).

New mobile communication services have to use new strategies for optimizing current spectrum resources and achieve the required higher

data rates [13, 14]. Among these techniques it can be mentioned an increase towards higher frequency bands such as millimeter bands or the application of new advanced modulation techniques such as carrier aggregation (CA). It is also important to highlight the coexistence of future 5G networks with the actual 3G and 4G standards.

In a recent releasable report [15] it is stated that 5G new radio (NR) gives a unified and more capable air interface providing diversity in three aspects: diversity in services (from critical services to massive Internet of Things –IoT- ones and enhancement of current mobile services), diversity in deployments and, finally, diversity in spectrum. This spectrum diversity for 5G NR provides a division in the frequency spectrum in three regions: low bands (below 1 GHz), mid-bands (between 1 and 6 GHz), and high bands (above 24 GHz). The first two bands (low and mid) constitute what is currently known as sub-6 GHz bands. This paper focuses on the mid sub-6 GHz band. Previously, in the Table 2 contained in [16], a survey on 5G technologies broadly uses the terminology "5G sub-6 GHz" to refer to widely distributed spectrum from 450 MHz up to 6 GHz. That classification comes from [17] where the operating bands for standalone services with carrier aggregation (CA) or dual connectivity (DC) were proposed. In particular, the bandwidth between 1427 MHz up to 2690 MHz is one of the proposed for NR-DC services. Therefore, the international administrations have allocated part of the L-band (1427-1518 MHz) to provide additional bandwidth for mobile communications. In particular, the standardizing of 5G [17] allows the bandwidth from 1427 MHz for NR-UE (user equipment). In addition, the European Union [18, 19], has included the harmonization of part of the L-band (1427 MHz to 1518 MHz) for the next- generation (5G) terrestrial wireless systems.

From the technological point of view, the associated mid-band for 3G and 4G services (between 1710 and 2690 MHz) has to be extended down to 1427 MHz resulting in a new extended band from 1427 MHz to 2690 MHz. In addition to the bandwidth extension, a reduction in size would also be welcome due to environmental issues. Then, for these new antennas, not only does the frequency band need to be extended but also the antenna element size has to be reduced while keeping suitable performance in its radiation pattern and matching and isolation parameters. [20]

1.3 Base Station Antennas

The base station antennas have to manage different signal channels with a defined radiation pattern for covering an specific region around themselves. The topology used for the antenna depends on the size of the coverage cell. Generally, in cellular communications, the different cells that are spatially separated can reuse the same frequency. [1]

An omnidirectional radiation pattern provides radiated energy uniformly around the tower in the horizontal plane (azimuth). In the beginning of cellular communications this was exclusively used, but nowadays most of them have been replaced by sector antennas which cover a specific angular region in the horizontal plane, with the exception of rural areas and some specific applications. The most common used cellular base station is composed by sector antennas, which enhances the number of user terminals.

The antennas used in cellular base stations for mobile phone communication have the appearance of a tall monopole as those used in radio broadcasting, but in fact it is a vertical array of elements. Often there are several of those array antennas on the same mount to provide for spatial diversity and for separating transmission and receive functions. Those elements forming the array are parallelly fed, often with uniform amplitude to achieve an overall high gain antenna. The combination of several arrays in the post leads to a uniform radiation pattern in azimuth, but it is directive in the elevation plane.

Following array theory, a linear phase taper across the array elements can be used to produce what is commonly named as electrical downtilt that moves the beam slightly down to reduce the interferences from adjacent cells. In the hypothetical case that the whole antenna is tilted mechanically, the toroidal pattern tilts down on one side but upside tilted on the opposite one, whereas using electrical downtilt produces a cone around the antenna array providing the same angle of downtilt for every azimuth direction.

Sector patterns are commonly used for cellular base station to cover a sector of angular space, rather than having uniform coverage around the

tower. One of the typical sector antenna arrangements is a triangular structure at the top of the post, using panel antennas on each face that cover 120° sector. Some common horizontal half power beamwidth values in the sector antennas are 65° and 90°. Even different sectors values can be used when users are not uniformly distributed in the space around the base station, this is the case for highways or football stadios where a huge ammount of users are concentrated over a determined angular region. Similarly to omnidirectional base station antennas, the sector antenna uses the vertical array properties to produce a narrow beam in the vertical axis to increase gain. The downtilt angles is adjusted by a trade off, small downtilt angle with the beam pointing in azimuth provides longer distance communication, whereas large downtilt angle reduces the interferences with adjacent cells that make frequency reuse.

Different kinds of antennas can be used as element in the antenna arrays. General specifications on sector panel antennas that are applied over the whole bandwidth are nearly constant in azimuth pattern, good impedance matching (VSWR 1.5 or RL -14dB), and front to back ratio of 28 or 30 dB. There are several broadband dipole architectures commonly used as elements, as four leaf clover or twin dipoles. Patch antennas can be used without dielectric for high power handling and low losses. Every type of antenna have a ground plane to reduce the back radiation. Dipole and patch antennas require the ground plane to produce a unidirectional beam.

Nowadays base stations are dual-polarized antennas, that characteristic allows for diversity using one dual-polarized receiving antenna, instead of two separated antennas with spatial diversity. The most popular polarization configuration is the dual orthogonal ±45° linear polarizations.

1.4 Base Station Requirements

In this section, the new requirements for the mobile communication base stations are explained. Mainly, they should cover the new bands with the same commercial requirements that are nowadays applied to previous generations base stations. The requirement sums up is also presented in Table 1.1. Although those are the main requirements, in

the last chapter there are different application proposals for different mobile communication base stations with new characteristics.

As it is explained in previous sections, the first challenging requirement is to extend the band to cover the required broadband from 1427 to 1690 MHz. Parallelly and not as technologically challenging, the lower band needs to cover 690 to 960 MHz.

The elements should cover those bands defined for a characteristic impedance of 50 Ω. Although, in communications is widely used a matching defined by return losses lower than -10dB, mobile communications systems generally use the definition of -14dB with is equivalent to a Standing Wave Ratio in Voltage of 1.5. In this application the polarization of electromagnetic waves needs to be ±45°, meaning elements have to be accomplished to achieve dual polarization for +45° and -45°. The two polarization ports has to satisfy an crosspolar isolation of -28dB.

The gain required in the array needs to be between 15 and 18 dBi, while for each element 8 dBi is generally accepted. The horizontal beamwidth defined as the Half Power Beamwidth should be at 65° with a margin of ±10°, this requirement is related to the final array, but as extension it is also a requirement for the individual elements.

The arrays have to include a vertical down tilt, which means that the beam can be moved in the vertical axis from 0° (azimuth) down to -12°. The Sidelobe Level can be defined in different ways, in this case the requirement is that the first upper sidelobe level suppression should be at least 10 dB. The purpose is to ensure not to interfere with different cells.

Finally, the size for the complete array should be similar to the base stations used nowadays, with a maximum length of 2000 mm, width of 500 mm, and the depth 350 mm.

1.5 Thesis Structure

This section presents the structure for the thesis in hands. The thesis is divided in chapters concerning different topics on the same overall objective. The chapters are organized as follows:

Table 1.1: Base Station Requirements for the New Generation of Mobile Communication Systems

Data	Requirements
Frequency Band (MHz)	1427 - 2690 MHz 690 - 960 MHz
Impedance [Ω]	50 Ohm
Polarization [°]	±45 degrees
VSWR ($S_{i,i}$)	1.5 (-14 dB)
Isolation (Crosspolar, Interband)	-28 dB
Gain [dBi]	15 - 18
Horizontal Beamwidth (-3dB) HHPBW [°]	65 ± 10
FirstUSLLSupp [dB]	10
Vertical Down Tilt [°]	0 - 12
Size Dimensions [mm]	2000x500x350
Ports	-

The Chapter 1 is the Introduction, in which the overall topic is presented. The chapter presents an introduction to mobile communications and base station systems, the need of new generations of mobile communication systems, as well as the commercial requirements for the antennas.

The Chapter 2 presents the design of a planar antenna element following the requirements. The Extended Ultrawideband (Ext-UWB) antenna element for new mobile base stations. New dual-polarized element is required for working in the microwave region in which the new

frequency bandwidth goes from 1.427 up to 2.69 GHz with the return losses lower than -14 dB and the crosspolar isolation larger than 28 dB.

The Chapter 3 includes the study of different ground plane shapes or reflectors in the element near field. A ground plane is needed to remove the back radiation and shape the radiation beam to obtain a directive antenna with the desired beamwidth that remains stable within the broadband frequency band. The key point to deal with is that the ground plane or reflector placed in the element near field disturbs both the matching and the radiation.

The Chapter 4 develops the integration of two elements to cover both required bands. While Chapter 2 presents a more challenging design objective for designing the ExtUWB element for the band 1.42 to 2.69 GHz, this chapter present a design for the band 690 to 960 MHz, easier to obtain. The core of the chapter is the integration of both band elements in the same space for developing the base station antenna providing dual band coverage.

The Chapter 5 presents the array of elements configuration. Different arrays are proposed with different objectives, as classic base station arrays and planar arrays for beam steering and Massive MIMO applications.

The Chapter 6 is the Conclusion of the thesis, in which the overall presented work is summarized. Some future lines of work in this topic are presented.

1.6 References

[1] W. L. Stutzman and G. A. Thiele, *Antenna theory and design*. John Wiley & Sons, 2012.

[2] E. P. Wenaas, "Edison—edmond morris (cambridge, ma, USA: MIT press, 2018, 800 pp.)," *IEEE Technology and Society Magazine*, vol. 40, no. 2, pp. 14–16, 2021.

[3] P. M. Harman and P. M. Harman, *The Natural Philosophy of James Clerk Maxwell*. Cambridge University Press, 2001.

[4] P. S. Ramsay, "Heinrich hertz, the father of frequency," *The Neurodiagnostic Journal*, vol. 53, no. 1, pp. 3–26, 2013.

[5] P. Kildal, *Foundations of Antenna Engineering: A Unified Approach for Line-of-Sight and Multipath*. Artech House Publishers, 2015.

[6] J. Hayes, "Titanic legacy," *Engineering Technology*, vol. 7, no. 3, pp. 32–33, 2012.

[7] T. Farley, "Mobile telephone history," *Telektronikk*, vol. 101, no. 3/4, p. 22, 2005.

[8] E. C. Niehenke, "Wireless communications: Present and future: Introduction to focused issue articles," *IEEE Microwave Magazine*, vol. 15, no. 2, pp. 26–35, 2014.

[9] C. Patil, R. Karhe, and M. Aher, "Development of mobile technology: A survey," *Development*, vol. 1, no. 5, 2012.

[10] A. Davies, "Covid-19 and ict-supported remote working: Opportunities for rural economies," *World*, vol. 2, no. 1, pp. 139–152, 2021.

[11] E. Sisinni, A. Saifullah, S. Han, U. Jennehag, and M. Gidlund, "Industrial internet of things: Challenges, opportunities, and directions," *IEEE Transactions on Industrial Informatics*, vol. 14, no. 11, pp. 4724–4734, 2018.

[12] "Gartner (symposium/itxpo 2015, noviembre 8-12, barcelona)."

[13] Y. Wang, J. Li, L. Huang, Y. Jing, A. Georgakopoulos, and P. Demestichas, "5g mobile: Spectrum broadening to higher-frequency

bands to support high data rates," *IEEE Vehicular Technology Magazine*, vol. 9, no. 3, pp. 39–46, 2014.

[14] E. Chavarria-Reyes, I. F. Akyildiz, and E. Fadel, "Energy-efficient multi-stream carrier aggregation for heterogeneous networks in 5g wireless systems," *IEEE Transactions on Wireless Communications*, vol. 15, no. 11, pp. 7432–7443, 2016.

[15] Qualcomm, "Making 5g nr a commercial reality," Feb. 2020, [Online]. Available: https://www.qualcomm.com/media/documents/files/making-5g-nr-a-commercial-reality.pdf.

[16] Y. Huo, X. Dong, W. Xu, and M. Yuen, "Enabling multi-functional 5g and beyond user equipment: A survey and tutorial," *IEEE Access*, vol. 7, pp. 116 975–117 008, 2019.

[17] "Technical specication group radio access network; nr; user equipment (ue) radio transmission reception; part 1: Range 1 standalone, document 3gpp ts 38.101-3 v15.3.0," Oct. 2018.

[18] "Ofcial journal of the european union. (apr. 26, 2018)." Commission Implementing Decision (EU) 2018/661 of 26 April 2018 amending Implementing Decision (EU) 2015/750, Apr. 2018, [Online]. Available: https://eurlex.europa.eu/eli/dec_impl/2018/661/oj.

[19] "European commission. directorate-general for communications networks, content and technology. electronic communications networks and services. radio spectrum policy, brussels, belgium. (mar. 14, 2017)." Mandate to CEPT to Develop Harmonized Technical Conditions in Additional Frequency Bands in the 1.5 GHz Range for Their Use for Terrestrial Wireless Broadband Electronic Communications Services in the Union., 2017, [Online]. Available: http://ec.europa.eu/newsroom/document.cfm?doc_id=45863.

[20] S. Martin-Anton and D. Segovia-Vargas, "Fully planar dual-polarized broadband antenna for 3g, 4g and sub 6-GHz 5g base stations," *IEEE Access*, vol. 8, pp. 91 940–91 947, 2020.

CHAPTER 2

EXT-UWB ELEMENT ANTENNA

The current chapter presents the design of an Extended Ultrawideband (Ext-UWB) antenna element for new mobile base stations. This work is based on the articles presented on [1] [2] [3].

The objective of this chapter is the design of an antenna working in the extended 5G band in order to fulfil the future 5G requirement in the microwave region, in which the new frequency bandwidth goes from 1.427 up to 2.69 GHz with the return losses lower than -14 dB and the crosspolar isolation larger than 28 dB.

Firstly, the proposed topology is a pair of folded dipoles placed with an elliptical cylinder reflector, providing single polarization.

Secondly, a fully planar dual polarized radiating element with internal embedded coupled dipoles is presented.

The inclusion of these internal parasitic elements allows achieving three different goals: on the one hand, an extension of the bandwidth towards lower frequencies (from 1.69 GHz to 1.427 GHz) as required in new 5G standards; whereas on the other hand, a reduction of the antenna size in comparison with other topologies for bandwidth extension and, finally, a reduction of the secondary lobes.

2.1 Introduction

In the last years, different broadband antennas for base stations have been developed. Patch and dipole-based antennas, such as crossed bow-tie dipoles, have been extensively used for base-station antennas. Whereas patch antennas are good because of their compactness, its performance when requested to work in bandwidths larger than 50% is more complicated. In fact they need the addition of parasitic elements or stacked structures to get the required bandwidth. So, as seen in the literature, crossed dipoles, folded dipoles, bow-ties, and, in general, dipole-based antennas have been a more common choice for this wide band performance. However, in general, the operating bandwidth of those antennas does not cover the desired extended band. Then, in [4,5] a pair of printed dipoles was proposed to achieve a slightly extended bandwidth (1.65-2.85 GHz) for LTE applications but for a general single polarization case. Eventually, a double element for dual polarization on a 130x130 mm^2 cell was proposed but leading to a much larger and asymmetric structure with tilted patterns.

In [6] - [11] different kinds of crossed bow-tie dipoles were presented to cover the non-extended band from 1.7-2.7 GHz. None of the previous works deal with the challenge of the extended bandwidth. In [12] a reduction of the antenna size was shown by using folded dipoles at a price of covering even a shorter bandwidth than the one for 2G-3G applications. In fact, although the dimensions of the antenna were certainly small, the antenna only covered the bandwidth between 1.7 and 2.25 GHz (far away from the required needs for the extended 1.427 GHz to 2.7 GHz).

Different attempts have been made to achieve compact designs. In [13] the use of multi-resonant cross-dipoles allowed obtaining compact antennas but without either covering the new extended bandwidth. The use of Artificial Magnetic Conductors (AMC) in [14,15] helped to reduce the height of the antennas but with higher values of the return losses (values around -10 dB instead of -14 dB) and, also, without covering the extended bandwidth.

It has not been till very recently that the proposed extended band has been included in the radiating elements for the newest base stations.

The challenge is great since a coexistence with the previous 3G and 4G communication systems has to be achieved. One attempt aiming at reducing the size, while covering part of the mid-band sub-6GHz 5G bands (between 1.7 and 3 GHz), can be seen in [16]. However, the lowest part of the extended band is not covered and its inclusion in array topology is not straightforward since the antenna is not planar. In [17] an example using crossed bow-tie dipoles is presented but the need of a conformal shape reflector yields to larger dimensions. Finally, two topologies have been presented in [18] where the inclusion of parasitic elements allows enhancing the bandwidth of previous bow-ties or dual dipoles. In that work, the inclusion of stacked parasitic capacitor made possible to add a new resonance in the higher band but at the price of having a multilayer non-compact design, what makes mass fabrication more difficult.

This chapter presents a compact and fully planar antenna for 3G-4G and sub 6-GHz 5G for large coverage area base stations. This challenge has been dealt by jointly acting on the radiating element and on the feeding structure. Concerning the radiating element, the inclusion of internal dipoles simultaneously coupled and fed by the feeding line and through the main dipoles allows extending the frequency band while keeping a compact and fully planar structure. In addition, the compactness of the new antenna prevents the multilobe effect at higher frequencies. Finally, concerning the feeding structure, the transition between the coaxial probe to the microstrip one has allowed achieving a nearly symmetric dual polarized broadband structure. Table 2.1 shows a comparison of the referenced dual-polarized broadband antennas and the presented in this work. For a fair comparison the size of any antenna is normalized in terms of λ_L (where λ_L is the wavelength at the lowest working frequency). The proposed antenna consists a fully planar one and shows the smallest size among all the ones covering either the extended bandwidth or a bandwidth larger than 60%.

The chapter is organized as follows. Section I gives the Introduction. Section II starts with a single-polarized element that focuses the efforts on broading the bandwidth. Section III starts the dual polarization achievement. Section IV deals with the need of a compact design with dual polarization and bandwidth extension. Section V provides the manufacturing issues and experimental results while Section VI con-

Table 2.1: Comparison of different dual-polarized broadband antennas for base station antennas

Ref.	BW (GHz) (%)	Element Size (mm) (λ_L)	Isolation(dB)
[7]	1.71-2.71 (45%)	67.2x67.2x29 0.38x0.38x0.16	30
[8]	1.7-2.7 (45%)	68.2x68.2x32 0.39x0.39x0.18	26
[9]	1.69-2.71 (45%)	70.38x70.38x27 0.4x0.4x0.15	28
[11]	1.61-2.71 (51%)	70.4x70.4x42 0.38x0.38x0.23	30
[12]	1.7-2.25 (28%)	80x80x34 0.45x0.45x19	25
[13].1	1.7-2.69 (45%)	46.7x46.7x32 0.27x0.27x0.1	35
[13].2	1.65-3.3 (66%)	52.2x52.2x34 0.44x0.44x0.26	28
[14]	1.7-2.7 (45%)	70x70x18 0.4x0.4x0.1	25
[16]	1.7-3 (55%)	150x150x100 0.35x0.35x0.23	20
[17]	1.427-2.9 (68%)	134x110x33 0.63x0.52x0.16	20
[18].1	1.4-2.7 (64%)	132.8x132.8x45.3 0.62x0.62x0.22	30
[18].2	1.4-2.7 (64%)	80x80x55.8 0.37x0.37x0.26	30
Present	1.4-2.7 (64%)	77x77x45 0.36x0.36x0.13	30

cludes the chapter.

2.1.1 Synthetic Dipoles Theory Demonstration

This subsection defines the theory behind the presented architecture, to deeper understanding the expected radiation pattern for the antenna element. Firstly, the 3D $\lambda/2$ dipole radiation pattern has been synthesized, to later, by applying the array theory presented in Chapter 5, achieve the results of combined dipoles with their images on a ground plane.

For a certain frequency, a $\lambda/2$ dipole has a radiation pattern defined by its electric field, shown in equations 2.1 for every dipole length and particularized in 2.2 for $\lambda/2$, which is a toroidal shape, i.e. omnidirectional in horizontal plane with a null in vertical axis (z-axis, or the direction of the dipole length). By integrating the complete 3D volume, the $\lambda/2$ dipole Directivity (or the maximum gain if no losses are assumed) is demonstrated to be 2.14 dBi. Continuous blue line in figure 2.1 shows the horizontal and vertical plane radiation pattern for a $\lambda/2$ dipole in free space, with the computed Directivity and the horizontal and vertical calculated half-power beamwidth.

$$E_\theta = j\eta \frac{I_0 e^{-jkr}}{2\pi r} \left[\frac{cos(\frac{kLcos(\theta)}{2}) - cos(\frac{kL}{2})}{sin(\theta)} \right] \tag{2.1}$$

as $k = \dfrac{2\pi}{\lambda}$ and $L = \lambda/2$ then

$$E_\theta = j\eta \frac{I_0 e^{-jkr}}{2\pi r} \left[\frac{cos(\frac{\pi cos(\theta)}{2})}{sin(\theta)} \right] \tag{2.2}$$

The designed element is composed of two dipoles simultaneously fed by a coplanar stripline, meaning two parallel dipoles spaced a $\lambda/2$ distance. The combination of both dipoles removes the side radiation, achieving a radiation pattern defined by a beam presented in front and back directions. Figure 2.1 in dashed green line presents the horizontal and vertical plane radiation patter for the two $\lambda/2$ dipole in free space,

with the calculated Directivity and horizontal and vertical calculated half-power beamwidth. The Directivity of the arrangement is calculated to be 5.14 dBi, i.e. 3dB increased. The horizontal HPBW is transformed from omnidirectional to 71.25°, while the vertical HPBW remains the same value (77.95°).

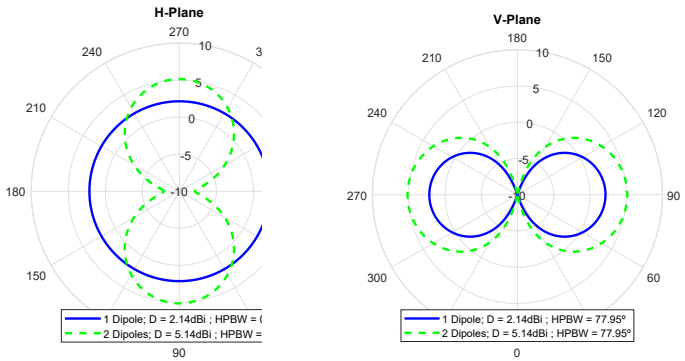

Figure 2.1: Synthetic Dipoles 1. One or two dipoles in free space.

When a $\lambda/2$ dipole is parallel placed over a $\lambda/4$ spaced ground plane, the image theory states a equivalence with having an image element radiating on the other side of the mirror. By including this information in the code, the synthesized result is a radiation pattern with removed rear radiation, pushing back radiation to front and increasing the maximum with 3 dB. Figure 2.2 in dash black line shows the horizontal and vertical plane radiation patter for a $\lambda/2$ dipole with an image dipole. In the horizontal plane, the omnidirectional pattern has been transformed into a cardiod shape, with removed back radiation and a 3 dB push in the front maximum, resulting in a 171.34° horizontal HPBW. Vertical plane evidences the back radiation removal and a front beam with 76.37° vertical HPBW.

The architecture for the designed element is defined by two dipoles simultaneously fed and a ground plane or reflector. After showing the intermediate steps, the resulting synthesized radiation pattern for two dipoles over a ground plane is presented. For the final case, the previously shown phenomena are now presented combined. Continuous red line in figure 2.2 shows the horizontal and vertical plane radiation patter for two $\lambda/2$ dipoles with their image dipoles. The total increase of

directivity leads to a value of 8.15 dBi. The resulting radiation pattern shows a front beam with an horizontal HPBW of 70.17° while the vertical HPBW is 76.37°.

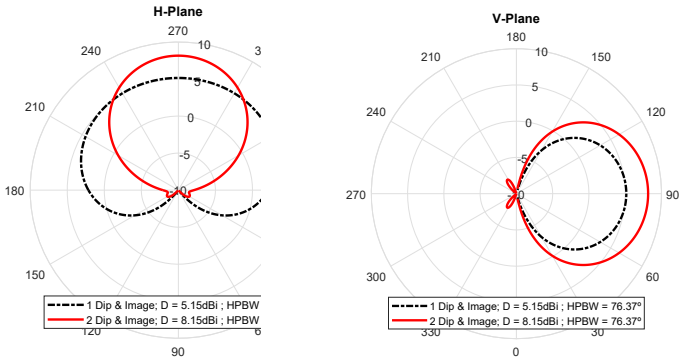

Figure 2.2: Synthetic Dipoles 2. One or two dipoles with reflective images.

Note that the presented synthesized results are valid for a single frequency, which can be even assumed for narrow band, while the design antenna needs to be broadband. Even though, it is a good point to understand the expected shape and values of radiation pattern.

Also, the results in the HPBW are presented for horizontal and vertical planes in a vertical polarized scenario. When the element is rotated in the following sections to achieve ±45° polarization, the resulting horizontal beamwidth leads to an intermediate value.

2.2 First Approach Broadband Antenna Design

2.2.1 Vertical Polarized Element

For the basic antenna the configuration of folded dipoles has been selected. The antenna, illustrated in figure 2.3, is composed of two folded dipoles connected in parallel through a coplanar stripline. The feeding of the antenna consists on a coupling fed by an L-shaped microstrip line on the other side of the substrate. H-shaped folded dipoles are printed on the substrate back side, while the L-shaped microstrip line

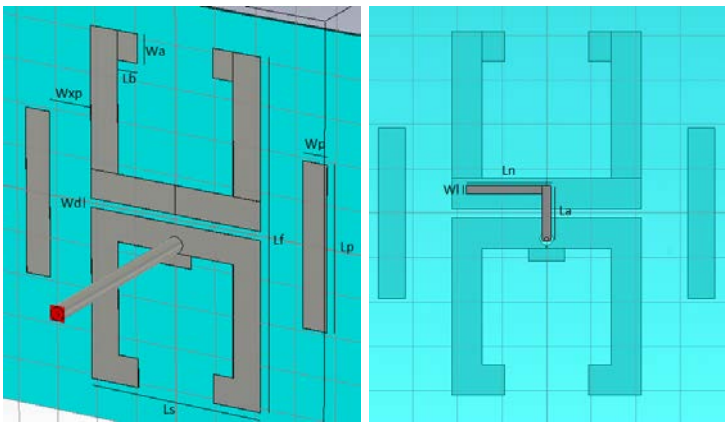

Figure 2.3: Front and Back pictures of the antenna element.

is on the front side. The L-shaped microstrip is connected to the inner conductor of a 50 Ω coaxial cable through a hole in the substrate, while the outer conductor of the cable, is connected to the coplanar stripline. The antenna is designed on a substrate Roger 4350B, with a relative dielectric constant of $\varepsilon_r = 3.48$ and a thickness of $h = 0.76mm$.

The dipoles length (Lf = 82 mm) is the dimension that selects the main working frequency of the antenna. The ipoles are connected through a coplanar stripline, its slot width (Wd = 2.1 mm) is an important parameter for impedance matching.

The length of the L-shaped coupling microstrip that makes the feeding is an important parameter for the matching and bandwidth. The values of Ln and La for obtaining an S11 parameter that fulfills the requirement was found to be Ln = 19 mm and La = 12.4 mm.

The non-connected microstrip lines that are placed at both sides of the folded dipoles act as side parasitic elements, that improve the matching and enhance the bandwidth. The values for the parasitic elements were chosen to be Lp = 38.5 mm of length, Wp = 6 mm of width, and Wxp = 10.5 mm of separation.

Table 2.2 shows the different values of the antenna dimensions. Figure 2.4 shows the reflection coefficient S11 of the antenna, in which a

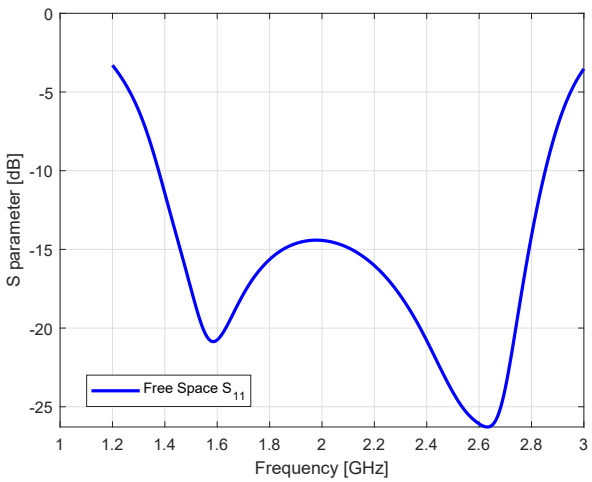

Figure 2.4: Reflection coefficient S11 of the folded dipole antenna.

matching of -14 dB is achieved along the whole bandwidth satisfying the industry requirements.

In the figure 2.5 a parametric study for parasitic dimensions and position is included for understanding their effects. The first picture shows the variation of the parasitic element length (Lp), which is related to its resonance frequency at the high frequency part of the band spectrum. Larger values imply resonance with high Q which is shifted down to lower frequency and results in mismatching at higher part of the band, while shorter values of length lead to low Q resonance in higher frequency with worse return losses at central ones. The second picture shows the variation in the parasitic width (Wp). It controls the relation between the second and the third resonance in the highest frequencies, while slightly affecting the central ones. The third picture is related to the position, precisely to the space or separation between the active dipole and the parasitic (Wxp). This separation controls the coupling between them and, consequently, the parasitic feeding, what affects the highest frequencies in both quality factor and resonance shifting and matching. As can be seen in the complete figure, parasitic variations mainly affect the high frequency spectrum of the working band. In that way the parameters, $Lp = 38.5mm$, $Wp = 6mm$ and $Wxp = 10.5mm$, are chosen to fit better the design goals.

Table 2.2: Parameters for Vertical Polarized Element

Parameter	Value [mm]
Wd	2.1
Ls	42.5
Lf	82
Wa	6.8
Lb	5
Wxp	10.5
Wp	6
Lp	38.5
Ln	19
La	12.4
Wl	1.9

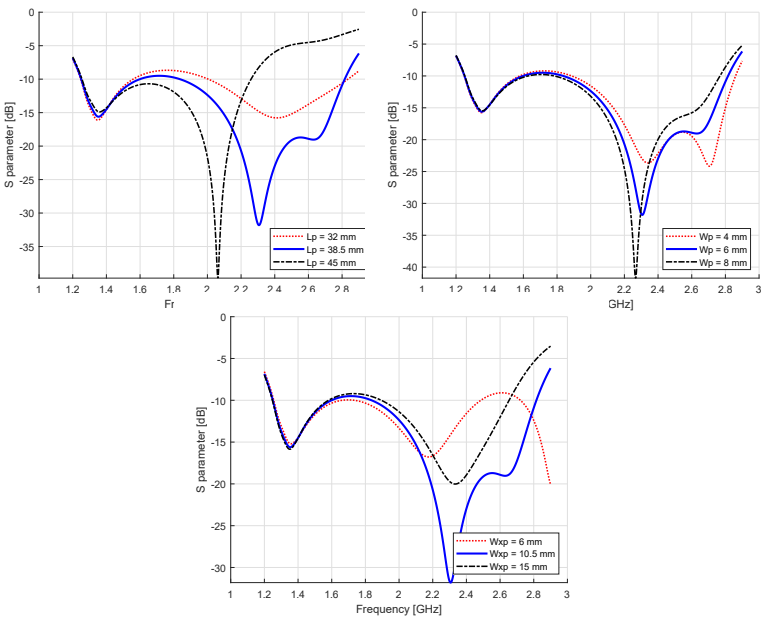

Figure 2.5: S_{11} Parameter for the proposed antennas with different values of parasitic dimensions.

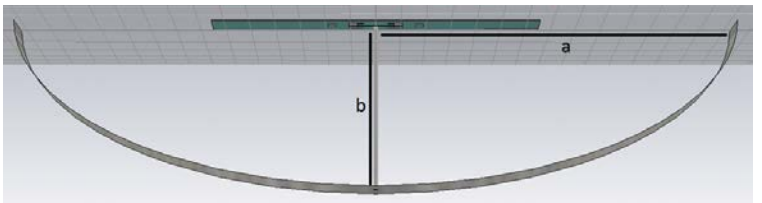

Figure 2.6: Picture of upper band element with elliptical ground plane.

2.2.2 Radiation pattern and ground plane

Dipole elements are omnidirectional antennas, so back radiation has to be removed to achieve the required beamwidth of 65 to 70 degrees on the horizontal plane. Using a ground plane is the main solution for that purpose. Although a flat one is the easiest to fabricate, due to its resonant behaviour as a narrow band reflector, it does not behave good enough for broadband antennas generally speaking.

Then, following that reasoning, the idea was using the broadband behaviour of parabolic reflector when the antenna phase center is nearly constant and placed at the focal point. But the parabolic cylinder was found to collimate the radiation pattern too much.

Finally, an elliptical shape was tested, due to the presence of two focal points the focal area would be wider obtaining better results. Figure 3.26 shows the geometrical setup where a = 90 mm, b = 45 mm. Values below -10 dB can be seen between 1.2 and 2.8 GHz in figure 2.8. Radiation patterns with simulation and measure are shown in figure 3.18, beamwidth is more similar to required as values around 60 degrees are found for 1.6 GHz.

After trying different ground plane configurations, the elliptical one was found to be better than other presented options. The reflector and ground plane topic is deeper studied in Chapter 3.

2.2.3 Fabrication and Measurement

The antenna elements have been fabricated with a laser machine. The coaxial cable is RG402 with an inner conductor welded in the L-

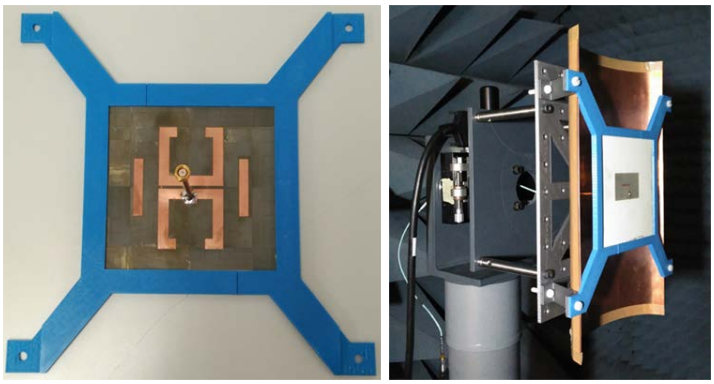

Figure 2.7: Manufactured Antenna with 3D printed holder and profile, performing the elliptical ground plane with copper metal sheet.

shaped microstrip. The outer conductor is connected to the coplanar stripline. While one branch of the coplanar stripline is physically attached to the outer conductor, the other branch is coupling fed by the L-shaped microstrip. With that process, the unbalanced signal coming from the coaxial is transformed into a balanced feed in the coplanar stripline.

To manufacture the elliptical ground plane, a 3D printed profile and holder makes a thin copper sheet fit and adapt its shape to the design. Figure 2.7 presents the vertical polarized element, in which the holder can be seen, and how the antenna with the copper elliptical ground plane is placed in the annechoic chamber.

Figure 2.8 shows the S parameter measurement and simulation for the antenna with elliptical ground plane. The radiation pattern for this antenna is shown in figure 2.9. The picture shows low values of cross polarization and high rejection of back radiation. Good agreement is observed between the simulation and the measurement, with 60 degrees of horizontal beamwidth at 1.6 GHz. Although different values of beamwidth are found for higher frequencies, this topic is developed in Chapter 3.

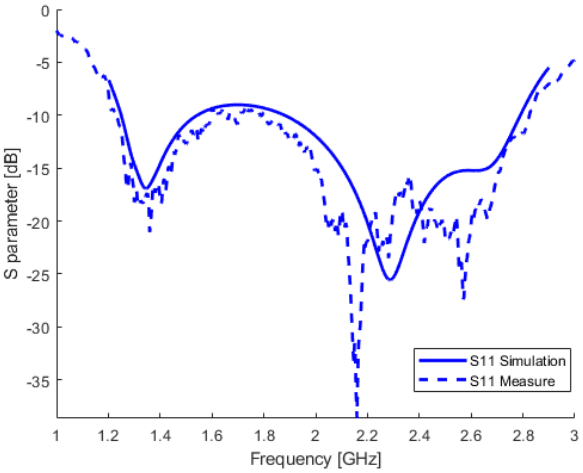

Figure 2.8: S11 for Manufactured Antenna with the implemented elliptical ground plane. Good matching below -10 dB is observed for the whole band of interest with agreement between simulation and measurement.

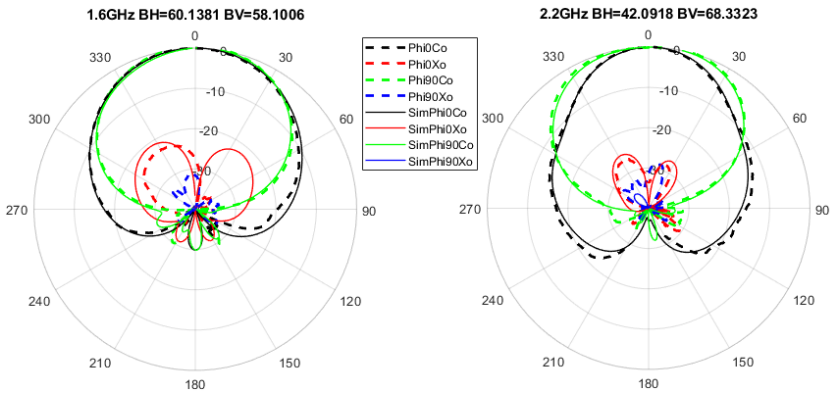

Figure 2.9: Measured radiation for Antenna with elliptical ground.

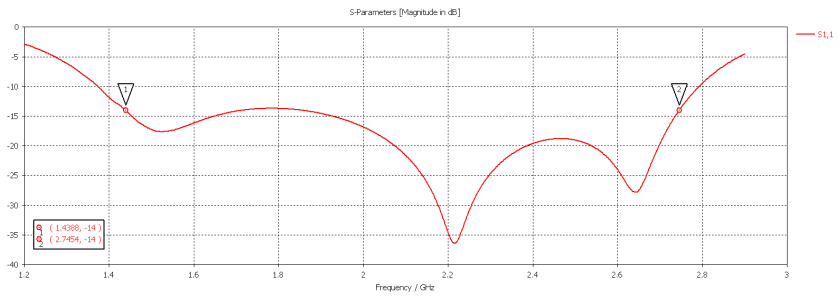

Figure 2.10: Optimized reflection coefficient S11 for rotated element at 45°.

2.3 Side-by-side Dual-Polarized Design

The previous section showed the design of a single polarized radiating element. However mobile communications need ±45° dual polarized ones. This section will deal with it.

When the element is rotated inside the elliptical ground plane to obtain the 45 degrees polarization, not noticeable modification in matching and radiation pattern is seen. So at that point, optimization to enhance the -10 dB return losses to get the required -14 dB of matching was developed.

The new parameters for the element can be found at table 2.3. The dipole length is now shorter, meaning that the lowest resonance at 1.3 GHz is now shifted up to 1.5 GHz. The dimensions of the parasitic element are modified to get better matching at higher frequencies. Figure 2.10 shows the resulting S11.

Then, for obtaining dual polarization there can be observed two main issues. Firstly, both polarization elements, achieved by ±45° rotations, have some difficulties to be combined in the same substrate plane or in the same space. Secondly, if they would be placed in the same reflector, following the reflector axis, the separation between them would entail an unaffordable distance between same polarization elements in a future vertical array design. For those reasons, it was decided to place both polarization in different elliptical reflectors, as shown in figure 2.11.

Table 2.3: Parameters for Dual Polarized New Design

Parameter	Value [mm]
Wd	2.1
Ls	42.5
Lf	73
Wa	6.8
Lb	5
Wxp	12.5
Wp	8
Lp	36.5
Ln	20
La	12.4
Wl	1.9

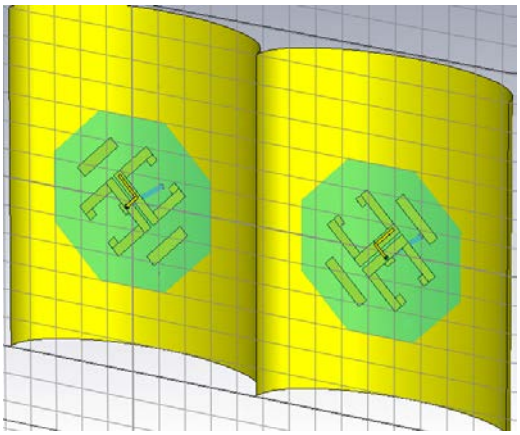

Figure 2.11: Dual Polarized Antenna for ±45 degrees polarization in side-by-side configuration.

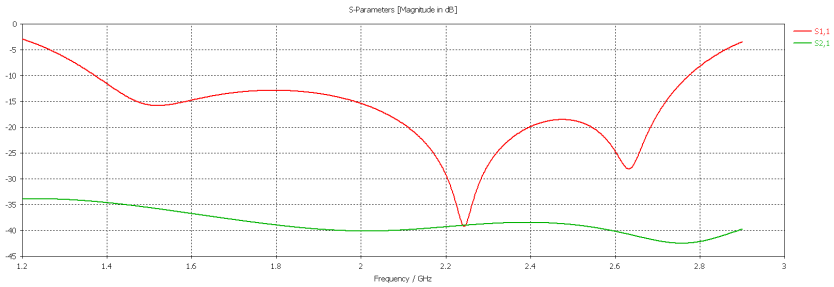

Figure 2.12: S Parameter for Dual Polarized Antenna side-by-side.

With this prototype, a really good isolation between polarization is obtained (around 35-40 dB). As can be seen in figure 2.12, the matching of the element is not modified by placing the other element next to it.

Although the proposed element works correctly, exposing that external capacitive parasitics enhance the matching bandwidth, the total size of the two polarization combination is huge. That size makes this proposal difficult and not interesting for making the arrays, integrate with low band elements, and manufacturing of a complete antenna. For those reasons it is important to obtain an element in which both polarizations are included, into a compact and planar design, as it is shown in next section.

2.4 Broadband Dual-Polarized Compact Antenna

2.4.1 Non-Compact Dual-Polarized Broadband Antenna

The challenge in the development of new antennas for sub 6-GHz 5G applications implies a somewhat contradictory request. On the one side, smaller and smaller sizes are required. On the other, larger and larger bandwidths are needed. It is well known that the antenna bandwidth is constrained by its electrical length [19]. Then, the extension to lower frequency bands, while keeping the largest ones and even reducing the size of the radiating element, is a challenge itself.

An arrangement of a double set of dual dipoles was used in [2] to achieve a dual-polarized configuration. The antenna, illustrated in Fig.

2.13, is composed of a pair of two dual dipoles connected in parallel through a coplanar strip on each side of the substrate. This dual polarized element (left part of Fig. 2.13) presents two resonances: one associated to the length of the dipole itself and the other one associated to the extended dipole coupled to the backside dipole.

The feeding of the antenna consists of a microstrip bridge that balances one of the coaxial conductors to connect it to one dipole branch through the substrate. For the first polarization the H-shaped dual dipoles are printed on the substrate backside whereas the microstrip bridge is on the front side. For the second polarization the process is just in the opposite sense.

The addition of external strips (right part of Fig. 2.13), acting as capacitive parasitic elements, enhances both the return losses and their associated bandwidth. The objective of placing these parasitic elements is to get another resonance that fulfills the bandwidth requirements. Including parasitic elements enhances the matching and bandwidth but also increases the size of the antenna.

The antenna is designed on a Rogers 4350B substrate, with a relative dielectric constant of $\varepsilon = 3.48$ and a thickness of $h = 0.76mm$. The proposed broadband antenna has to cover the extended frequency bandwidth between 1.427 and 2.69 GHz while maintaining the original base station specifications such as $VSWR < 1.5$, $isolation < -28dB$ and $beamwidth = 65^\circ \pm 10$.

The realization of the current antenna requires a flat ground plane reflector placed 45 mm below the radiating element (corresponding to $\lambda/4$ at the central frequency). This assures the best matching condition while keeping a trade-off with the desired beamwidth. The dipole length, $Ld = 68.8mm$, is chosen to select the intermediate resonance frequency. Concerning the coplanar strips, the width of the line will be the same as the one of the dipole ($Wa = 5.8mm$) whereas the spacing between the lines has been set to $1.2mm$ (Wd). Finally, concerning the external parasitic strips, it can be said that are placed at both sides of the dual dipoles acting as side capacitive elements to improve the matching at higher frequencies and enlarge the overall bandwidth. The values for the parasitic elements were chosen to add a third resonance frequency around

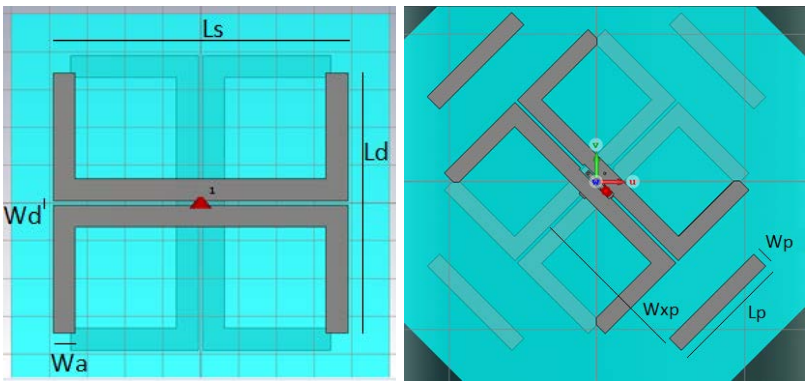

Figure 2.13: Schematic of the proposed antennas: the left part shows the non-extended bandwidth while the right one shows the extended bandwidth non-compact antenna. Darker colour means the metal forming the dipoles in the substrate front face, while the backside dipoles are shown in lighter colour.

2.6 GHz resulting in the following values: $Lp = 38.5mm$, $Wp = 6mm$, and the $Wxp = 87.5mm$ as can be seen in the right part of Fig. 2.13. A comparison of the impedance bandwidth between the antennas at the left and right part of Fig.2.13 is shown in Fig. 2.14. The proposed impedance bandwidth has been clearly achieved with the inclusion of these capacitive elements.

The inclusion of the parasitic element has allowed increasing the impedance bandwidth at a price of enlarging the electric dimensions of the antennas. This fact is particularly critical on the antenna radiation pattern that tends to have a multilobe performance at higher frequencies, when the dimension of the overall antenna is larger than λ. This can be seen in Fig. 2.15 that shows the horizontal plane of the radiation pattern for both antennas, non-extended and extended frequency antennas. A non-desired lobe appears in the extended frequency antenna due to its dimension, larger than a wavelength ($D > \lambda$).

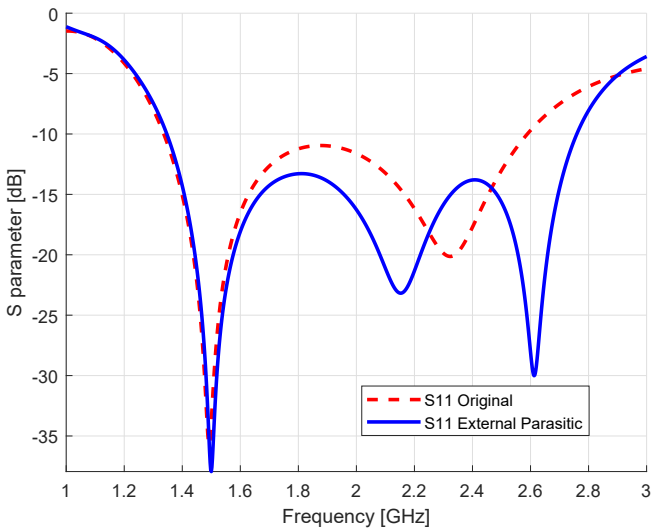

Figure 2.14: S_{11} Parameter for the proposed antennas (continuous line shows the extended frequency non compact antenna while the dashed line shows the non-extended frequency).

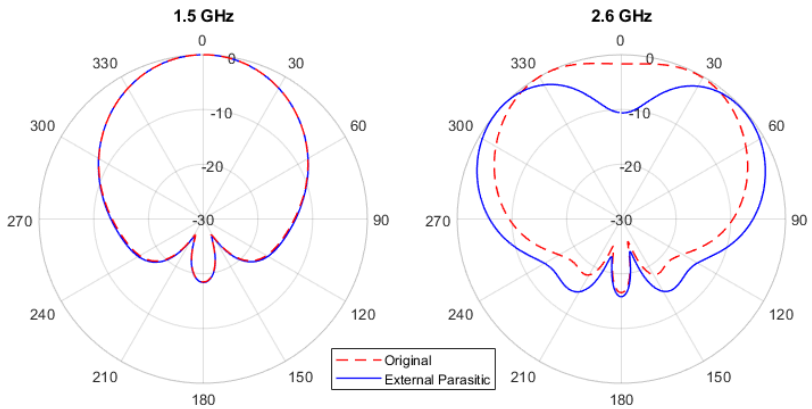

Figure 2.15: Radiation Pattern of External Parasitic Antenna present lobulation for highest part of frequency band (Discontinuous red line for original element, continuous blue line for external parasitic).

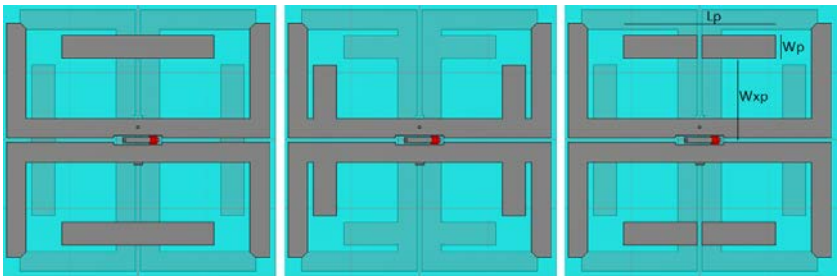

Figure 2.16: a) Internal Parasitic. b) Internal fed Dipoles. c) Internal Parasitic Dipoles.

2.4.2 Extended Bandwidth Dual-Polarized Compact Antenna

While external parasitics have been proved to enhance the bandwidth in terms of matching, the increase of the size results in lobulation for the highest frequencies. For that reason, it is necessary to achieve a new method to increase the bandwidth in a compact design to prevent that lobulation, which is proposed in this section.

The inclusion of internal dipoles simultaneously coupled and fed by the feeding line and through the main dipoles allows extending the impedance bandwidth while keeping a compact and fully planar structure. In addition, the compactness of the new antenna prevents the multilobe effect at higher frequencies. The final goal is the reduction of the multilobes in the previous non-compact dual polarized broadband antenna.

Fig. 2.16 shows three possibilities to extend the bandwidth and reduce the antenna size. In all of them the total dimension of the antenna is smaller than the wavelength at the highest frequency in order to avoid multilobe radiation patterns as desired for the whole frequency band.

The first option (shown in Fig. 2.16a) is the addition of a fully parasitic strip integrated inside the element in a similar way to the one proposed for the non-compact antenna (it is called as internal parasitic in Fig. 2.16a). These strips are intended to provide an additional resonance

at the highest frequency band (in this case around 2.7 GHz). The strips have to be placed on the opposite side of the substrate in order to avoid physical contact with the original conductors. These continuous strips affect the feeding coplanar strips and perturb the original dipoles of the antenna and the matching of the element. Despite the similarity with the antenna of the previous section, the optimized parameters (the strip length, L_p, the strip width, W_p, and the separation with the main dipole, W_{xp}) do not turn out a good performance of the antenna in terms of impedance matching and sidelobes.

The second option consists on making the internal dipole active by feeding it through the line. This internal dipole is placed in ohmic contact with the coplanar strips generating a new resonance at higher frequencies. Although the impedance bandwidth is extended and the lobes have been reduced, there is an increase in the return losses at central frequencies that is not easily controlled.

By acting on the impedance and on the coupling of the added dipole (mostly by means of modifying both the width of the new internal dipole, W_p, and its position with respect to the main dipole, W_{xp}) a control on the overall impedance bandwidth, in particular at middle frequencies, can be achieved. However, due to physical limitations, the dipole has to be placed in antipodal configuration at the opposite side of the main dipole as shown in Fig. 2.16c. Then, the final arrangement of the proposed antenna is as follows. For the central frequency, 2.3 GHz, the dipole length approximately equals $\lambda/2$, generating a resonance for that frequency. This can be appreciated in the central part of Fig. 2.17. Another resonance is found at 1.5 GHz. This is due to the coupling between the original dipole and its antipodal part, as can be appreciated in the left part of Fig. 2.17. A current distribution along the dipole and its antipodal part flows along a length of 140 mm, what approximately matches $\lambda/2$ at 1.5 GHz. Finally, as shown in the right part of Fig. 2.17, another resonance appears at 2.7 GHz associated to the coupled inner dipole in the antipodal part of the main dipole. The dimensions of all the design parameters of the antenna are shown in Table 2.4. This table also shows the distance with the ground plane, H_G, which has been set to 45 mm.

In the figure 2.18 a parametric study for parasitic dipole dimensions

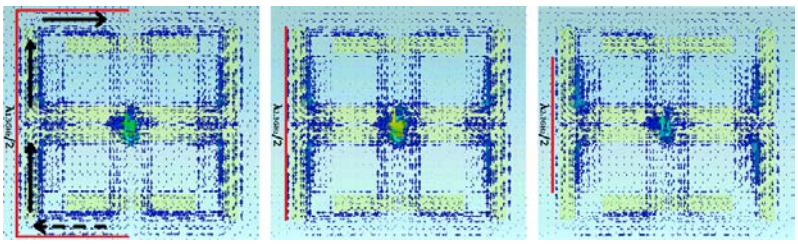

Figure 2.17: Currents for vertical excitation. 1.5, 2.3 and 2.7 GHz frequencies are presented.

and position is included for understanding their effects. The first picture shows the variation with the parasitic element length (Lp). It is related to the third resonance frequency in the high frequency part of the band spectrum. The second picture shows the variation with the parasitic width (Wp), affecting both the matching and Q. The third picture is related to the position, concisely to the X-position with respect to the center (Wxp), this implies the separation between the active dipole and the parasitic coupled feed dipole, that separation controls the coupling between them and the parasitic feeding, affecting the higher frequencies in both quality factor and resonance shifting and matching. As can be seen in the complete figure, the parasitic variations mainly affect to the high frequency spectrum of the working band.

The control of the coupling between both layer dipoles that creates the first resonance can be done by cutting a small piece in the dipole corner to modify the overlapping. This technique is used in [11], and can be seen in figure 2.19. The figure shows how the dimension of the cut essentially modifies the shape on the first resonance due to changing the coupling, while other frequencies are modified consequently. When $\Delta = 0$ there is no cut, so the coupling is strong with a sharp resonance and worse broadband behavior. The selected $\Delta = 1.4mm$ is considered to be the best trade off, with the minimal physical overlapping, while in the S_{11} a noticeable resonance for low frequency is found and better broadband matching. Finally, the value $\Delta = 2.8mm$ shows the results when there is no overlapping between the dipoles, instead some small gap is presented, the low frequency resonance is now very subtle and shifted due to the low coupling, and bad behaviour in higher frequencies is obtained.

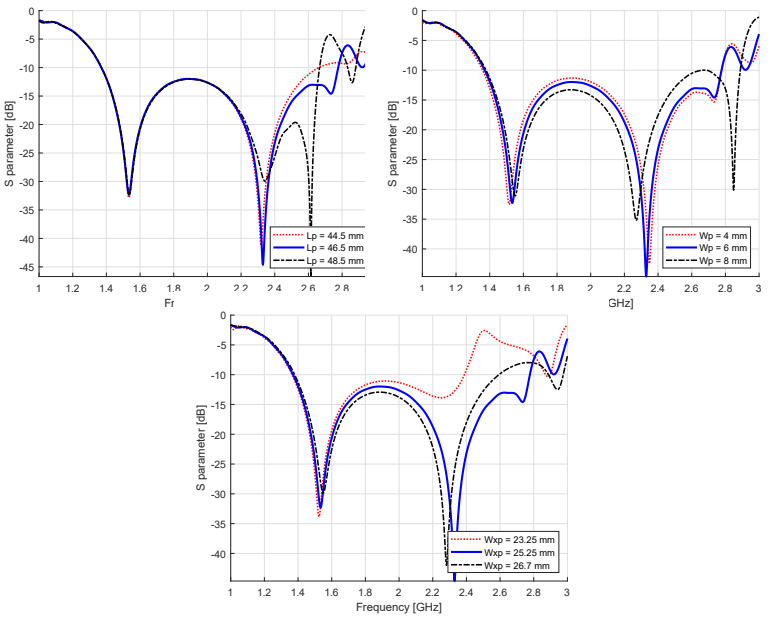

Figure 2.18: S_{11} Parameter for the proposed antennas with different values of parasitic dimensions (Lp, Wp, Wxp).

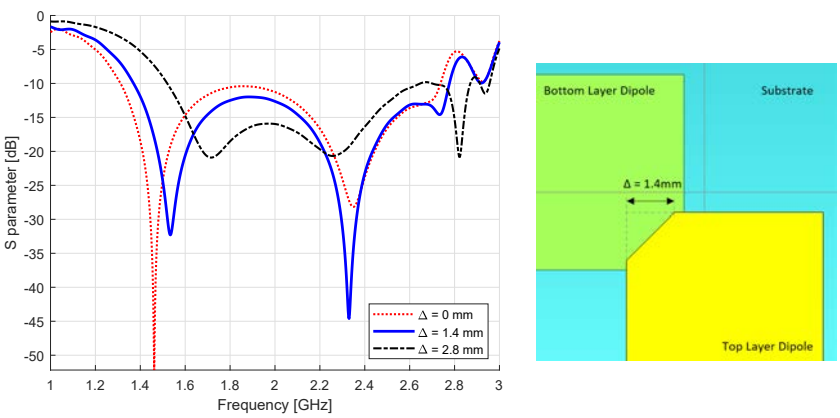

Figure 2.19: Left figure shows the S_{11} parameter for the proposed antennas with different values of Δ, controlling the overlapping between dipoles. Right picture is a detail zoom to the element corner to clarify the meaning of the Δ parameter.

Table 2.4: Parameters for New Design with Internal Parasitic Dipoles

Parameter	Value [mm]
Wd	1.2
Ld	68.8
Ls	77
Wa	5.8
Lp	46.5
Wxp	25.25
Wp	6
H_G	45

Once the impedance bandwidth has been studied, two additional points have to be addressed concerning the radiation pattern. The first one is associated to the presence or not of multilobes. According to the current distribution shown in Fig. 2.17 it can be seen that the inclusion of the new dipole has avoided the presence of multiple lobes in the current distribution and in the radiation pattern along the whole band.

The second point is the crosspolar radiation that could be high, at least at the lowest frequencies due to the coupling between the dipole and its corresponding antipodal part. Fortunately, this does not happen and the cross-polar component is low enough. This can be explained, for one polarization (the other one is equivalent), as follows. When the vertical dipoles are fed, the phase associated to its input port 1 (P1) is maximum while the one associated to port 2 (P2) is null. Under these conditions the currents in the extended vertical dipole (vertical dipole plus the coupled horizontal arms) are shown in Fig. 2.17a. These currents allow having an extended length for the dipole, what makes the working frequency be reduced for the radiation copolar component. However, for the crosspolar component the horizontal currents are cancelled out since

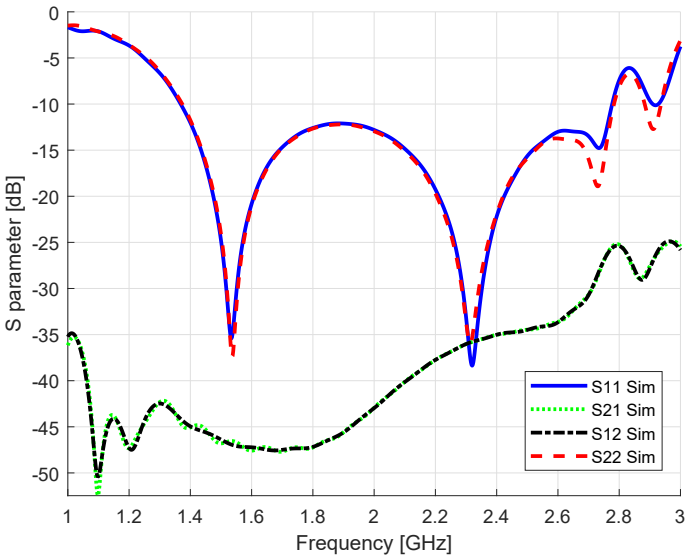

Figure 2.20: S parameters for internal parasitic dipoles antenna.

the upper part of the current (a continuous trace has been added in the right part of Fig. 2.17) is 180° out of phase in comparison with the bottom one (dashed trace) producing a cancelation of the horizontal current contribution and a subsequent reduction of the crosspolar component.

The resulting S-parameters are shown in Fig. 2.20. The return losses are lower than -13 dB for both ports along all the frequency band, between 1.4 to 2.8 GHz (and lower than -15 dB for most band). In addition, the isolation is larger than 35 dB along the bandwidth between 1.4 and 2.6 GHz and larger than 30 dB in the whole extended band up to 2.8 GHz.

2.4.3 Feeding

The final step for the design is the feeding network. This stage is critical, especially, because of the broadband performance of the structure and the balanced arrangement of the antenna itself. Then, a broadband balun to balance the coplanar feeding for the two pairs (horizontal

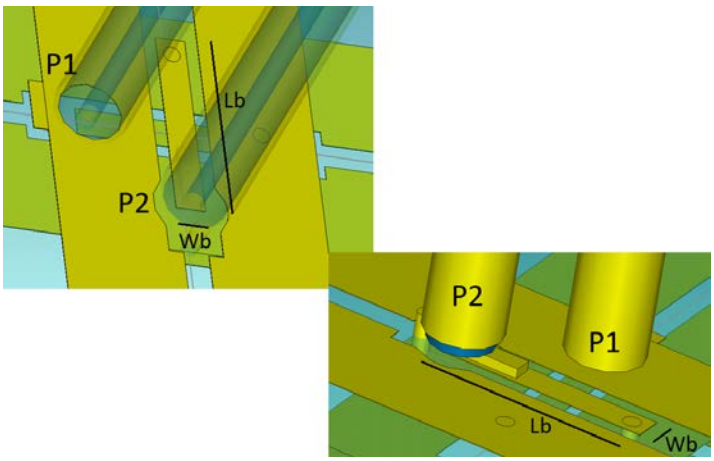

Figure 2.21: Coaxial feeding architecture. Picture shows both coaxial inner conductor connected to the bridge and the jacket to one dipole branch.

and vertical) of dipoles with the unbalanced coaxial line is needed. Fig. 2.21 shows the overall structure of the balun. For the horizontal pair of dipoles the feeding will be made through the coaxial port 1. Its outer part is directly welded to one branch of coplanar strips, whereas the inner conductor crosses the substrate through a hole. The double side cladding substrate allows creating a metal strip between the coplanar conductors of the vertical pair of dipoles placed on the other side of the substrate. This metal strip will serve to create a bridge with the horizontal dipoles via a hole and an ohmic contact. The described overall structure will act as a balun and will balance the signal from port 1 to the horizontal dipoles. The dimensions of this global microstrip bridge are important parameters for achieving the desired impedance matching along the desired broadband. The values of its width, W_b, and length, L_b are: $W_b = 1.4mm$ and $L_b = 9.3mm$. This procedure has to be repeated for the feeding structure through the coaxial probe P2 for the vertical polarized antenna as shown in Fig. 2.21.

Finally, a microstrip taper has also been included to match the impedance to 50 ohm. This transition will be placed on the other side of the ground plane and will improve the impedance matching to values below -15 dB between 1400 MHz and 2800 MHz. This can be appreci-

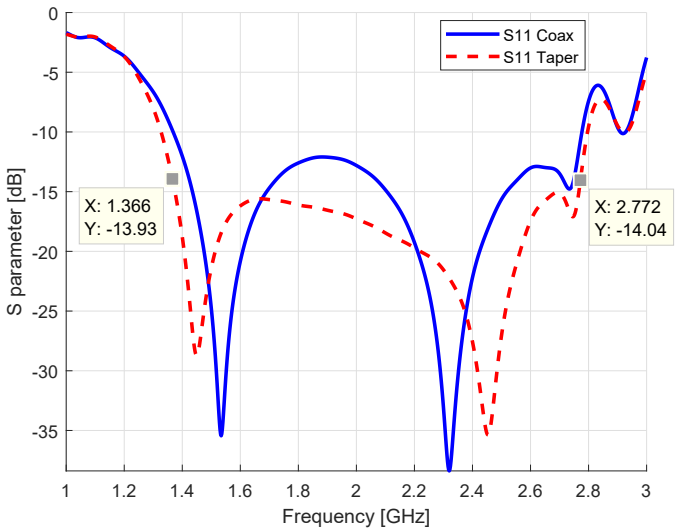

Figure 2.22: Return losses with and without taper feeding

ated in Fig. 2.22 and 2.23 that compares the impedance matching with the taper and without the taper.

2.5 Experimental Results - Manufacture and Measurement

The antenna has been fabricated with a routing laser machine. The balun has been realized with two coaxial cables that connect the two branches of the dipole through a bridge with dimensions L_b and W_b as described in Section II.C. A flat ground plane has been added since it is easier to fabricate than a conformal one and shows good performance for our application. The reflector also acts as a ground plane for the needed circuits, in particular for the proposed microstrip taper for the feeding. In addition some nylon posts have been added to provide mechanical robustness and assure the required distance between the antenna and the ground plane. It has been previously proved that the presence of the posts does not affect the electromagnetic properties of the antenna. This arrangement can be seen in Fig. 2.24 that shows the antenna to be measured in the anechoic chamber.

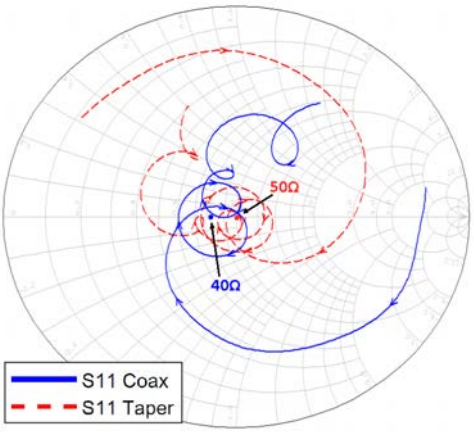

Figure 2.23: Return losses with and without taper in Smith Chart. Blue coninuous line show the S_{11} from the coaxial, centered at 40Ω, while red dash line add a taper to center the return losses at 50Ω.

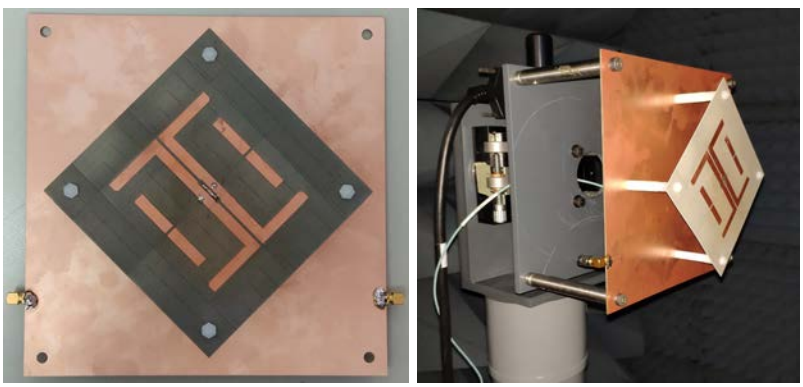

Figure 2.24: Pictures of the antenna prepared to be measured in the anechoic chamber.

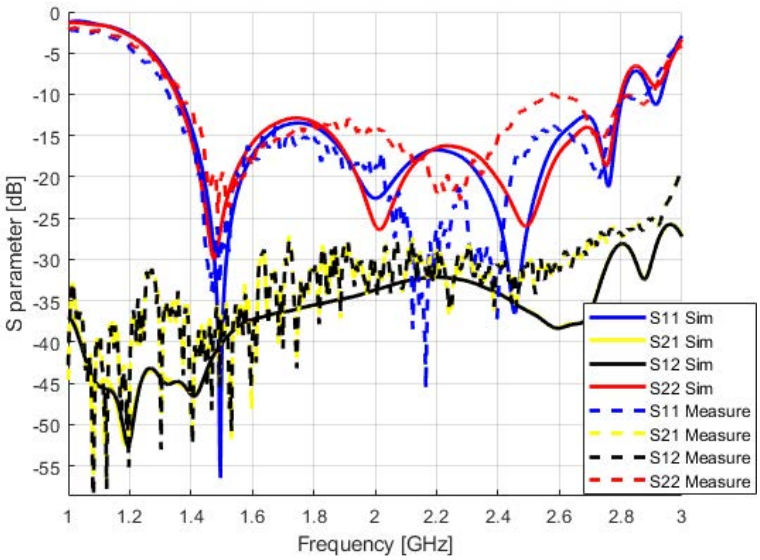

Figure 2.25: S parameters of the antenna. Simulated in continous line and measured in dash line.

Fig. 2.25 shows the S parameter of the final prototype for the presented antenna. Both the reflection coefficient and the isolation between ports are shown. A comparison between simulations and measurements has been undertaken. Good agreement between simulation and measurements can be seen in Fig. 2.25. The reflection coefficient at port 1, S_{11}, is below -14 dB, both in simulation and measurement for the whole frequency band, from 1.4 to 2.8 GHz. The same happens for the second port, S_{22}, except a small mismatching (but always below -10 dB) in the upper part of the band (between 2.5 and 2.7 GHz). This prominence between 2.5 and 2.7 GHz is probably due to the different and more laborious coaxial welding. The isolation between both polarizations fully meets the requirements around 30 dB for the whole frequency band achieving a value below -28 dB between 1.427 and 2.69 GHz.

Finally, with regards to the radiation pattern, it is well known that base stations usually have sector architecture what means that the different sectorial antennas are combined in one place to obtain the required omnidirectional diagram. When applied to one sector antenna, it means

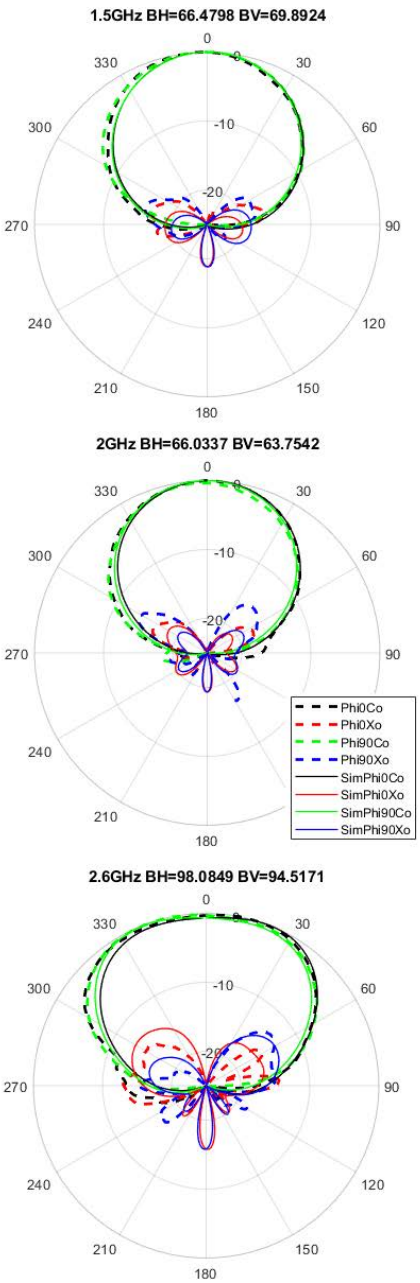

Figure 2.26: Simulated and measured radiation pattern.

that the broadband design has to achieve a stable radiation pattern within the desired bandwidth for both polarizations with a horizontal radiation pattern around 65 degrees. Fig. 2.26 shows the radiation pattern at three frequencies (1.5 GHz, 2 GHz and 2.6 GHz) for both horizontal and vertical planes for copolar and crosspolar polarization ($\pm 45^{\circ}$). As illustrated, there is a good agreement between simulations and measurements. The horizontal half-power beamwidth, as required, is very stable for most of the band with values of 66°. It can be appreciated, however, that wider beamwidths (98°) are found at the highest frequencies. This increase can be due to the fact that potential lobes are close to appear implying an increase in the corresponding beamwidth.

It can also be appreciated that the copolar-crosspolar ratio is larger than 25 dB are achieved for a beam range between $\pm 30^{\circ}$ for the whole frequency range (between 1.4 GHz and 2.7 GHz). For larger beamwidth ranges (up to $\pm 90^{\circ}$) the copolar-crosspolar ratio is always larger than 15 dB. This is coherent with the fact that the feeding structure and the arrangement of the dipoles cancels out the currents orthogonal to the desired one, as it was explained in Section II.B. The same can be said for the vertical beamwidth, good agreement with the simulation can also be seen.

Finally Fig. 2.27 summarizes the values for the realized gain at boresight and the corresponding $VSWR$ for the whole bandwidth. The gain in simulation shows values around 9 dBi whereas the measurement is around 8 dBi. This small difference can be due to some transition and connector losses. Finally, the small difference between port 1 and port 2 can be associated to the inequality between the feeding at port 1 and 2, meaning that small differences observed in matching are also presented in the realized gain values. Regarding the decrease in gain that can be observed for the highest frequencies of the band, as it is related to the reflector and beam shape, this topic is addressed in Chapter 3. Concerning the $VSWR$ it can be seen that it is always lower than 1.5 except in the upper part of the band at port 2 due to the welding process.

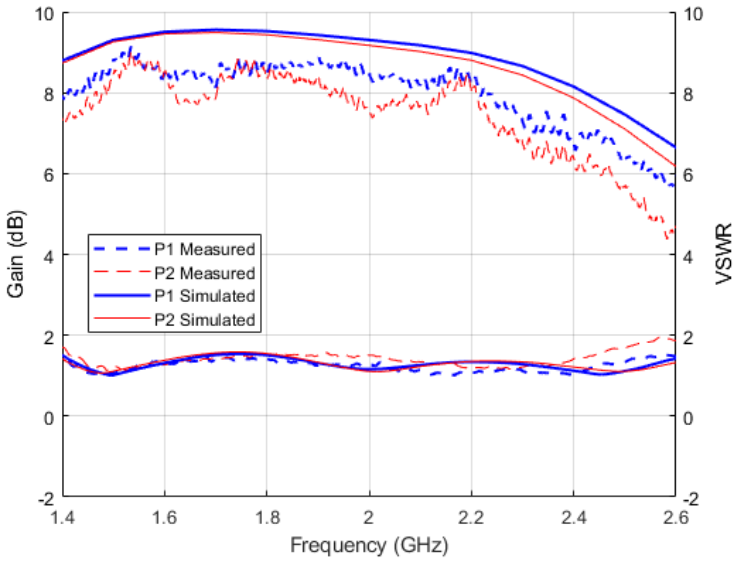

Figure 2.27: Antenna gain at boresight. Simulated and measured for both ports.

2.6 Conclusions

This chapter has presented a broadband antenna to work in the sub 6-GHz frequency band for 3G to 5G standards. The antenna has been designed and fabricated in a cost-effective and affordable way presenting a compact and fully planar topology. The main idea behind the goal is the inclusion of active embedded dipoles in the antipodal part of the antenna itself. Compactness and dual polarized performance have been achieved for working in the whole frequency bandwidth between 1.427 and 2.69 GHz. The performance of the antenna has been shown as good in terms of matching (below -14 dB), isolation (larger than 28 dB), and radiation pattern for a dual-polarization performance of $\pm 45^{\circ}$.

2.7 References

[1] S. Martin-Anton and D. Segovia-Vargas, "Fully planar dual-polarized broadband antenna for 3g, 4g and sub 6-GHz 5g base stations," *IEEE Access*, vol. 8, pp. 91 940–91 947, 2020.

[2] S. Martin-Anton and D. Segovia-Vargas, "Broadband antenna design for new mobile communication systems," in *12th European Conference on Antennas and Propagation (EuCAP London)*, 2018, pp. 1–5.

[3] S. Martin-Anton and D. Segovia-Vargas, "Dual-polarized broadband antenna for new mobile communication base stations," in *13th European Conference on Antennas and Propagation (EuCAP Krakow Poland)*, 2019, pp. 1–3.

[4] Y. Cui, R. Li, and P. Wang, "A novel broadband planar antenna for 2g/3G/LTE base stations," *IEEE Transactions on Antennas and Propagation*, vol. 61, no. 5, pp. 2767–2774, 2013.

[5] Y. Cui, R. Li, and P. Wang, "Novel dual-broadband planar antenna and its array for 2g/3G/LTE base stations," *IEEE Transactions on Antennas and Propagation*, vol. 61, no. 3, pp. 1132–1139, 2013.

[6] Y. Cui, R. Li, and H. Fu, "A broadband dual-polarized planar antenna for 2g/3G/LTE base stations," *IEEE Transactions on Antennas and Propagation*, vol. 62, no. 9, pp. 4836–4840, 2014.

[7] H. Sun, C. Ding, T. S. Bird, and Y. J. Guo, "A base station antenna element with simple structure but excellent performance," in *Proc. Australian Microwave Symp. (AMS)*, 2018, pp. 35–36.

[8] N. Xu and Q. Chu, "A broadband dual-polarized antenna with coupling-resonators for base-station applications," in *Proc. Int. Workshop Antenna Technology (iWAT)*, 2018, pp. 1–3.

[9] H. Sun, C. Ding, T. Yang, Y. J. Guo, and P. Qin, "A wideband base station antenna with stable radiation pattern," in *Proc. Australian Microwave Symp. (AMS)*, 2018, pp. 5–6.

[10] X. Gao, Y. Cui, and R. Li, "Broadband vertically/horizontally dual-polarized antenna for base stations," in *Proc. Propagation and EM Theory (ISAPE) 2016 11th Int. Symp. Antennas*, 2016, pp. 79–80.

[11] Y. Cui, X. Gao, H. Fu, Q. Chu, and R. Li, "Broadband dual-polarized dual-dipole planar antennas: Analysis, design, and application for base stations," *IEEE Antennas and Propagation Magazine*, vol. 59, no. 6, pp. 77–87, 2017.

[12] D. Wen, D. Zheng, and Q. Chu, "A dual-polarized planar antenna using four folded dipoles and its array for base stations," *IEEE Transactions on Antennas and Propagation*, vol. 64, no. 12, pp. 5536–5542, 2016.

[13] H. Sun, C. Ding, H. Zhu, and Y. J. Guo, "Dual-polarized multi-resonance antennas with broad bandwidths and compact sizes for base station applications," *IEEE Open Journal of Antennas and Propagation*, vol. 1, pp. 11–19, 2020.

[14] M. Li, Q. L. Li, B. Wang, C. F. Zhou, and S. W. Cheung, "A low-profile dual-polarized dipole antenna using wideband amc reflector," *IEEE Transactions on Antennas and Propagation*, vol. 66, no. 5, pp. 2610–2615, 2018.

[15] M. Li, R. Wang, J. M. Yasir, and L. Jiang, "A miniaturized dual-band dual-polarized band-notched slot antenna array with high isolation for base station applications," *IEEE Transactions on Antennas and Propagation*, vol. 68, no. 2, pp. 795–804, 2020.

[16] A. Alieldin, Y. Huang, S. J. Boyes, M. Stanley, S. D. Joseph, Q. Hua, and D. Lei, "A triple-band dual-polarized indoor base station antenna for 2g, 3G, 4G and sub-6 GHz 5g applications," *IEEE Access*, vol. 6, pp. 49 209–49 216, 2018.

[17] Q. Zhang and Y. Gao, "A compact broadband dual-polarized antenna array for base stations," *IEEE Antennas and Wireless Propagation Letters*, vol. 17, no. 6, pp. 1073–1076, 2018.

[18] L. Wu, R. Li, Y. Qin, and Y. Cui, "Bandwidth-enhanced broadband dual-polarized antennas for 2g/3G/4G and imt services," *IEEE Antennas and Wireless Propagation Letters*, vol. 17, no. 9, pp. 1702–1706, 2018.

[19] R. C. Hansen and R. E. Collin, "Small antenna handbook," 2011.

CHAPTER 3

EFFECT OF DIFFERENT REFLECTOR SHAPES

Some of this work is based on the articles presented on [1] [2].

This chapter deals with the need of a ground plane to remove the back radiation caused by the omnidirectional pattern of a dipole, as is the architecture presented in Chapter 2. This ground plane or reflector should shape the radiation beam to obtain a directive antenna with a desired beamwidth that remains stable within the frequency band.

From theory [3] it is known that a ground plane should be placed in a distance of $\lambda/4$ from the feed at the selected frequency, so that in that case, from image theory, a constructive interference is obtained. The problem here is that the ground plane or reflector is in the element near field, which disturbs both the matching and the radiation.

Furthermore, we are dealing here with a very broad bandwidth, which makes it even more difficult. So the objective of the chapter is to get a good matching and fulfill the radiation pattern requirement with frequency stability, ie, in a very broadband scenario.

To deal with this task, different ground plane shapes are tested here. Finally it is proposed to use optical structures with several focal points or areas as near field reflectors.

In the introduction different techniques and options are explained, in which it is exposed why commonly used techniques as ray theory can not be used, and instead full wave simulation, taking into account the electromagnetic field behaviour, is needed.

3.1 Introduction

Reflector antennas are widely used in communication, radar and radio astronomy [4]. The fine art of analyzing and designing reflectors of many various geometrical shapes started with the World War II for radar applications. Some years later, spectacular progress were done in the development of sophisticated analytical and experimental techniques in shaping the reflector surfaces and optimizing illumination over their apertures [3].

One of the goals of using a ground plane as a reflector is to focus radiation energy in some specific direction or region in the space, usually from a less directive or even omnidirectional primary source [5].

It has been demonstrated that the overall system properties (radiation pattern, impedance, directivity, efficiency, sidelobes, etc) can be improved if the structural configuration of reflector surface is upgraded with different shapes, source polarization, or distance [3–5]. The objective of this work is to apply this principle to use tailored reflector as ground plane for new generations of mobile communications arrays in base stations. But at the same time it will also depend on the physical and economical feasibility of the proposals for the mobile communcations market.

In the field of working with reflector ground planes, there have been some proposal with different techniques. From earlier studies as [6] in the search of directivity increase, to the newer ones. In [7] a flat plane is proposed, but instead of using a metal plane as a Perfect Electric Conductor PEC, a periodic metamaterials structure is used to generate an Artificial Magnetic Conductor AMC, leading to a change in boundary conditions and hence reduction in antenna height. Other authors as [8] modify the ground plane by cutting or milling some slots in the ground plane modifying its currents and its behaviour.

More related to our topic, some publications as [9] and [10] use some metallic walls with the purpose of conforming the beam to the required radiation pattern without any deeper study. This kind of complex structures as [11] [12] led to a more expensive production cost, and furthermore, the near arbitrary shapes used for the reflective surfaces are not explained or their studies presented. Also, reflective elements published in [13] [14] could work in a base station scenario with a modification to the flat ground plane, but the new extended band is not covered, which is a challenge itself.

In this chapter the starting element is the ultra wide band antenna (1.4 - 2.7 GHz) based on dual dipoles presented in Chapter 2, with an omnidirectional radiation pattern when no reflector is used. On the other hand, the desired beamwidth is to be around $60 - 70°$.

The purpose of this reflector is to tailor the radiation pattern removing back radiation, obtaining stable diagram for the whole ultra wide frequency band, while maintaining an acceptable matching for the antenna.

3.1.1 Theoretical Background and Analysis Methods

Now we are going to study the reflector theory and analysis methods from the state of the art. Most of the theory explained here is based on well-known books as [4,5]. Then, a conclusion is obtained to decide how to analyze the work in this chapter.

Dipole antennas are often located above an electric conducting plate which is commonly referred to as the ground plane. In consequence, the radiation field is directed into half-space becoming a unidirectional radiation pattern. Image theory can be used to calculate the radiation field.

Image theory, is a technique which can be used to construct field solutions satisfying the boundary conditions at a specific surface. In practice, it is only used in connection with simple feeder and infinite plane PECs or PMCs. For other geometries the imaging equations become so complicated that they hardly represent any simplification over a numerical solution.

When an elementary dipole is in the presence of a perfect electrical conductor plane, currents are induced in the conductor that contribute to radiation. The conductor effect is translated as the produced by a mirror image dipole with the same currents as the original.

The optimal distance to place the ground plane is $\lambda/4$ from the feed at the working frequency, so that a constructive interference is obtained in the radiation direction, according to image theory and the array theory for two elements $\lambda/2$ spaced. For that case the directivity is optimized, and the dipole radiation resistance is close to that in free space.

In addition to flat ground planes, reflector antennas can have many different forms. Normally they consist of one or more reflectors which are designed to collimate an incident plane wave by reflection to a focal point at a convenient location.

On transmit, the electromagnetic analysis can be performed considering a locally plane-wave emerging from the antenna feed located in the reflector focus, illuminating the reflector system such that a desired field distribution is generated in the aperture plane in front of the main reflector. The wave could be considered plane-wave since the dimensions, focal length, diameter and radius of curvature are usually large in terms of the wavelength. In the discussion that follows, it is assumed that the reflector is in the feeder far-field, which is usually true for more common feeders. Although, it is fair to anticipate that this is not the case for the present work.

Geometrical Optics (GO), or ray theory, is an approximate method to determine electromagnetic fields. It is asymptotically correct for high frequencies. In GO, all fields in free space geometrically propagate along straight lines, referred to as rays, and these rays are reflected at material interfaces by the classical reflection law.

Physical Optics (PO), or induced currents method, is developed by computing the induced currents on the reflector, and calculate the radiated field as the currents integral. Then, the total field is found by summing up the contributions from both actual and induced sources. This method considers the feed at the focal point, also plane waves and large dimensions are considered to use far-field and physical optics approximation in a locally infinitesimally flat surface. In fact, the computed

integration is difficult to compute, nonetheless PO integration method is very accurate for large reflector antennas ($D \gg \lambda$).

In the aperture integration method it is assumed that all the rays reflected from the reflector are parallel, which is rarely true, and never true when the feed is not exactly at the focal point. By applying the Huygens equivalence principle, the reflector end can be considered as a plane aperture in free space, knowing the aperture fields by the optic reflection of feed fields, the equivalent currents can be computed, and with them it is possible to obtain the radiation pattern.

Reflector Synthesis is the art of designing shaped reflectors. Modern reflector antennas often need surfaces that are shaped in order to provide a desired radiation pattern. They may be shaped to maximize the gain, reduce the sidelobes in particular regions or to generate a contoured beam. Originally, reflector synthesis is based on solving differential equations to obtain a desired aperture distribution by Geometrical Optics (GO) reflections. This technique was used to maximize gain in the large ground stations for satellite communications used in the 1980s.

Otherwise, there is a method named Finite Elements and Modal Segmentation (FEM-MS), presented in [15] and particularized for lenses or reflector in [16, 17], in which a different point of view is exposed.

Reflector and lens designs are usually carried out according to classical methods as GO, which, in general gives the shape and profile that meet the specifications while providing also the structure focal point. Nevertheless, the reflector must be fed by a radiating element which computed phase center should match the focal point, achieving theoretically the best gain performance. However, in most lenses cases and in near field reflectors, the distance between them and the feeder position does not allow to apply GO. Moreover, the interaction between them are not taken into account in the design process with that approximation, and hence, performance is degraded. In summary, full-wave analysis is needed, while repeatability and scalability sometimes make it prohibitive in computing time.

The work presented for FEM-MS is a method that begins with the

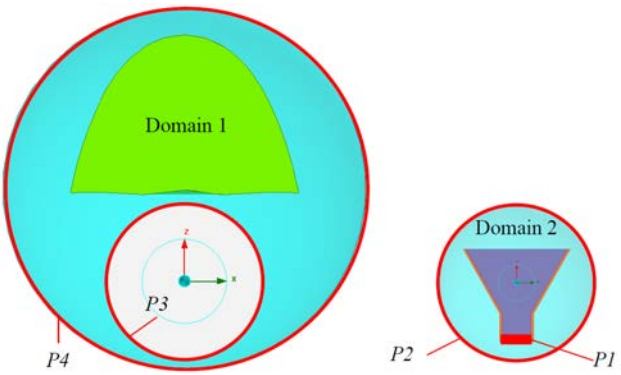

Figure 3.1: Application of Domain Decomposition based on Modal Expansion. Extracted from [16].

decomposition into domains or segments of the device, in order to calculate the corresponding multimode-multiport matrices of each of them. The analytical connection of these matrices gives rise to the global matrix of the device, and hence the complete performance. The technique combines the power of Finite Element Method (FEM) with the flexibility and speed of the Domain Decomposition techniques.

Figure 3.1 shows the proposed segmentation in an example, where there are two domains, Domain 1 containing the lens or reflector and two ports (P4 for radiation, and the interior P3), and Domain 2 being the smallest one, containing the feeder and two ports (P1 for excitation, and P2 for connecting with P3). Connecting both domain matrices, the complete structure matrix is obtain.

As results, taking advantage of Domain Decomposition in addition to matrix analytical manipulations yield to speed up the resolution of the whole structure when computing its electromagnetic parameters over different transformations as position or steering angle, whereas accuracy is kept thanks to the use of mathematically consistent formulations.

To conclude this section it can be said that classical methods for reflector designs (as GO, PO, etc) are not valid for our near field study, due to starting from some far field assumptions, and locally flat large reflectors, where there is a one-point source and flat wavefront with straight

parallel rays, and in that case there is not interaction between reflector and feed apart from the reflection properties.

On the other hand, new methods as the explained FEM-MS have their particular strength in the speed and repeatability for achieving more simulations with less computational weight. While the final results, if the method is correctly developed, are the same as the obtained by full-wave simulations.

According to image theory, a first directivity approximation can be done for our dual dipole design. As exposed, the reflector will enhance the element gain, and for an approximation 3dB increase can be assumed for a flat reflector spaced $\lambda/4$ from the feed. So the total directivity of the element antenna would be one dipole directivity (2.15 dBi) added with the second dipole due to the dual dipole architecture (3 dB can be assumed, although array theory will be explained later in Chapter 5), plus the assumed 3 dB from the flat reflector image, which in total is 8.15 dBi as a first approximation. This is presented in the Chapter 2 Section 2.1.1.

Furthermore, specific designs as $\lambda/4$ spaced are only true for a single frequency, being different spaced in term of lambda for each frequency, not fulfilling the design requirements for a wideband as the present work is dealing.

It is worth mentioning that for wideband frequencies as the interested, dealing with classical reflector theory does not make any good, because the objective is not to collimate the energy in one only direction as a parabolic antenna pointing to a satellite. Otherwise, this work should be handled from the viewpoint of conforming the ground plane or reflector in a way that the radiation pattern is shaped into the desired beamwidth approximately stable in the wide frequency band, while, at the same time, get a good matching in terms of return losses.

Due to the presented reasons, this chapter is based on a designed work developed and checked with full-wave simulator, and finally with actual measurements.

3.2 Study of Different Reflector Shapes in a Single Polarization Scenario

In this section the used feed is the single polarized element presented in Chapter 2, a dual dipole element with single polarization, working in the band 1.4 to 2.7 GHz. Dipole elements are omnidirectional, so back radiation must be removed to achieve the required beamwidth around 65 to 70 degrees in the horizontal plane.

Reflector shape and distance are the main characteristics that determine the performance. If the spacing is too small, the radiation resistance decreases which leads to an inefficient antenna. For very large spacing, the system produces undesirable multiple lobes [3].

While other papers make use of complex radiation elements to deal with multilobulation, beam stability and matching problems [18,19], this chapter focus on optimizing reflector design to handle those goals.

To know the starting point of this single-polarized element, figures 3.2 and 3.3 shows the characteristics in free space. Firstly, in the radiation pattern, both horizontal and vertical planes are shown for different frequencies, while H-plane evidences the omnidirectional diagram, V-plane shows the nulls located at top and bottom, those characteristics are the expected in a dipole kind antenna radiation pattern. Secondly, the return losses of the antenna in free space is around -15 dB for the frequencies 1.4 to 2.8 GHz.

3.2.1 Flat Ground Plane

The simplest type of reflector is a plane reflector introduced to remove the back radiation and direct energy in the desired direction.

Although a flat reflector is the simplest and easiest to fabricate, due to its narrow band resonant behavior it does not behave good enough for this broadband antenna. With distance equal to 0.3λ, the matching is good enough in the whole band, with $S_{11} < -9dB$. While the horizontal beamwidth is not consistent because it starts with 98° for 1.4 GHz,

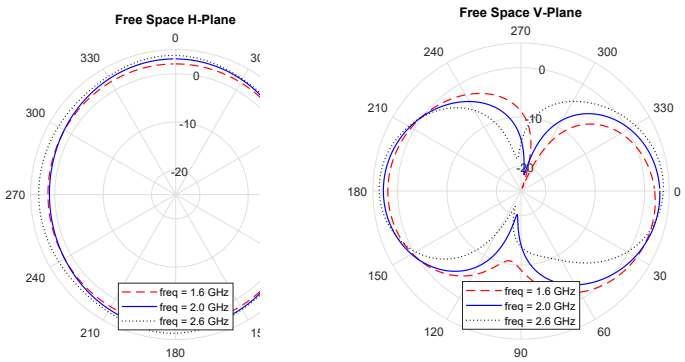

Figure 3.2: Horizontal and vertical radiation pattern for the single-polarized element in free space.

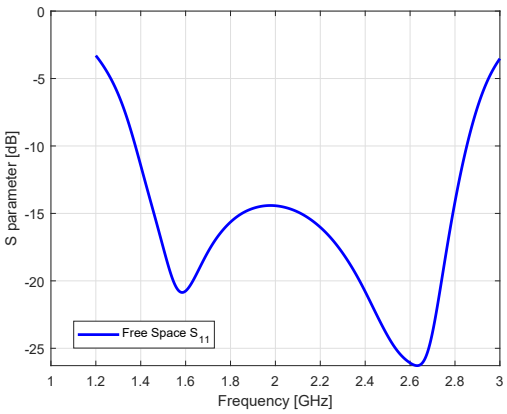

Figure 3.3: S_{11} Parameter for the single-polarized element in free space.

Figure 3.4: Flat Reflector with single-polarized element.

widening with the frequency, and lobulates at the highest part of the bandwidth.

From this first case it is notorious that is not only a matching problem to deal with, which can be achieved by furthering apart the ground plane to a distance in which they do not interact or find a distance that does it in a constructive way. Nevertheless, a flat ground plane does not shape the radiation pattern to the requirement, obtaining beamwidth values too large for low frequencies, while at higher frequencies it splits to the sides and lobulate, which is mainly caused by the element used in this section. For that reason, it is necessary to use a shaped ground plane, which should avoid and redirect side radiation and shape the radiation pattern to the center.

Figures 3.5 and 3.6 shows the results in return losses (S_{11}) and horizontal radiation pattern respectively for different values of height (H), i.e. space between the feed and the flat plane. Used values of distance are 37.5, 45 and 52.5 mm, which correspond to 0.25λ, 0.3λ and 0.35λ at central frequency. With respect to the S parameter, the height tunes the resonance frequency for the reflector, meaning that lower values enhance lower frequencies matching while higher values enhance higher frequencies matching and viceversa. Regarding the radiation pattern, none of the height values are good according to specifications, huge values of beamwidth is obtain with the flat ground plane regardless the selected height, furthermore the beamwidth increases with frequency even arriving to lobulate in twin beams in high frequency.

3.2.2 Parabolic Cylinder Reflector

It has been shown by geometrical optics that if a beam of parallel rays is incident upon a reflector whose geometrical shape is a parabola,

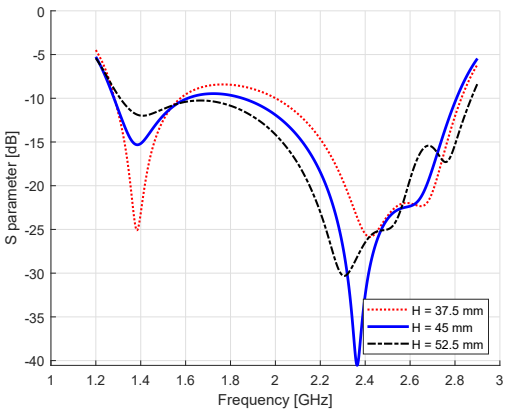

Figure 3.5: S_{11} for flat ground plane antenna with different values of plane height

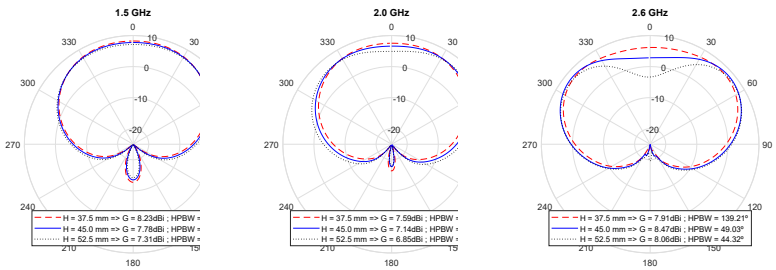

Figure 3.6: Radiation pattern for flat ground plane antenna with different values of plane height.

the radiation will converge (focus) at a spot which is known as the focal point. In the same way, if a point source is placed at the focal point, the rays reflected by a parabolic reflector will emerge as a parallel beam [3].

The idea at this point is to use the well known characteristic of a parabolic reflector, that is shown to have good broadband performance when the antenna phase center is nearly constant in frequency and placed at the focal point.

To bring the element closer to the focal point, it is important to know which is the element phase center. The phase center was computed with the tool included in full-wave simulator. Table 3.1 shows the phase center coordinates for different frequencies of the band. X-coordinates are almost zero because of the horizontal symmetry, Y-coordinates are a bit shifted to positive values due to the feeding but it is not important due to the cylindrical architecture of the parabola, finally Z components are less static receding almost 20 mm in higher frequencies. This is not very precise, because as can be seen, the maximum standard deviation is also increasing the same amount, meaning that the lower frequency estimation is more realistic while the highest frequency appraisals are more uncertain.

Table 3.1: Phase Center for High Frequency Band Antenna

Freq (GHz)	x (mm)	y (mm)	z (mm)	σ (max Std Dev)
1.6	0.32	3.58	-0.82	4.01
1.8	0.19	4.65	-2.84	4.75
2.0	0.12	5.27	-5.32	6.23
2.2	0.14	5.73	-8.45	8.75
2.4	0.42	6.19	-12.59	13.46
2.6	0.53	7.16	-18.67	23.63

From the table it can be assumed the phase center to be approximately in the coordinate origin. A parabolic cylinder reflector is placed

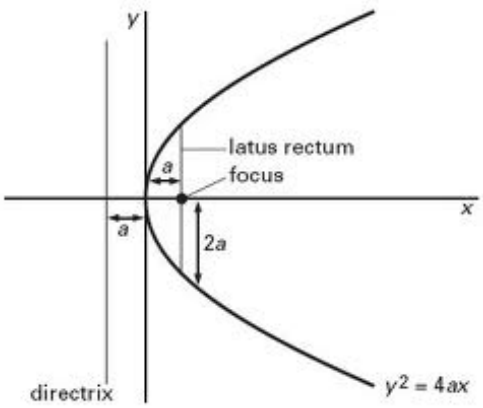

Figure 3.7: Mathematical Concepts of the Parabola.

on the antenna in a position such as the focal point is around the obtained values for the phase center. In that case the antenna is placed at the reflector focal point, 45 mm (0.3λ) from the parabola vertex. That configuration is shown in figure 3.8.

It is fair to mention that, according to the parabola properties, there is only one parabola in the sense that each parabola is a scaled version of each other parabola. The semi-latus rectum of a parabola is always twice the focal distance, and consequently, the proportions are always the same although the figure is scaled. Any parabola size can be used as reflector as far as the focal point matches the feed or is near its phase center. However, there is a trade off to notice. When the parabola is bigger and the feed is further apart, it will disturb less the matching but a very collimated diagram with narrow beamwidth will be obtained. Whereas on the other hand, if the parabola is smaller and closer to the feed, it will affect and disturb much more to the radiation resistance and hence deteriorate the matching, but obtaining wider values for the beamwidth.

The architecture has been probed better for a parabolic cylinder in which the element is placed in the parabola focal point. The focal distance from the parabola to the element is 0.3λ. The S-parameter for the element is similar to that of the flat ground plane, but in this case the maximum value is -7 dB. The radiation pattern is more collimated

Figure 3.8: Parabolic cylinder with single-polarized element.

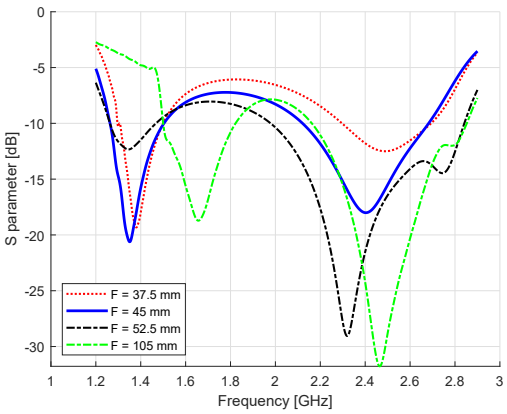

Figure 3.9: S_{11} for for parabolic cylinder reflector antenna with different values of focal distance

due to parabola properties. The horizontal beamwith is 68° for 1.4 GHz, decresing because of lobulation at higher frequencies.

Figure 3.9 shows the S parameters for a parametric study in the parabola focal distance (F). The selected values are the same as before (37.5, 45 and 52.5 mm) including the larger value of 105 mm (0.7λ at central frequency) for a case in which the parabola is much bigger. Once again the distance between the antenna element feed and the metal reflector is related with a shift in the enhanced frequency, while near reflector perturbate more the return losses and further reflector applies less perturbation being more similar to free space presented ones. Figure 3.10 shows the radiation pattern obtained with the parabolic ground plane with the mentioned focal distances. While none of the cases are stable with frequency for the beamwidth values, the results shows narrower beams for larger reflectors leading to very noticeable lobulations

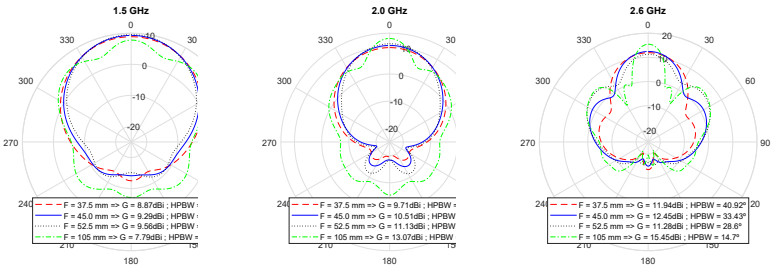

Figure 3.10: Radiation pattern for parabolic cylinder reflector antenna with different values of focal distance.

in high frequency. At the same time, collimation with larger parabolas are stronger in the whole frequency band leading to very narrow beams.

3.2.3 Elliptical Cylinder Reflector

An ellipse is the set of all points on a plane whose distance from two fixed points (the foci) is constant, for that reason an elliptical cylinder is used here. Due to the two focal points characteristic of an ellipse, the overall focal area would be wider obtaining better results. The antenna here is placed centered in the plane containing the two focal points that has been converted to two focal lines in the elliptical cylinder. To manufacture the elliptical ground plane, a 3D printed profile makes a thin copper sheet fits and adapts its shape to the design. Figure 3.16 presents the antenna, in which the holder and the reflector can be seen, the shortest radius is 0.3λ and the longest one is 0.6λ, 45 and 90 mm respectively.

Figure 3.17 shows the S parameter measurement and simulation for the high band antenna with elliptical ground plane, values around -10 dB for the whole band. In the figure 3.18 the radiation pattern for this antenna is shown, in which good agreement between simulation and measure is seen. The horizontal beamwidth at 1.6 GHz is 60°.

With an elliptical cylinder, the parametric study can be developed in two values, the larger radius (a) and the shorter radius (b), both of them are shown below with the consequence of moving the focal points or focal lines closer or further together in the same aperture plane.

The shortest radius (b) controls the distance to the reflector, similarly to the height. The values for this study have been 37.5, 45 and 52.5 mm ($0.25\lambda_c$, $0.3\lambda_c$ and $0.35\lambda_c$). Figure 3.11 shows the S parameter for those cases. In the same way as for the previous shapes, the closeness of the reflector controls some shifting in specific frequencies and, more importantly, the perturbation in the near field. Figure 3.12 shows the horizontal radiation pattern, not very significant differences are obtained in this parameter sweep because the reflector aperture remains constantly the same. But slightly differences can be seen in high frequency, because lower values of b results in slightly larger values of beamwidth.

The largest radius (a) controls the lateral distance to the reflector, what is related to the aperture area. The values for this study have been 75, 90 and 105 mm ($0.5\lambda_c$, $0.6\lambda_c$ and $0.7\lambda_c$). The S parameter results are shown in figure 3.13. As seems to be coherent, larger values makes less perturbation with acceptable results by increasing the size, while the lower value makes a more significant perturbation in the return losses. Figure 3.14 shows the horizontal radiation pattern, while in lower and medium frequencies the results are similar with different values of a, for high frequency the differences are more noticeables, as expected, as the radius increases the beamwidth become smaller at the same time as the lobulation increases, this behaviour is due to the characteristic of a bigger antenna according the aperture size or effective radiation area.

It is interesting to note that the best performanced ellipse is found to match its dimensions, ie. major and minor radii, with the ones on the parabola, ie. focal distance and semi-latus rectum, being the major radius twice the minor one, which is the same that happens in parabola properties, being the semi-latus rectum twice the focal distance. Nonetheless, the only finite focus on a parabola is centered, while on a ellipse there are two separated focuses located in the major axis. Specifically, in the ellipse with radiuses of 90 and 45 mm, the focuses are placed at:

$$c = \pm\sqrt{90^2 + 45^2} = \pm 45\sqrt{3} = \pm 77.94mm$$

This means that the focal points in the ellipse are 155.88 mm aparts,

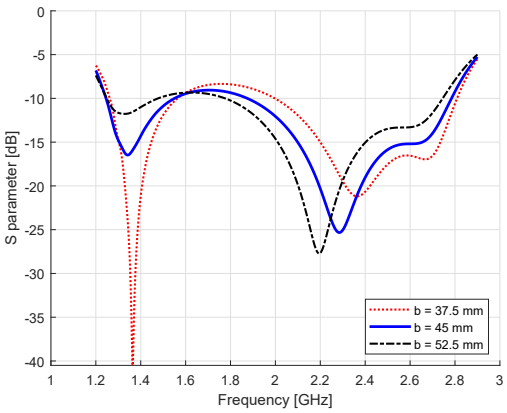

Figure 3.11: S_{11} for elliptical cylinder reflector antenna with different values of b (shorter radius).

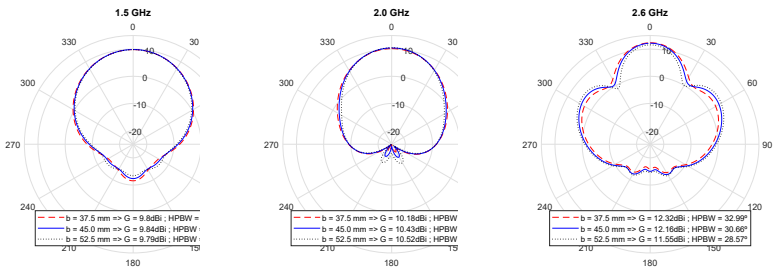

Figure 3.12: Radiation pattern for elliptical cylinder reflector antenna with different values of b (shorter radius).

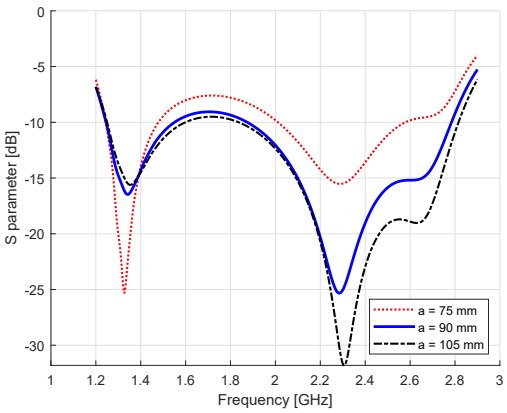

Figure 3.13: S_{11} for elliptical cylinder reflector antenna with different values of a (larger radius).

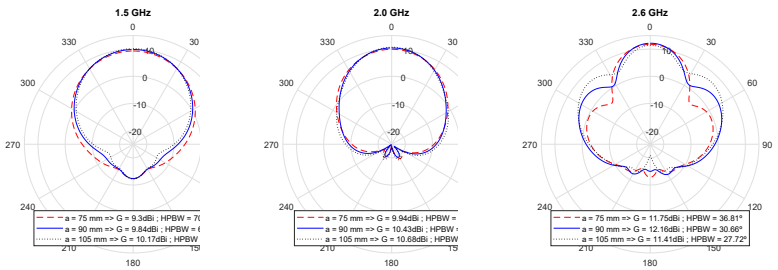

Figure 3.14: Radiation pattern for elliptical cylinder reflector antenna with different values of a (larger radius).

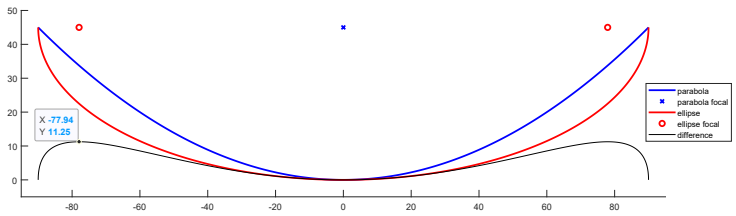

Figure 3.15: Comparison between parabola and ellipse shapes. Both profiles are shown together with their focal points and the computed difference between both shapes.

contributing to an extended focal area where the feed is placed and more homogenously illuminated, and hence a slightly better matching obtained with this elliptical reflector than with the parabolic one.

Figure 3.15 shows a comparison for both profiles. The parabola and the ellipse profiles are presented with their focal points and the vertical difference between both shapes. The maximum value for the difference is 11.25 mm, and it is located 77.94 mm away from the center, what is the same as the ellipse focal points. Being in that area 11.25 mm ($0.1\lambda_{@2.7GHz}$) further than the parabola from the aperture plane explains two different items. From the matching point of view, it explains less interaction between feed and reflector and hence better return losses values. From the radiation point of view, broader and more open reflector explains wider values for the highest frequencies obtaining more lateral suppression meaning less lobes magnitude, and consequently a more stable radiation pattern in broadband with the ellipse than with the parabola profile.

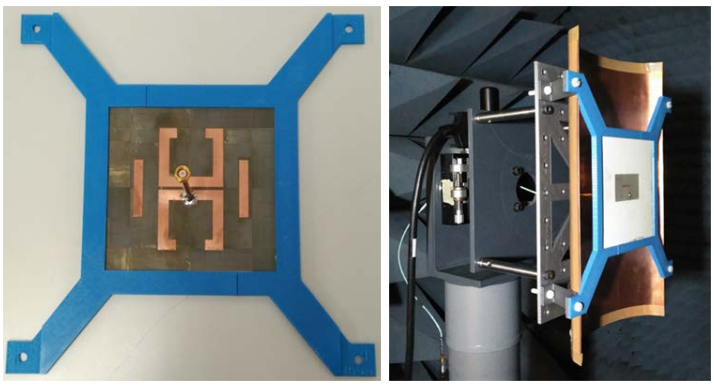

Figure 3.16: Manufactured Vertical Polarized Element with 3D printed profile, to perform the elliptical ground plane with copper metal sheet.

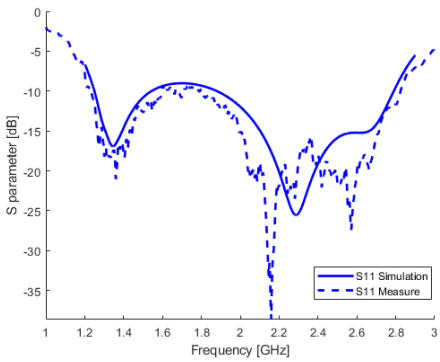

Figure 3.17: S11 for vertically polarized element with elliptical ground plane.

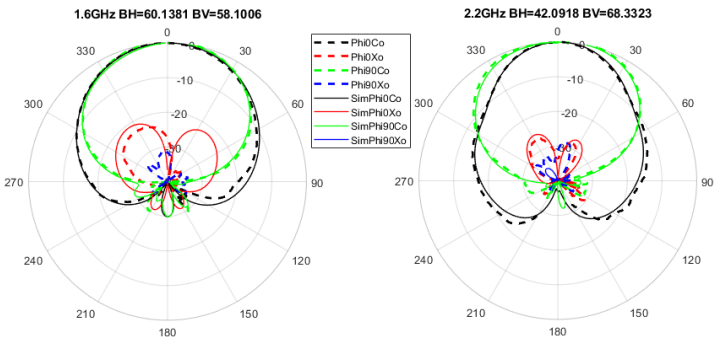

Figure 3.18: Measured radiation for vertically polarized element with elliptical ground.

3.3 Study of Different Reflector Shapes in a Dual Polarization Scenario

Dual polarized element in this section is an extension of the previous one based on dipoles, with a dual dipole architecture on each substrate side, rotated to achieve $\pm 45^{\circ}$ of polarization. The dual polarized element is presented in Chapter 2.

Figures 3.19 and 3.20 shows the characteristics in free space when no reflector is used. In this case the radiation pattern is not equivalent to an omnidirectional dipole, mainly due to two reasons, firstly because the dipoles are now rotated to get the slant polarization, but secondly, due to the interactions between the two polarization elements and the architecture itself explained in previous chapter, which makes a radiation pattern with the energy more concentrated. The figure 3.20 shows the return losses of the free space element, in which a mismatching can be observed specially in low frequency. This is not a problem because the interaction with the reflector will be used to modify the S parameter in an enhanced way.

3.3.1 Flat Ground Plane

The dual polarized element is a more compact design with the parasitic elements embedded inside. It prevents lobulation for high frequency

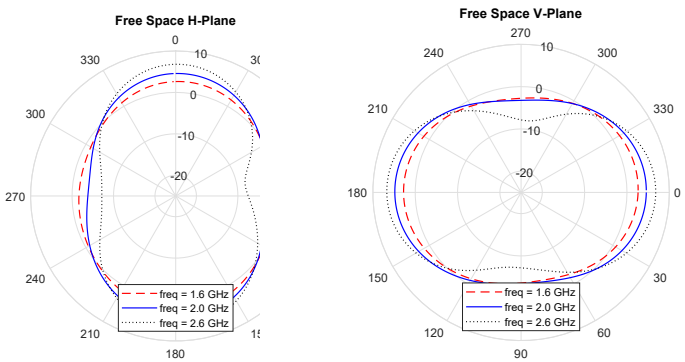

Figure 3.19: Horizontal and vertical radiation pattern for the dual-polarized element in free space.

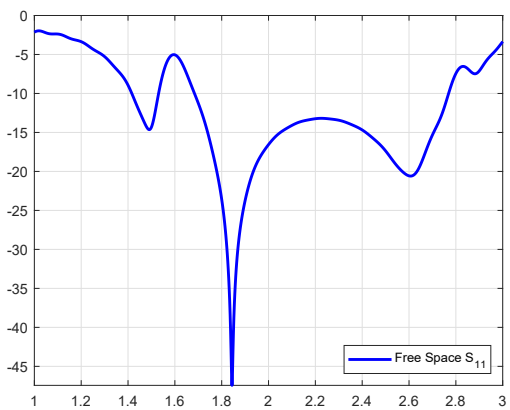

Figure 3.20: S_{11} Parameter for the dual-polarized element in free space.

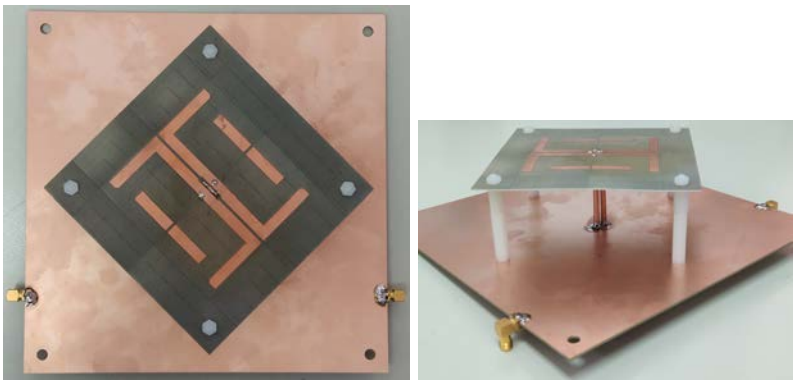

Figure 3.21: Dual Polarized Antenna with flat reflector.

and makes radiation pattern more compact when using a flat ground plane than previous single polarized element.

Figure 3.21 shows the dual polarization element with a flat ground plane in 0.3λ distance. Figure 3.22 shows the S parameter of the prototype for the presented antenna. The simulated and measured data is presented, with good matching of $S_{11} < -14dB$. The radiation pattern can be seen in figure 3.23. Both horizontal and vertical planes are presented for copolar and crosspolar polarization ($\pm 45°$). The matching between the simulation and measurement is really good. The horizontal half-power beamwidth is very stable for most of the band with values of $66°$ but wider values are found for higher frequencies.

A parametric study of the ground plane distance is presented in figure 3.24 for return losses and 3.25 for radiation pattern. The presented study can be seen for distances 30, 37.5, 45 and 52.5 mm, which correspond to $0.2\lambda_c$, $0.25\lambda_c$, $0.3\lambda_c$ and $0.35\lambda_c$ at central frequency. For the return losses, larger values of H as 52.5mm shows a mismatching for higher frequency, while lower values as 30mm is very near increasing the perturbation and obtaining worse return losses for the whole band. On the other hand, height values as 37.5 and 45 mm are below -10 dB in the complete frequency band, while 45mm was selected as the best in Chapter 2 to get -15dB with a matching network, the height value of 37.5mm is slightly not as optimal but it is also good enough in S parameter result to try a matching network as long as the radiation pattern is worthy.

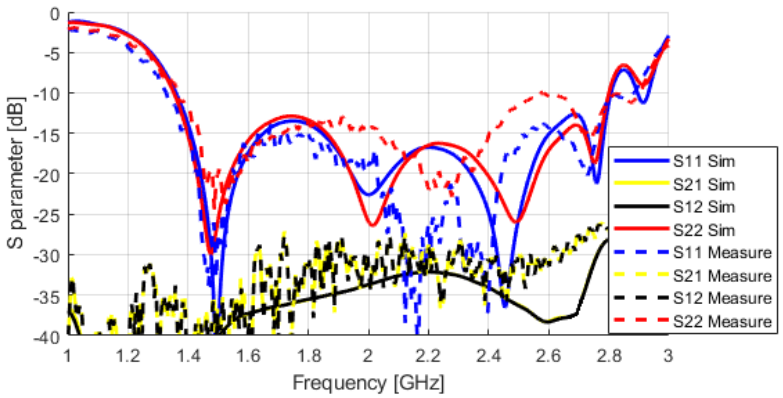

Figure 3.22: S parameters of dual polarized antenna with flat reflector at H=45mm. Simulated in continuous line and measured in dash line.

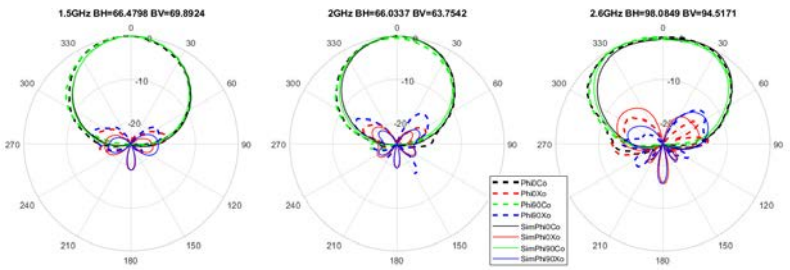

Figure 3.23: Simulated and measured radiation pattern for dual polarized antenna with flat reflector at H=45mm.

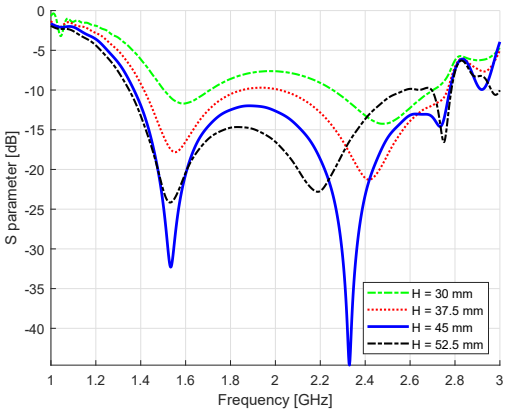

Figure 3.24: S_{11} for flat reflector dual-polarized antenna with different values of height.

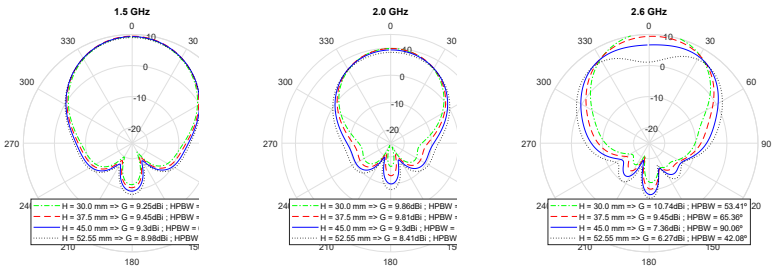

Figure 3.25: Radiation pattern for flat reflector dual-polarized antenna with different values of height.

Regarding the radiation pattern seen in figure 3.25, generally lower values of beamwidth are found for lower heights, except in the high frequency with larger value of height that leads to lobulation. While $H = 45mm$ obtain values from 63° to 90° of beamwidth and a decrease with frequency in the realized gain from 9.3 to 7.3 dBi, the parameter $H = 37.5mm$ leads to more stable values in the radiation pattern with beamwidth from 57° to 65° ($61° \pm 4$) and realized gain 9.4 to 9.8 dBi ($9.6dBi \pm 0.2$). Those convenient results are now stable in frequency and within the requirements, which is a good improvement in the design.

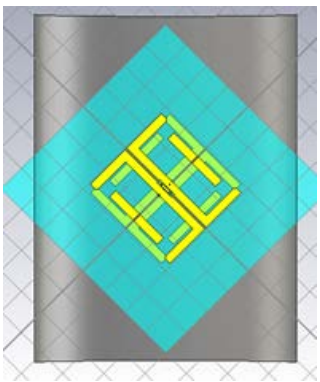

Figure 3.26: Elliptical Cylinder Reflector with dual-polarized element.

3.3.2 Elliptical Cylinder Reflector

The same previously mentioned dimensions ($a = 90mm, b = 45mm$) are used for the ellipse in this dual-polarized scenario. The elliptical cylinder works fine, as it achieve $S_{11} < -10dB$ in the whole band (Fig. 3.27). It achieves relatively good values (62° to 40° for Horizontal beamwidth), but not completely symmetric, being more notorious for high frequencies (Fig. 3.28). Dipoles arms are not homogenously illuminated, especially taking into account that the vertical plane has not been conformed. That makes evidence how, in the elliptical cylinder, reflector horizontal plane is curved, while vertical is not, versus the rotated dipoles arms at ±45° for achieving the required polarization.

3.3.3 Ellipsoid Reflector

The ellipsoid is the 3D shape made by the revolution of the ellipse curve. The ellipse is rotated along its radiation axis to produce an ellipsoid reflector, meaning that the spacing to the element is still 0.3λ as the shorter radius, and 0.6λ for large one ($a = 90mm, b = 45mm$).

With this configuration the matching is similar to the previous ones. The S-parameters do not significantly vary but achieve better values for the whole band. Now due to its shape, the reflector behaves in the same

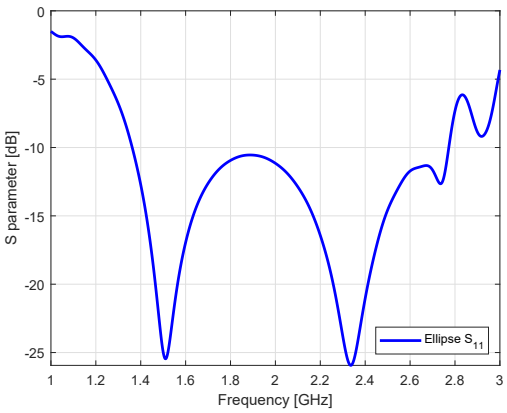

Figure 3.27: S_{11} for for elliptical cylinder reflector dual-polarized antenna.

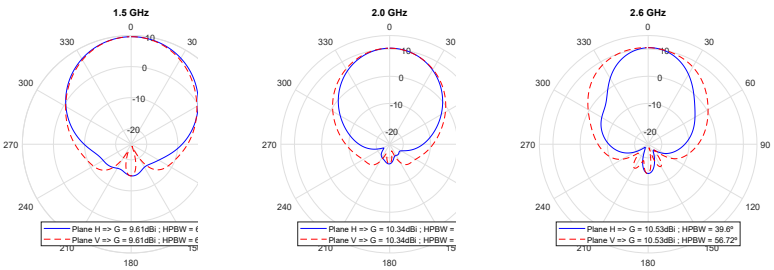

Figure 3.28: Radiation pattern for elliptical cylinder reflector dual-polarized antenna.

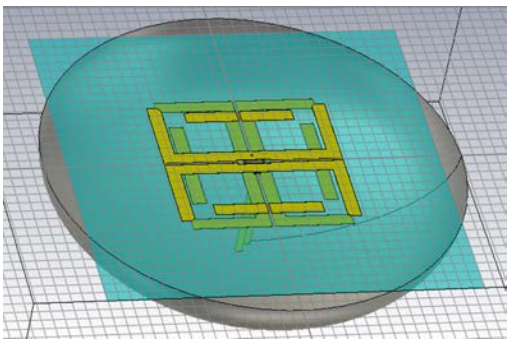

Figure 3.29: Ellipsoid reflector with dual-polarized element.

way for both polarizations and planes, obtaining value of 66° to 43° of beamwidth.

As in an ellipse, with an ellipsoid the parametric study can be developed for two values, the larger radius (a) and the shorter radius (b), both of them are shown below with the consequence of moving the focal points or redimensioning the focal circle in the same aperture plane.

The shortest radius (b) controls the distance behind the reflector, similarly to the height. The values for this study have been set to 37.5, 45 and 52.5 mm ($0.25\lambda_c$, $0.3\lambda_c$ and $0.35\lambda_c$). Figure 3.30 shows the S parameter for those cases. In the same way as for the previous shapes, the closeness of the reflector controls the mutual effects between feed and metal reflector, being closer leading to more perturbation and worse return losses, whereas larger values lead to few perturbation and more similarity to the original free space results which has the original missmatching at low frequency. Figure 3.31 shows the horizontal radiation pattern, not very significant differences are obtained in this parameter sweep because the reflector aperture remains constantly the same. In general terms, the beamwidth reduces with frequency from 65° to 43° and similar gain values regardless the radius b.

Larger radius (a) controls the lateral distance to the reflector, what is related to the aperture area. The values for this study have been chosen as 75, 90 and 105 mm ($0.5\lambda_c$, $0.6\lambda_c$ and $0.7\lambda_c$). The S parameter results are shown in figure 3.32. As previously explained, larger values

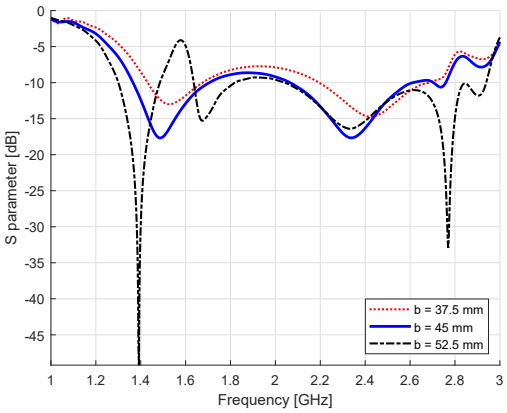

Figure 3.30: S_{11} for ellipsoid reflector dual-polarized antenna with different values of b (shorter radius).

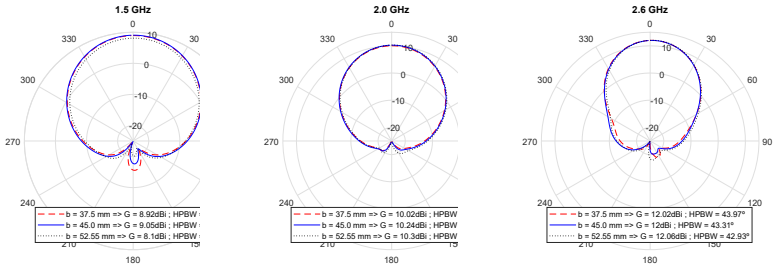

Figure 3.31: Radiation pattern for ellipsoid reflector dual-polarized antenna with different values of b (shorter radius).

makes less perturbation with acceptable results by increasing the size, while the lower value makes a more significant perturbation with worse return losses. Figure 3.33 shows the radiation pattern. As before, the beamwidth reduces with frequency, but now it is also affected with the aperture area, meaning that larger values of a leads to larger aperture areas and narrower beamwidth, affecting at the same time to the gain results.

3.4 Conclusions

Due to the characteristic of near field reflectors, it has been exposed the influence of the shape both in the radiation pattern and the matching.

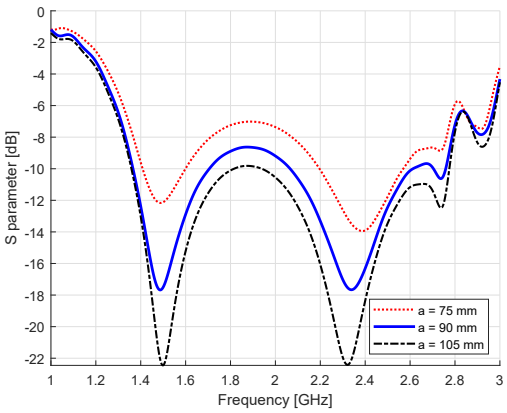

Figure 3.32: S_{11} for ellipsoid reflector dual-polarized antenna with different values of a (larger radius).

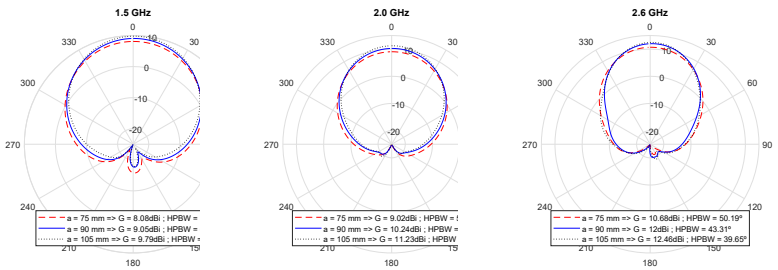

Figure 3.33: Radiation pattern for ellipsoid reflector dual-polarized antenna with different values of a (larger radius).

For that reason, classical analysis method for far field reflectors can not be used, and hence full-wave simulator is necessary.

Different reflector shapes have been tested with single and dual polarization very broadband elements. It has been shown that the choice of focal reflectors (elliptical cylinder and ellipsoids) improves the performance with better matching and stable radiation pattern.

As presented feeders are electrically large in this near field reflector scenario, it makes necessary to illuminate them with the reflector shape that achieves equal power along the element points.

Presented single polarization element lobulates at high frequency due to its characteristics, making necessary to use a conformal shape as elliptical to have similar behaviour in the wide frequency band. Meaning that simple flat reflector is unusable due to differences in beamwidth through frequency and lobulation. In general, this single polarized element makes difficult to achieve the requirements, because it extends the bandwidth with external parasitics that produce multilobe in the highest frequencies. The conclusion with the separation is similar regardless the reflector shape, being closer reflectors cause of perturbation and bad behaviour in return losses, whereas further reflector tends to better return losses with narrower beamwidth and more important lobes.

On the other hand, dual polarization element is a compact design that prevent lobulation, making possible to use and fabricate a flat reflector with good performance. Furthermore, as the element includes two pairs of dipoles placed in perpendicular polarizations, the cylinder reflectors presented previously do not achieve the best radiation performance. Consequently, dual polarization elements require to use a reflector shape which is symmetrical along radiation axis to provide same distance and power to feeder dipole arms. It can be a flat plane or a revolution shaped reflector.

According to the results and coherently with previously exposed, the key of this near field reflector search is to achieve the trade off in which the reflector is spaced the specific distance in which the perturbation is positively affecting being the return losses good enough to be worked with, and the aperture area is not too big that the beamwidth is narrower

than needed, obtaining at the end a well matched antenna with stable beamwidth values along the frequency band.

Tables 3.2 and 3.3 show the different shapes results summary to observe the differences and the achieved improvement.

Table 3.2: Results Comparison with Different Reflector Shapes for Single-Polarized Antenna

Reflector Case	Horizontal HPBW [deg]	Gain [dBi]
Flat Ground Plane	80.7 ± 31.7	7.8 ± 0.7
Parabolic Cylinder	49.3 ± 15.9	10.9 ± 1.6
Elliptical Cylinder	47.0 ± 16.2	11 ± 1.2

Table 3.3: Results Comparison with Different Reflector Shapes for Dual-Polarized Antenna

Reflector Case	Horizontal HPBW [deg]	Gain [dBi]
Chapter 2 Flat Ground Plane h=45mm	76.3 ± 13.7	8.3 ± 1
Flat Ground Plane h=37.5mm	**61 ± 4**	**9.6 ± 0.2**
Elliptical Cylinder	51 ± 11.4	10 ± 0.5
Ellipsoid Reflector	54.5 ± 11.2	10 ± 1

3.5 References

[1] S. Martin-Anton, P. Fernandez-Martinez, and D. Segovia-Vargas, "Effect of different reflector shapes on sub 6-ghz 5G dipole-based antennas," in *Proc. IEEE Int. Symp. Antennas and Propagation and USNC-URSI Radio Science Meeting. (APS Montreal Canada)*, 2020.

[2] S. Martin-Anton and D. Segovia-Vargas, "Broadband antenna design for new mobile communication systems," in *12th European Conference on Antennas and Propagation (EuCAP London)*, 2018, pp. 1–5.

[3] C. A. Balanis, *Antenna Theory: Analysis and Design.* John Wiley & Sons, 2005.

[4] P. Kildal, *Foundations of Antenna Engineering: A Unified Approach for Line-of-Sight and Multipath.* Artech House Publishers, 2015.

[5] A. Cardama Aznar, L. J. Roca, J. M. R. Casals, J. R. Robert, S. B. Boris, and M. F. Bataller, *Antenas.* Edicions UPC, 1998.

[6] G. V. Trentini, "Partially reflecting sheet arrays," *IRE Transactions on Antennas and Propagation*, vol. 4, no. 4, pp. 666–671, 1956.

[7] M. Li, Q. L. Li, B. Wang, C. F. Zhou, and S. W. Cheung, "A low-profile dual-polarized dipole antenna using wideband amc reflector," *IEEE Transactions on Antennas and Propagation*, vol. 66, no. 5, pp. 2610–2615, 2018.

[8] Q. Li, S. W. Cheung, and C. Zhou, "A low-profile dual-polarized patch antenna with stable radiation pattern using ground-slot groups and metallic ground wall," *IEEE Transactions on Antennas and Propagation*, vol. 65, no. 10, pp. 5061–5068, 2017.

[9] Y. Cui, R. Li, and H. Fu, "A broadband dual-polarized planar antenna for 2g/3G/LTE base stations," *IEEE Transactions on Antennas and Propagation*, vol. 62, no. 9, pp. 4836–4840, 2014.

[10] Z. Yang, Y. Cui, X. Mo, and R. Li, "A wideband crossed-dipole antenna for LTE700/GSM850/GSM900 Base stations," in *Proc. IEEE-APS Topical Conf. Antennas and Propagation in Wireless Communications (APWC)*, 2019, pp. 030–033.

[11] C. Hsiao and W. Chen, "Broadband dual-polarized base station antenna for LTE/5g c-band applications," in *Proc. Cross Strait Quad-Regional Radio Science and Wireless Technology Conf. (CSQRWC)*, 2018, pp. 1–3.

[12] J. Y. Yin and L. Zhang, "Design of a dual-polarized magnetoelectric dipole antenna with gain improvement at low elevation angle for a base station," *IEEE Antennas and Wireless Propagation Letters*, vol. 19, no. 5, pp. 756–760, 2020.

[13] and Yejun He and Yadong Yue, "A novel broadband dual-polarized dipole antenna element for 2g/3G/LTE base stations," in *Proc. IEEE Int. Conf. RFID Technology and Applications (RFID-TA)*, 2016, pp. 102–106.

[14] Y. He, W. Tian, and L. Zhang, "A novel dual-broadband dual-polarized electrical downtilt base station antenna for 2g/3G applications," *IEEE Access*, vol. 5, pp. 15 241–15 249, 2017.

[15] J. Rubio, J. Arroyo, and J. Zapata, "Analysis of passive microwave circuits by using a hybrid 2-D and 3-D finite-element mode-matching method," *IEEE Transactions on Microwave Theory and Techniques*, vol. 47, no. 9, pp. 1746–1749, 1999.

[16] P. Robustillo, J. Rubio, J. Zapata, and J. R. Mosig, "Application of modal domain decomposition for fast analysis of lens-based antennas with steering capabilities," in *Proc. of the 10th European Conference on Antennas and Propagation, EuCAP, Davos, Switzerland*, 2016.

[17] R. G. Alcala, J. Rubio, M. A. G. de Aza, J. Garcia, J. M. G. P. Robustillo, and J. Zapata, "El metodo de elementos finitos con segmentacion modal (fem-ms) aplicado al diseno de antenas," in *URSI 2018 UGR - XXXIII Simposium Nacional de la Unión Científica Internacional de Radio.*, 2018.

[18] L. Wu, R. Li, Y. Qin, and Y. Cui, "Bandwidth-enhanced broadband dual-polarized antennas for 2g/3G/4G and imt services," *IEEE Antennas and Wireless Propagation Letters*, vol. 17, no. 9, pp. 1702–1706, 2018.

[19] H. Sun, C. Ding, B. Jones, and Y. J. Guo, "A wideband base station antenna element with stable radiation pattern and reduced beam squint," *IEEE Access*, vol. 5, pp. 23 022–23 031, 2017.

CHAPTER 4

DUAL BAND INTEGRATION

The present chapter introduces how to deal with integrating two different bands in mobile communications antennas. While in previous chapters the ExtUWB element was presented for the band 1.42 to 2.69 GHz, there is also another band to be covered, from 690 to 960 MHz.

Integrating those two bands in the same space is a key task in mobile communications antennas. On the one hand, it is due to size, space and physical and mechanical reasons for the base stations. But also on the other hand, it is related to economy in the base station market, as providing the two bands with different base station antennas would be a step back, been one base station per band very unprofitable and a misuse of resources.

The beginning of this chapter deals with the design of new element antennas for the lowest band. After the design of the element, the integration with the highest band has to be aboarded. Finally, a dual polarization $\pm 45^{\circ}$ scenario is presented.

Finally, the importance of integrating the previously presented ExtUWB element with different standardized low band commercial elements is addressed. Different shapes are studied and discussed, showing the advantages that the proposed architecture presents.

4.1 Introduction

Classical mobile communication systems are based on the well known 2G/GSM 900 MHz and 1800 MHz bands. In the following years, the 2100 MHz and 2600 MHz bands were introduced to provide spectrum to the incoming technologies, 3G/WCDMA and 4G/LTE. [1]

The inclusion of 4G/LTE also brought a new band in the additional lower frequency, the 800 MHz band, which had been previously used by analog television broadcasting, becoming the so-called "Primer Dividendo Digital" in which television started to use the digital DVB-T system in their lower spectrum, while 4G LTE was seatled in the 800 MHz band for mobile communication. This process started in 2010 and ended in 2015. [2]

Nowadays, the aforementioned bands are included in the same radome (i.e. in the same antenna panel). Inside the mentioned base station the mobile communication bands are usually covered by two broadband radiating elements, one for the low frequency band (790 - 960 MHz) and other for the high frequency band (1710 - 2690 MHz).

With the coming of new 5G technology, new bandwidth extensions have also arrived. In the high frequency band, the working frequency is extended down to the 1500 MHz band. In the low frequency band it is extended down to the 700 MHz band to achieve higher and deeper coverage, producing the "Segundo Dividendo Digital" [3].

The new low frequency band should now be covered by an element working in the bandwidth 690 to 960 MHz, that has to be integrated with the element presented previously for 1427-2690 MHz. The integration of both elements is the goal of the chapter.

From the commercial point of view it is necessary to obtain an integrated antenna covering both new bands, without modifing the requirements and specifically without increasing the overall size. For that reason, separated base station arrays for each band would be a mistake in terms of commercial, deployment, visual impact and spacial use.

While the new frequency band extended in the 690-960 MHz band is

not such a huge challenge in terms of relative bandwidth, it is necessary to design the element in this band to achieve the mentioned integration.

In this chapter, the low band frequency is covered by a new own-design element integrated with the ExtUWB element previously presented, while the chapter ends with the integration of ExtUWB element with different architectures and shapes low band elements commercially developed provided by Telnet company.

Regarding the integration with commercial elements, the company provided elements are subject to legal restrictions, for that reason in this chapter similar or standardized elements used in the industry will be shown, while specific architectures or company results with restrictions are not specifically provided.

During the last years, different proposals have been developed for integrating both bands in base stations. Some of them can be found for the classical bands interleaving low and high frequency band elements as in [4]. Otherwise, publications as [5] present multiband elements in which different bands are cover with a complex element that can make difficult the overall array structure in the different bands. In [6] an integration of GSM elements with 3.5GHz band elements is presented, although their integration is easier to develop due to their inherent smaller size. Although different integration for covering both mobile phone bands have been developed in the literature and in the market, the increment of the bandwidth has not been achieved which makes this a novel challenge to deal with.

4.2 Single Polarized First Integration Approach

This section is based on the work previously published in [7]. The first approach is a single polarized design relying on a scaled version of the presented in Chapter 2, in which dimensions are modified to make the antenna work in the lower band.

As it is presented in the next subsections, this element is not the optimal solution but a good first approach in the integration path. According to the studies developed in previous chapters, a single polarization element would need a reflector ground plane shaped into a larger elliptical

cylinder and, at the end, with an incompatibility in the integration point of view due to different reflector size needs. Furthermore, the whole integration of both band in the single polarized approach is too big, which demonstrates the needs of dual polarized compact designs.

4.2.1 Lower Band Element

Following the same procedure presented in Section 2.2, a broadband element for working in lower band of frequencies (690-960 MHz) has been designed.

In that way, the element shown in figure 4.1 is obtained, using a dual dipole element with side parasitic elements.

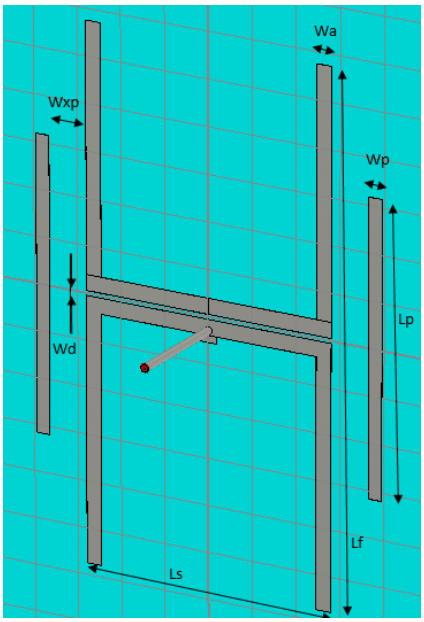

Figure 4.1: Single Polarized Antenna element for lower band.

The different values of dimensions for this antenna element is shown in table 4.1. As can be seen, most parameters have been enlarged in comparison with the original design to cover the low band frequency, particularly, the dipole length Lf is now set to 230mm.

Table 4.1: Values for the Parameters of the Single Polarized Antenna for Lower Band Element

Parameter	Value [mm]
Wd	2.1
Ls	112
Lf	230
Wa	6.8
Wxp	17
Wp	6
Lp	127
Ln	66
La	13.2
Wl	1.7

For this element the reflection coefficient is simulated in figure 4.2, in which the required matching of -14 dB can be observed for frequencies from 557 to 977 MHz. As previously explained for this architecture, the element achieves two main resonances, the lowest one at 600 MHz due to the dipole length itself and the highest one at 862 MHz due to the parasitic resonance.

4.2.2 Dual-Broadband Integration

For integrating both elements the idea is to make use of the space in the lower band element to place the higher frequency elements there, placing two high frequency elements on the lower frequency one. Those embedded elements are shown in figure 4.3.

To optimize the integration, minimizing coupling and achieving

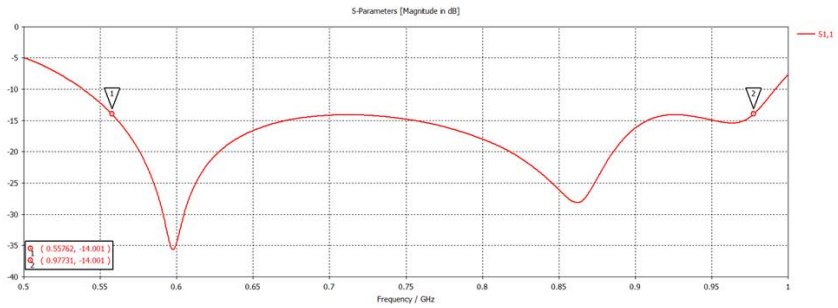

Figure 4.2: Reflection coefficient S11 of the Single Polarized Antenna in lower band.

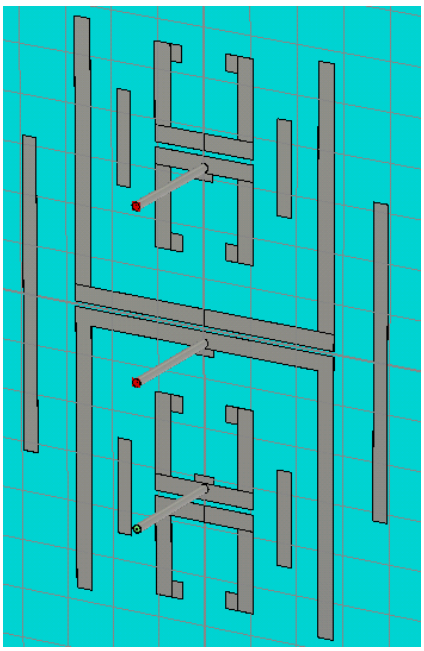

Figure 4.3: Integration of both single polarized elements.

matching, a parametric simulation was developed, where the position of the small element was selected to be 70 mm from center to center. In figures 4.4 and 4.5 the S parameters for different positions of the higher frequency band element can be seen, so 70 mm was selected as a good tradeoff.

Figure 4.4 shows the parameter S11 of the integration, which is the port for the lower frequency band. A matching of -14dB was obtained for the bandwidth 568-969 MHz.

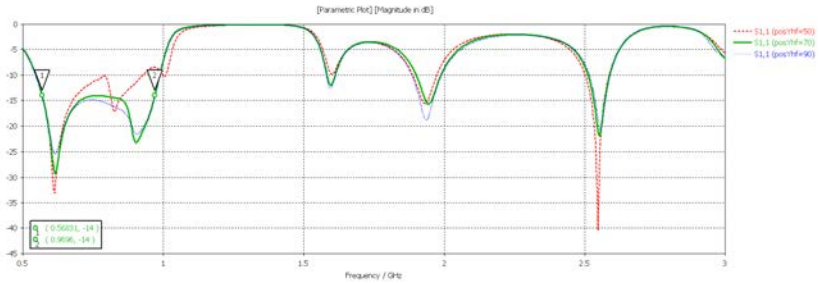

Figure 4.4: S11 parameter of the integrated single polarized antenna. Corresponding to lower band element reflection coefficient.

S22 is the reflection coefficient for the higher frequency port, which is shown in figure 4.5. This port has a good matching for the frequencies from around 1.43 to 2.82 GHz.

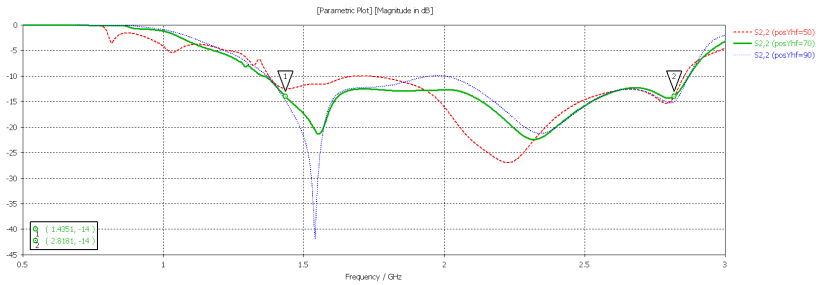

Figure 4.5: S22 parameter of the integrated single polarized antenna. Corresponding to upper band element reflection coefficient.

Furthermore, the parameters S12 and S21 are obtained, these parameters correspond to the isolation between both ports. As can be seen in figure 4.6, the isolation is not good enough, so a better optimization should be undertaken, to achieve at least 20 dB of interband isolation.

The prototype has been manufactured, as can be seen in figure 4.7, where the two high frequency band elements are integrated in the same plane with the low frequency band element. They are printed in the

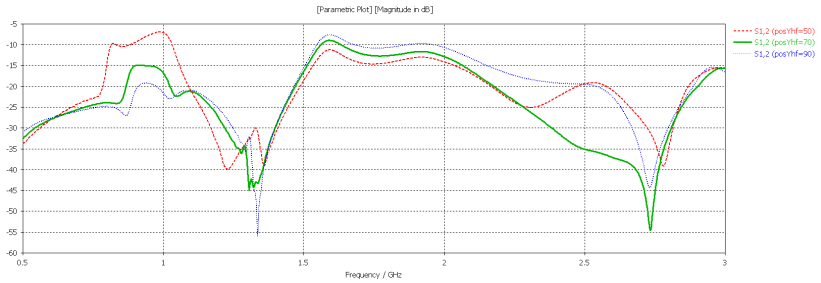

Figure 4.6: S12 parameter of the integrated single polarized antenna. Corresponding to the isolation between both ports.

same substrate and the coaxial cables and connector are presented, in the same procedure previously shown in Chapter 2.

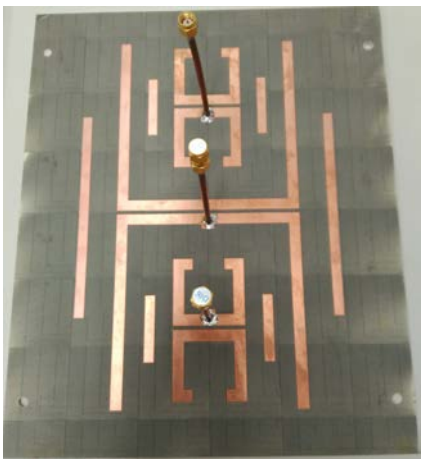

Figure 4.7: Single Polarized Dual Band Integration Antenna. Manufactured Picture.

In a free space scenario, figure 4.8 presents the return losses measurement for both bands in dashed lines, for comparing them with the simulated values in continuous lines. As can be observed, the measured results obtain good values and they are very similar to the expected in simulations.

This prototype has some drawbacks although it is a first approach to the integration solution. Firstly, as exposed, it is a vertical single-

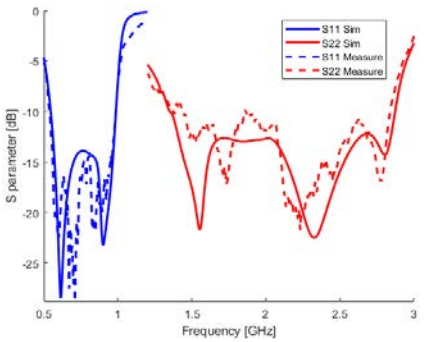

Figure 4.8: Single Polarized Dual Band Integration Antenna. S Parameters in Free Space. Continuous lines for simulation and Dashed lines for measurement.

polarized antenna, while the final objective needs to be dual polarized. Secondly, the overall size of the integration, and the elements themselves, is larger than expected, meaning that in an array configuration the elements will be very far apart, so hence, the prototype can not evolve into a correct array structure.

For the free space scenario, the measured matching is good, however, for obtaining the required beamwidth, the low band element would need a elliptical cylinder reflector in a different size than the designed for high frequency elements. If both reflectors would be placed in the prototype, they would be interacting and perturbing each other and both band elements behaviour, furthermore their design and manufacture would be impracticable.

4.3 Dual-Polarized Dual-Dipole Low Band Element Integration

Once shown the need of a new element with dual polarization for the low frequency band, in this section an element antenna with dual dipoles is presented. Basically, it is a scaled and modified version of previously presented element in Chapter 2 for ExtUWB with which it is later integrated to achieve the dual band behaviour.

The element for covering the (LBF) Low Band Frequencies (690 -

960 MHz) is presented in figure 4.9. It is based on dual-dipole as the ExtUWB element presented in Chapter 2, but now with different dimensions to fulfill the different band. The element has two pairs of dipoles fed by coplanar strip obtaining dual polarization. This element presents the two resonances associated to the length of the dipole and the other associated to the extended dipole coupled to the backside dipole.

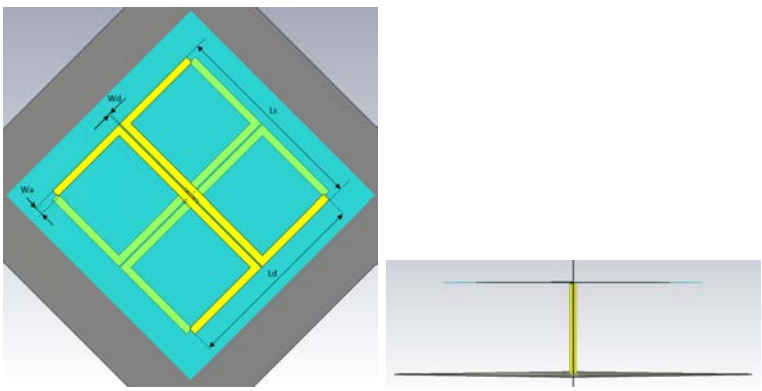

Figure 4.9: Dual Polarized Low Band Element. Front and Side view.

The length of the dipole arms is Ld = 189 mm, while the line width is Wa = 7.9 mm. The length of the coplanar strip is Ls = 201 mm, giving the dipoles the required feed, and obtaining a shape of a rotated square to the element. The element is designed over a flat ground plane spaced a distance of 130 mm, corresponding to $0.35\lambda_c$ at central frequency (825 MHz). The parameter values are summarized in the table 4.2.

The results for the element alone are shown in next figures. Figure 4.10 shows the return losses for the LBF element, the two resonances can be seen at a matching below -10 dB between 0.51 and 0.96 GHz, while the required bandwidth is 690-960 MHz. Due to the lowest resonance and the architecture restriction it is enhanced even more in the lowest part, which can be even a good characteristic for future extension of the band in next generations. The radiation pattern is shown in figure 4.11, the horizontal beamwidth is 70.7 ± 0.2 degrees in the required band, with an gain of 8.5 dBi. Those are good results for this design.

Table 4.2: Values for the Parameters of the Dual Polarized Antenna for Lower Band Element

Parameter	Value [mm]
Wd	1.2
Ld	189
Ls	201
Wa	7.9
H_G	130

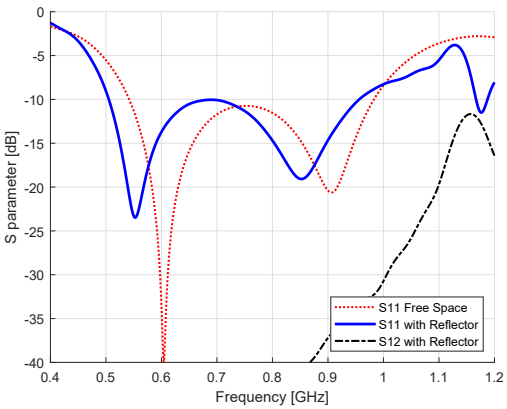

Figure 4.10: S parameter for the low band frequency dual polarized element.

4.3.1 Dual Polarized Elements Integration

The benefit of using this fully planar architecture of dual-dipoles is taking advantage of the shape of the square and the space between the metal shaped into squares, to use them as the location to place the high band frequency element (ExtUWB), embedded into the low band frequency element.

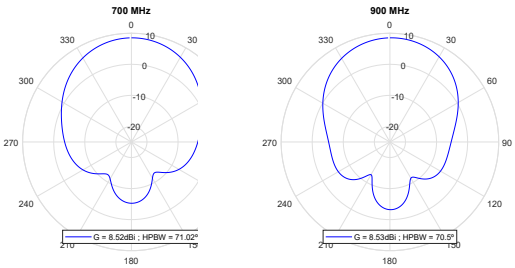

Figure 4.11: Radiation pattern for the low band frequency dual polarized element.

Firstly, the main idea is to use the upper and bottom squares to place two elements in the vertical axis, the direction for a later vertical array. Due to physical reasons, and the actual sizes of the elements, the distance between centers from low band element to high band element has been chosen to be 70 mm, as the limits only allow a couple of millimiters of tolerance. Finally, the physical restrictions are the reason that constrain and determine the distance between element centers.

Figure 4.12 shows how to make use of the square shapes to embed and place one element into the other, but placing them in the same plane lead to a bad performance regarding the S parameters. As can be seen in figure 4.13 the element matching is unacceptable, firstly displacing the low band frequency toward lower frequencies, and mismatching the high frequency band. Moreover, the radiation pattern for this first case is shown in figure 4.14.

The physical height distance from the elements to the ground plane has to be different for high and low band elements, as it would be different in terms of lambda. For that reason, ExtUWB should be H = 37.5 mm $0.3\lambda@2GHz$ high over the ground, while the low band element H = 130 mm $0.25\lambda@825MHz$. In other words, the distance for the ground plane to the elements should be chosen in terms electrical distance, ie. in term of lambda per each band, consequently, the different band elements have to be placed in different planes, as seen in figure 4.15.

Figure 4.16 shows the resulting S parameters which are better than before, with a matching near -10 dB for each band. Radiation pattern is shown in figure 4.17. Low band element presents a gain of 7.5 dBi and

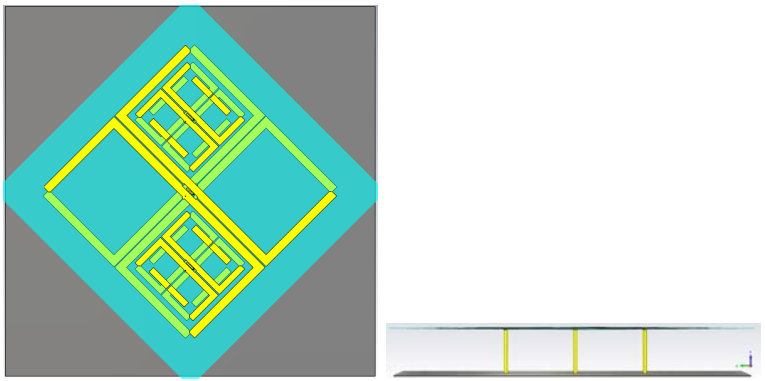

Figure 4.12: Dual-Band Dual-Polarized Integration. Front and Side view. Both band elements placed at same height.

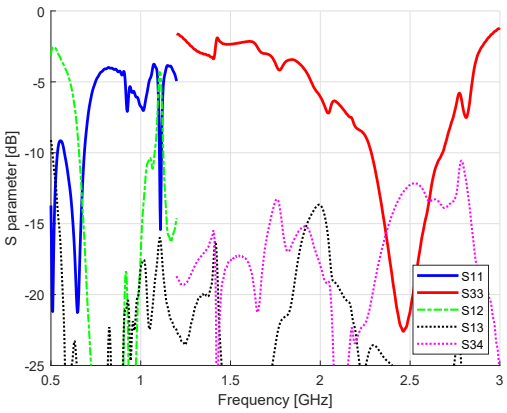

Figure 4.13: S parameters for Dual-Band Dual-Polarized Integration. Both band elements placed at same height, destroying the elements matching.

a horizontal beamwidth of 75.8 degrees. High band element presents a gain of 6.4 ± 1.6 dBi and a horizontal beamwidth of 61 ± 15 degrees.

For symmetry reasons, and to make a good use of the overall space, it was decided to place four high frequency elements, one in each square, instead of placing only two in the vertical axis. With this, it is expected to enhance the radiation pattern, trying to avoid some asymmetries, and increase the radiating elements having more flexibility for future designs.

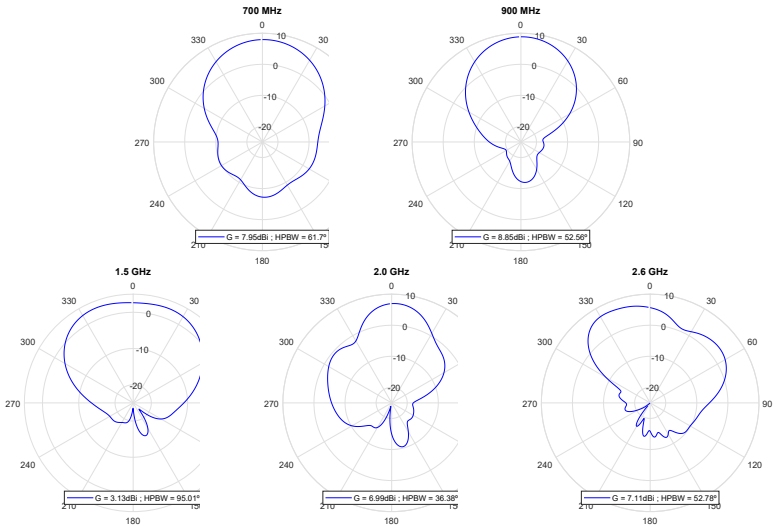

Figure 4.14: Radiation pattern for Dual-Band Dual-Polarized Integration. Both band elements placed at same height.

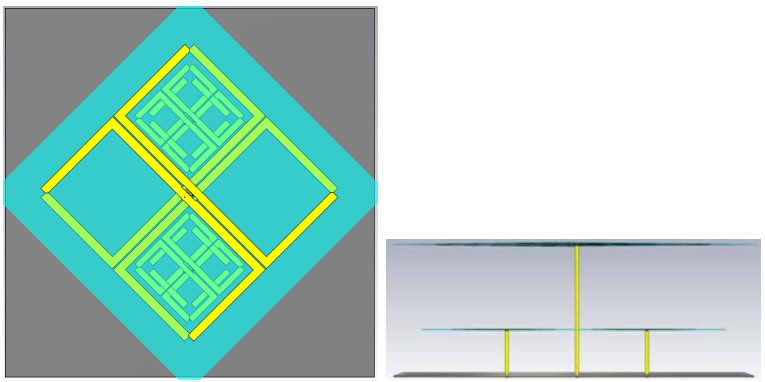

Figure 4.15: Dual-Band Dual-Polarized Integration. Front and Side view. Each band elements placed at different height.

Placing the low band elements at higher height means that there is a substrate on the top of the antenna system. The top substrate can produce some occlusion and shadow for the high band elements placed in a lower level. To solve that situation, the low band elements placed on top can be cut out from the substrate as much as possible, removing

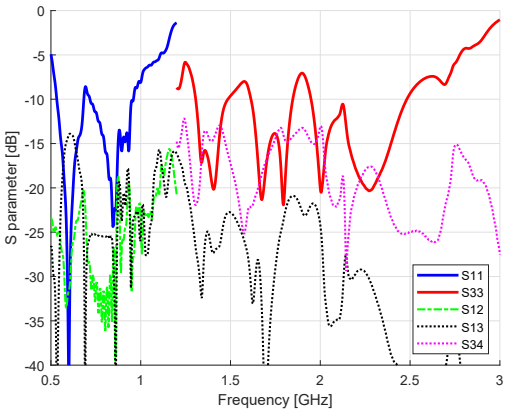

Figure 4.16: S parameters for Dual-Band Dual-Polarized Integration. Each band elements placed at different height.

all the excess of substrate where it is not necessary. The element is now printed in a substrate square of 210 mm side in which four smaller squares (windows) of 74.1 mm are milled out. The lines that conforms the low band element are now printed in a substrate which is 9.5 mm wider than the lines, that margin ensures that the general behaviour of the antenna is maintained without performance modifications. By removing all the substrate excess, the top substrate is more transparent and the occlusion for the high band elements is more released.

The architecture with four high band elements and the windows in the upper high band element can be seen in figure 4.18. Figure 4.19 shows the resulting S parameters with a matching near -10 dB for each band. The radiation pattern is shown in figure 4.20. The low band element presents a gain of 7.5 dBi and a horizontal beamwidth of 76.2 ± 2.8 degrees. High band element presents a gain of 7.8 ± 1.0 dBi which is better, with a small increase and more stable values. The horizontal beamwidth is 38.8 ± 3.6 degrees which is more stable than before. Note that, although the horizontal beamwidth value is lower than expected and a bit tilted for one of the elements, this will be compensated with the symmetric element when performing the array, as it will be deeper explain in Chapter 5.

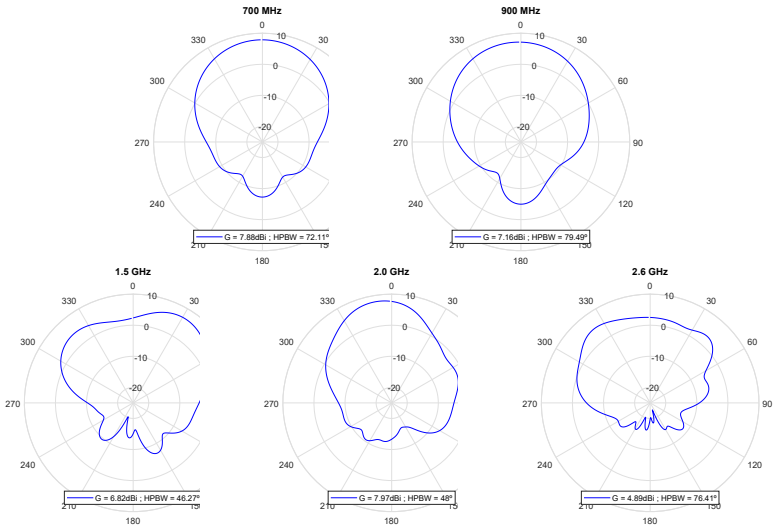

Figure 4.17: Radiation pattern for Dual-Band Dual-Polarized Integration. Each band elements placed at different height.

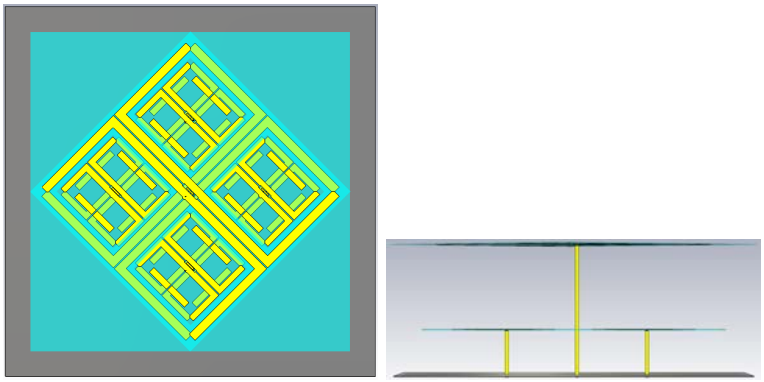

Figure 4.18: Dual-Band Dual-Polarized Integration. Front and Side view. Four high band elements are located in lower substrate, High band element is place in the upper substrate which has been cut out to reduce occlusion.

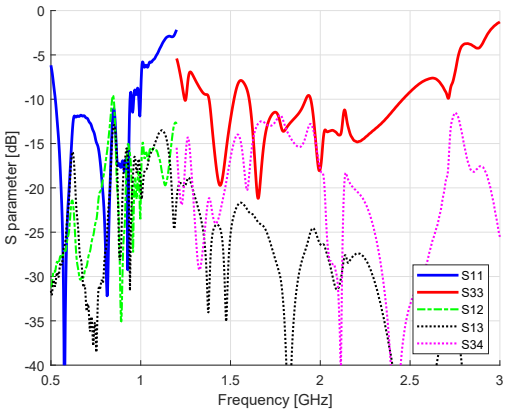

Figure 4.19: S parameters for Dual-Band Dual-Polarized Integration. Four high band elements placed at lower substrate.

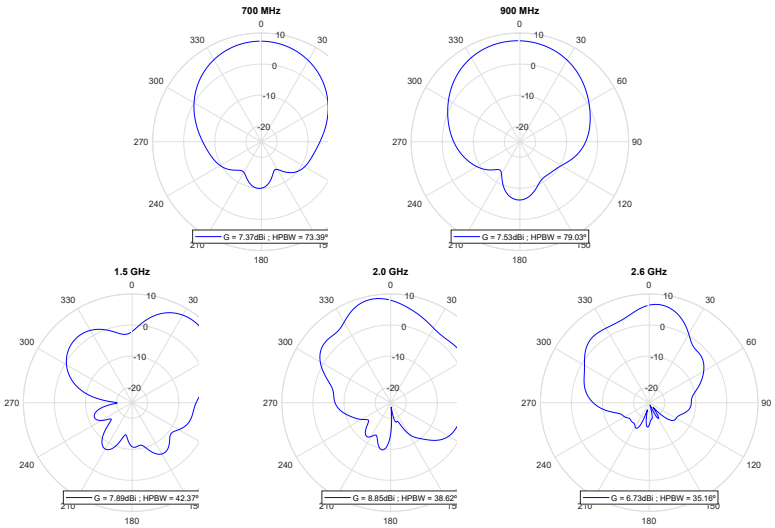

Figure 4.20: Radiation pattern for Dual-Band Dual-Polarized Integration. Four high band elements placed at lower substrate.

4.4 Commercial Elements

In the market there are different architectures for providing the lower band coverage. In this section, two elements of the most standardized

architectures are used for integrating our ExtUWB element into low band frequency commercial elements provided by companies, showing some examples of offering the whole dual band coverage. These elements are under legal rights, so non explicit pictures can be shown, although general and extensively used architectures are used here.

4.4.1 Crossed Dipoles Element

The crossed dipole antenna is generally chosen for the low band due to its simplicity in antenna design. Crossed dipoles are elements with the shape of blades in an old windmill. The basic architecture is made up of two simple dipoles, usually substrate printed, perpendicularly crossed together in order to achieve dual polarization. Dipoles are placed over a parallel ground plane behind which the feeding is provided. [8] [9] [10]

As the ExtUWB element shape is a rotated square piece of PCB, it is easy to assume that the best way of integrating them with the cross shaped low band element is to approximate them and to fit them with the cross 90 degrees angles.

Crossed dipoles can be physically quite narrow, so the element can be closer, but the objective is to get a position in which the coupling between the elements is low enough to be assumed. The distance between ExtUWB element has been set to 130 mm, which means that there is 65 mm between cross dipole element and ExtUWB element centers.

The height of the crossed dipoles on these frequencies is usually larger than the ExtUWB height, which is positive for low coupling, but not too much, meaning that the radiation pattern should not be heavily affected by occlusion.

The architecture of the cross dipoles integrated with two ExtUWB elements can be seem in the figure 4.21.

Figure 4.22 shows the resulting S parameters with a matching near -10 dB for the whole band that could be enhanced with the matching and feeding network. Radiation pattern is shown in figure 4.23. High band element presents a gain of 7.6 ± 0.9 dBi. The horizontal beamwidth is 69.9 ± 7.5 degrees.

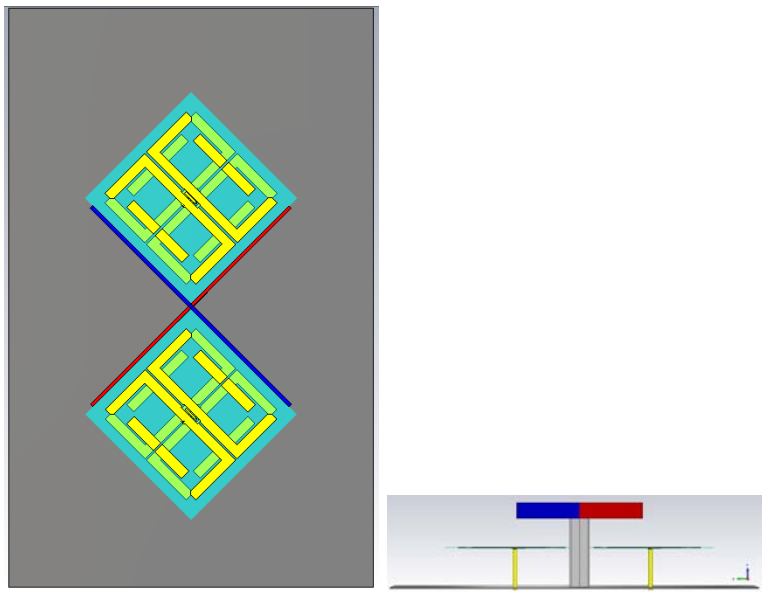

Figure 4.21: Crossed Dipoles Element Integration. Front and Side view.

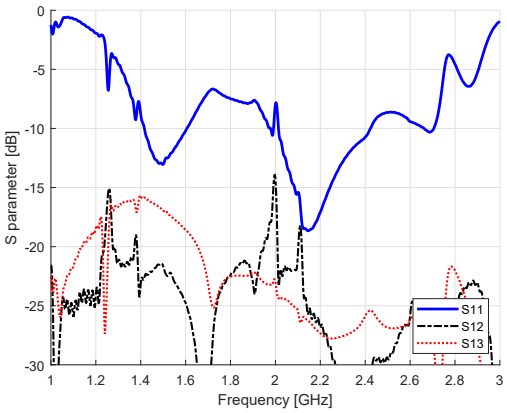

Figure 4.22: S parameters of the ExtUWB element integrated with Crossed Dipoles.

4.4.2 Bowl-Shaped Dipoles Element

This element is an antenna in which dipole arms are placed in a circular or polygonal shape, being the top border of a bowl or container,

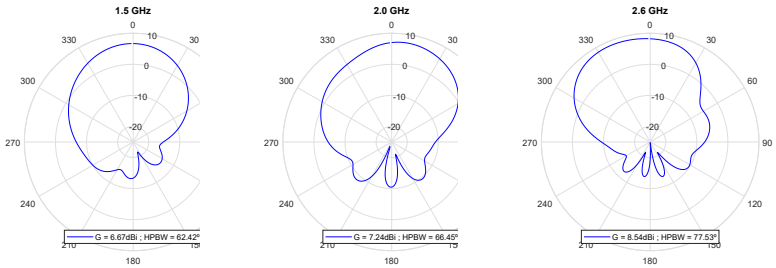

Figure 4.23: Radiation pattern of the ExtUWB element integrated with Crossed Dipoles.

the feeding structure is made of twins lines curved to the ground plane in the shape of a bowl or a vessel. [11] This kind of element is very used for covering low band frequency as it can contain a high band frequency element inside. [4, 12, 13]

As the ExtUWB element behavior has been studied in Chapter 3 for different ground plane shapes as flat reflector and ellipsoidal one. And being the bowl shaped dipoles element something similar to a revolution container as the ellipsoid but with some apertures. It can be expected, that placing the ExtUWB element in the center of the bowl could lead to a blended behavior between the influence of the flat ground plane under the bowl, and the pseudo-ellipsoid made by the bowl element.

As explained before, the lower band element is usually higher than the ExtUWB height, meaning that the high frequency element need to be placed inside the bowl, to place the element with the required height. The size of the bowl determines the space and distance between the elements, being big enough meaning that the coupling values between elements are under control.

The architecture of the bowl-shaped dipoles integrated with ExtUWB elements can be seem in the figure 4.24. One ExtUWB element is embedded in the center of the bowl, while other elements are outside de bowl, placed next to it. Note that the outer elements are placed 37.5 mm over the flat ground plane reflector, while the inner element is affected by the 37.5 mm ground plane and being inside the bowl which is nearer, being consequently an shorter effective distance to the ground plane and and overall different surrounding.

The distance between ExtUWB element has been set to 130 mm, which give a margin for the outer element to not be placed below the bowl arms.

Figure 4.25 shows the resulting S parameters with a matching near -10 dB for the whole band, being the inside element (S11) slightly better than the outer (S33). The radiation pattern is shown in figure 4.26 for the inner element and figure 4.27 for the outer one. The high band element presents a gain of 9.7±0.9 dBi for the inner element and 8.3±1.0 dBi for the outer one. The horizontal beamwidth is 55.4±2.4 degrees for the inner element and 73.2 ± 11.2 degrees for the outer one. Both gain and beamwidth show good results, and although inner elements beam can be a bit narrow and outers one a bit wider, they will compensate with each other when performing the array in Chapter 5.

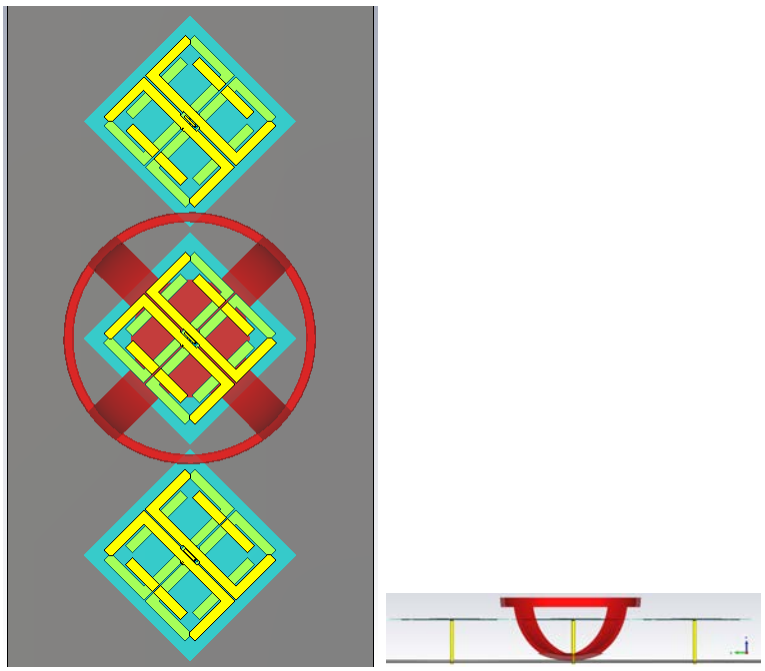

Figure 4.24: Bowl-Shaped Element Integration. Front and Side view.

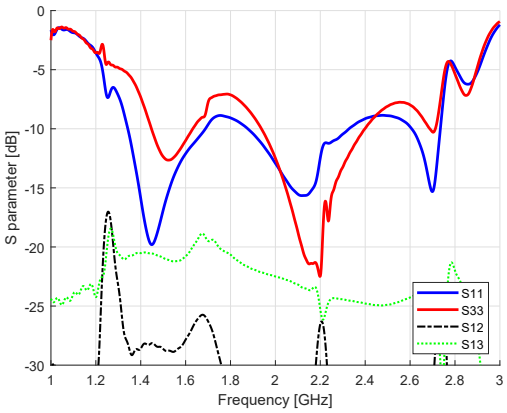

Figure 4.25: S parameters of the ExtUWB element integrated with the Bowl-Shaped element. S11 is the return losses for the element embedded inside the bowl, whereas S33 is for the element placed outside.

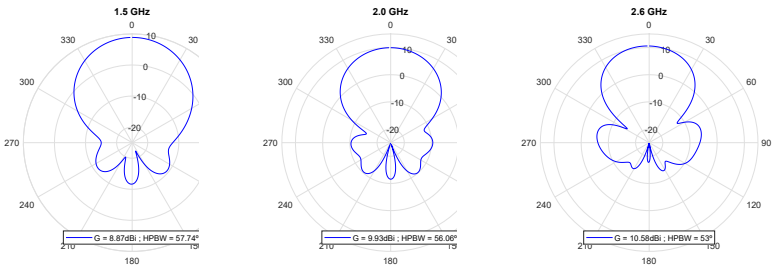

Figure 4.26: Radiation pattern of the ExtUWB element embedded inside the bowl-shaped element.

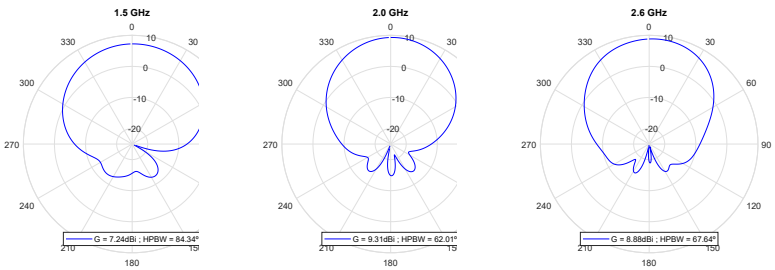

Figure 4.27: Radiation pattern of the ExtUWB element placed outside, next to the bowl-shaped element.

4.5 Literature Elements Integration Comparison

The most used element in mobile communication is usually based on crossed dipoles [14], in order to integrate those elements with each other or with different bands elements, the crossed dipoles are inscribed into a square, with corners in the 45 degrees directions. Moreover, the ExtUWB is inscribed into a 45 degrees rotated square. The fact that the corners are placed in vertical and horizontal direction could be apriori considered as a drawback for disturbing when the elements are approaching, but on the contrary, it is a benefit for integrating with other elements as it is now exposed.

The elements which corners are in the 45 degrees directions and flat in the vertical can be usually placed together in closer distances (d_{scd}) to achieve an array of the same element. While on the other hand, for ExtUWB element with corners in the vertical direction, the distance (d_{sext}) between elements can be limited due to touching corners. See figure 4.28.

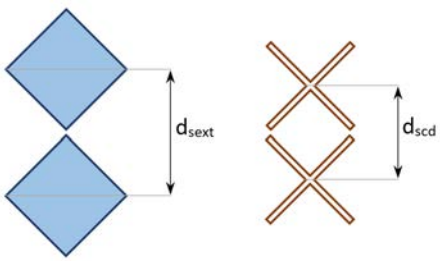

Figure 4.28: Comparison between the minimum element distance in two topologies.

However, in mobile communication the objective is not to achieve simple arrays of antennas with one element but integrating both element architectures to achieve dual band coverage. With this scenario and the requisite of integration, the presented ExtUWB element is more favourable as can be better integrated with low band elements because its limit sides are rotated 45 degrees corresponding with the polarization and hence the shape of the lowest frequency element architectures, as it is shown in figure 4.29.

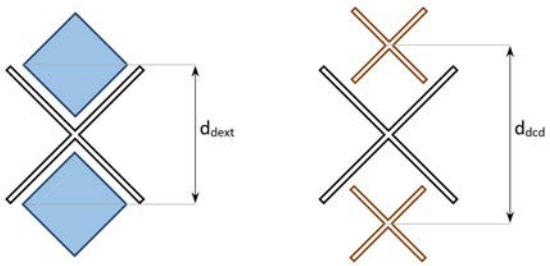

Figure 4.29: Comparison between the minimum element distance that can be achieve in two topologies when they are integrated with a low band element.

Furthermore, the geometrical integration with the new architecture presented in this chapter for the low band frequency is shown in figure 4.30. Left picture shows the fits between square shapes in the LBF element and the ExtUWB element square shapes. Nevertheless, right picture shows how same size cross-dipoles elements would be seen in the same spaces, the dipoles tips would be in contact with each other and out of the space, as the cross-dipoles elements would be larger than the available space.

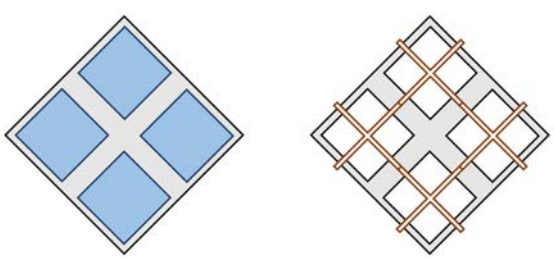

Figure 4.30: Comparison between ExtUWB elements and Cross-Dipole elements integrated in the own-designed low band frequency element. Left picture shows the fitting with square shapes, while right picture evidences the dificulty of using cross-dipole elements in this scenario.

To sum up, for those reasons, the presented ExtUWB element proposes an improvement in terms of integration with the elements used for low band, offering a full dual band coverage with a good element integration.

4.6 Conclusions

It has been shown the need of integrate the antennas for two different mobile communication bands. Firstly, an antenna element has been designed to cover the low frequency band (690 to 960 MHz). At the beginning a single polarized element is shown, to later focus on the dual polarized design.

Once both band elements are designed, some development has been done to integrate both elements and join them to achieve the coverage in both band within the same physical space. In this chapter, the new designed antenna for low frequency band presents some spaces that has been used as an advantage to allocate high frequency band elements. Finally the integrated results are appealing, with good behaviour for both bands.

The presented chapter finished with the importance of integrating the presented ExtUWB element with different elements that cover the low band frequencies. Those elements have different shapes due to the topologies and architectures that can be found in the market.

Although some of the results are not completely optimal, it has to be noticed that they are not the complete results. It will be seen that the elements behaviour have some changes when the complete array is formed in the neighbourhood, and some element misaligments in radiation pattern will be compensated with symmetric element radiation patterns.

To sum up, for those reasons, the presented ExtUWB element proposes an improvement in terms of integration with the elements used for low band, offering a full dual band coverage with a good element integration.

4.7 References

[1] M. Bartolacci, *Advancements and Innovations in Wireless Communications and Network Technologies.* IGI Global, 2012.

[2] J. I. Gallego, M. Fernández-Sande, and N.Limón, *Trends in Radio Research: Diversity, Innovation and Policies.* Cambridge Scholars Publishing, 2018.

[3] "Technical specication group radio access network; nr; user equipment (ue) radio transmission reception; part 1: Range 1 standalone, document 3gpp ts 38.101-3 v15.3.0„" Oct. 2018.

[4] F. Jia, S. Liao, and Q. Xue, "A dual-band dual-polarized antenna array arrangement and its application for base station antennas," *IEEE Antennas and Wireless Propagation Letters*, vol. 19, no. 6, pp. 972–976, 2020.

[5] A. Alieldin, Y. Huang, S. J. Boyes, M. Stanley, S. D. Joseph, Q. Hua, and D. Lei, "A triple-band dual-polarized indoor base station antenna for 2g, 3G, 4G and sub-6 GHz 5g applications," *IEEE Access*, vol. 6, pp. 49 209–49 216, 2018.

[6] Y. Zhu, Y. Chen, and S. Yang, "Integration of 5g rectangular MIMO antenna array and GSM antenna for dual-band base station applications," *IEEE Access*, vol. 8, pp. 63 175–63 187, 2020.

[7] S. Martin-Anton and D. Segovia-Vargas, "Broadband antenna design for new mobile communication systems," in *12th European Conference on Antennas and Propagation (EuCAP London)*, 2018, pp. 1–5.

[8] A. B. Asrokin, A. B. Abas, R. H. B. Basri, and N. B. Jamlus, "Design of x-polarized GSM 900 Base station antenna with field test measurement," in *Proc. Second Int. Conf. Computer Engineering and Applications*, vol. 2, 2010, pp. 94–98.

[9] Z. Yang, Y. Cui, X. Mo, and R. Li, "A wideband crossed-dipole antenna for LTE700/GSM850/GSM900 Base stations," in *Proc. IEEE-APS Topical Conf. Antennas and Propagation in Wireless Communications (APWC)*, 2019, pp. 030–033.

[10] D. Su, J. Qian, H. Yang, and D. Fu, "A novel broadband polarization diversity antenna using a cross-pair of folded dipoles," *IEEE Antennas and Wireless Propagation Letters*, vol. 4, pp. 433–435, 2005.

[11] Y. He and W. Tian, "A broadband dual-polarized base station antenna element for european digital dividend, CDMA800 and GSM900 applications," in *Proc. 13th Int. Wireless Communications and Mobile Computing Conf. (IWCMC)*, 2017, pp. 659–663.

[12] Y. He, Z. Pan, X. Cheng, Y. He, J. Qiao, and M. M. Tentzeris, "A novel dual-band, dual-polarized, miniaturized and low-profile base station antenna," *IEEE Transactions on Antennas and Propagation*, vol. 63, no. 12, pp. 5399–5408, 2015.

[13] Y. He, W. Tian, and L. Zhang, "A novel dual-broadband dual-polarized electrical downtilt base station antenna for 2g/3G applications," *IEEE Access*, vol. 5, pp. 15 241–15 249, 2017.

[14] J. Volakis, *Antenna Engineering Handbook*, fifth edition ed., J. L. Volakis, Ed. New York: McGraw Hill Education, 2019. [Online]. Available: https://www.ebook.de/de/product/31184088/john_volakis_antenna_engineering_handbook.html

CHAPTER 5

ARRAY DESIGN

The aggregation of elements is known as antenna array. The combination of several elements is recognized for increasing the overall directivity in comparison with the element and some properties that are presented in this chapter.

The objective of the chapter is to design arrays working in the extended band to be used as base stations in the new generation of mobile communication.

Firstly, as a design tool, the chapter presents a new software based on array theory. The purpose of the software is to obtain accurate array simulations with low computational cost. avoiding the high computational cost associated to full-wave simulations.

Secondly, a linear array working in the 1.42 - 2.69 GHz band is presented with the actual elements designed in Chapter 2. Dual band integrated arrays are presented for covering both bands, 690-960 MHz band and 1.42-2.69 GHz band. Within this section, classic base station arrays are covered with the extension of the new bands.

At the end, a new topology solution is presented, in which by using planar array properties it is possible to achieve beamsteering in both θ

and ϕ direction for the ExtUWB, which is a novelty that can be used for future MMIMO applications.

5.1 Introduction

The requirements that are needed (such as gain) can not be fulfilled by single elements. For that reason, the solution is to combine several identical elements working together in what is called an array of antennas. The antenna array increases the directivity of the element by an amount defined by the distance between them, the working frequency, etc.

Figure 5.1 shows a complete base station tower in which the array of elements used is in the inside part of the panel array.

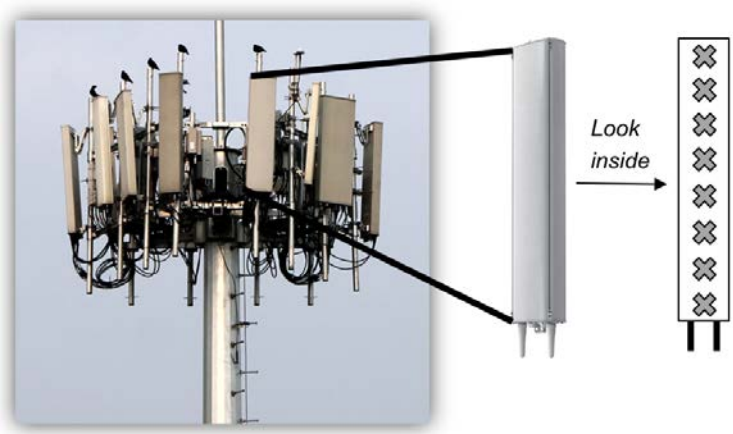

Figure 5.1: Base Station Tower with Sector Panel Antennas. An array of elements is shown in the interior of one panel antenna. Picture extracted from [1].

Usually, the array is composed by parallelly fed elements, with uniform amplitude to obtain high gain. For a vertical array consisting of a line of elements, the pattern is uniform in azimuth and directive in the elevation plane. Longer arrays produce narrower elevation pattern and, hence, higher gain and longer communication distance. Nevertheless, a very narrow pattern will lead to coverage loss near the tower.

A linear phase taper across the array, consisting in small time delays between element feeds, is used to produce an electrical downtilt that tilts the radiation beam slightly downward to reduce the interferences with adjacent cells. If the electrical downtilt were mechanically developed by tilting the whole antenna (mechanical downtilt), the radiation pattern would tilt down on the front but up on the back, whereas an electrically downtilted array produces the same angle of downtilt in all azimuth directions.

Commonly, cellular base stations use sector patterns to cover each sectors of the angular space, instead of having omnidirectional antennas with uniform coverage around the tower. The typical sector antenna arrangement is a triangular structure at the tower top, using panel antennas on each face that cover a 120° sector. The most common value for the half power beamwidth in the horizontal plane is in the range of 65°. [2]

For large antennas, the maximum available directivity is defined by the common aperture directivity formula. In the case of small antennas, it is given by the directivity of the Huygens source. When both expressions are combined in a heuristic manner to a continuous maximum directivity limitation, the result is a function of the diameter of the smallest sphere that can surround the antenna. [3]

An array of antennas generates a continuous electromagnetic field defined by its currents, that is as big as the total array dimensions, whereas the elements are as small as the working frequency requires. It is that large size current that generate EM field and hence a radiation pattern in which the gain is larger than the gain found in a single element.

The model for the basic array antenna study consists of two parts, the radiation pattern of one of the elements by itself, called the element pattern, and the pattern of the array with the elements replaced by isotropic point sources, the Array Factor. The total radiation pattern of the array is then the product between the element pattern and the array factor. [2]

The concept of array is used in base station for mobile phone antennas, by placing several elements in a vertical linear broadside array,

the gain is increased by narrowing the radiation pattern in the vertical plane, while the horizontal plane is theoretically kept the same as the one found in the designed element.

When a group of elements in an array is placed not in a line pattern, but in a meshgrid, the planar configuration of the elements can be considered as a planar array. A planar array can often be considered as a linear array of linear arrays, so the theory of linear arrays is also valid for planar arrays. Planar arrays extend the array properties to the two coordinates in which it is located. If linear array shrinks the radiation pattern in one plane, the planar array can do it in both planes. And more important, the scanning property expands not only to the array axis, but to both of them. In other words, if linear arrays can scan in different values of θ for a ϕ defined by the array axis, the planar array achieves scanning properties for different values of θ for every ϕ, defined in spherical coordinates. [4]

Arrays of antennas are also popular due to the ability to shape the radiation pattern through spacing and excitation adjustment obtaining the capability of scanning in angular space by dynamically adjusting the excitation phase electronically. Those arrays are referred as phased arrays. Before that innovation, the traditional method of scanning a directive beam was to mechanically move an aperture antenna such as a reflector antenna. But nevertheless, mechanical scanning requires a rotation and position system that is usually large, expensive and too slow. [2]

The evolution presented in the use of array can be defined with the first widely used Yagi-Uda array invented in 1926, followed by other fixed-phase arrays with mechanical scanning. Mechanical phase shifters brought the emergence of phased arrays during the World War II, and later with ferrite phase shifter, electronic scanning became possible. Later, in the 1960s solid-state phase shifters allowed for more affordable and compact phased arrays, the recent innovations are related to active phased array with individual electronic per element. [2]

There are different concepts regarding the new technologies in the array field of knowledge. Switched beam array is when a software algorithm is used to select from different previously defined beams in the

antenna array, with the purpose of choosing the strongest signal. For example, nowadays in the base station market, there are antennas in which it can be selected between two sectors, -30 to 0 degrees or 0 to +30 degrees in the horizontal plane.

Adaptive arrays or smart antennas produce beam or beams in determined directions. By processing the signal from the individual elements, the array can react intelligently to its environment, steering the beam toward a desired signal while simultaneously steering a null toward an undesired, interfering signal and thereby maximizing the signal to noise and interference ratio of the desired signal. [5]

With the sampling and digitalizing of the signals at each element, a computer processing can be done to run a smart antenna. Different weights of beams could be simultaneously directed toward many signals and directions. Those antennas are sometimes referred as Digital Beam Forming antennas. Although, any antenna in which the pattern is dynamically adjusted by the system as required is usually called as a smart antenna. [5, 6]

The concept of shifting the antenna main beam with the properties of phased array is called scanning or beamsteering, and can be used for developing smart antennas and use them in Massive MIMO communications. The applications of MMIMO is being developed nowadays in much higher frequency as dozens of GHz [7], although there are several researches to apply it to a new band in communications at 3.5GHz and 6 GHz [8, 9]. The use of Massive MIMO in higher frequency is due to the reduced physical size, as higher frequency elements are much smaller, they can be physically very close to eachother, and the final size of the planar array is not huge. But as mentioned, due to size deals, it has not been developed for lower bands of frequency. The novelty with this respect here is to present a final Massive MIMO beam steerable array for the interest band of ExtUWB 1427-2960 MHz, which has not ever been proposed, and include them in the same reduced size of a classical BTS antenna, which would be very interesting for the community in a near future.

Nowadays, in the state of the art, MMIMO arrays can be found for higher frequency as mentioned in the previous paragraph (3.5 GHz, 6

GHz, and dozens of GHz), but not for the cell phone bands. Also, some references as [10] and [11] can be found, where different shapes and architectures are used in classical mobile communication bands arrays with the purpose of obtaining the requirements and improve the results. But the new extended bands are not achieved in those publications. Furthermore, regarding 5G and phased array design, a hard push is being developed in papers such as [12] and [13], trying different architectures, methodologies and perspectives for the design of those new arrays, with array synthesis and adaptive arrays according to the channel scenarios.

In next sections, different details are explained, in which it is explained why array design is not as easy as easily compute an array factor and apply it to an isolated element. For that reason, the first objective of the chapter is to develop and present all the theory behind arrays, and implement a more realistic simulation in a computed based software.

The rest of the objectives in the chapter is to present new array architectures in which the new ExtUWB is included, firstly in a classical linear array configuration, and afterwards, in a beam steerable array for MMIMO applications.

5.2 Array Theory and Implementation

This section presents the theory behind the arrays development, while some conclusions and opinions are expressed. The end of the section finishes with the implementation of a new software tool developed for obtaining more realistic arrays results with less computational cost.

When combining several radiating elements, the resulting far field radiation pattern is the superposition of each element contribution. It can be seen in equation 5.1, where G_n is the radiation pattern for the n element, I_n is the current fed to the element and the exponential represents its position.

$$G_{Array}(r) = G_1(r)I_1e^{jkr_1} + G_2(r)I_2e^{jkr_2} + ... \tag{5.1}$$

When it is assumed that all elements are identical and have the same far field function, it can be simply written as presented in equation 5.2.

$$G_{Array}(\theta,\phi) = G_{Element}(\theta,\phi)AF(\theta,\phi) \tag{5.2}$$

AF is the common factor and it is referred to as the Array Factor that expresses the sum of the contributions of all the elements in the array as if they were ideal. Thus, the far field function of an array of equal and co-oriented elements is the product of the element pattern factor (the far field function of the element) and the array factor.

In the case in which the elements are placed in a straight line, the array is known as a linear array, and the array factor can be express as equation 5.3.

$$AF(\theta,\phi) = \sum_{m=1}^{M} I_m e^{j(m-1)(kd_x sin(\theta)cos(\phi)+\beta_x)} \tag{5.3}$$

where I_m is the excitation coefficient of each element. The spacing and progressive phase shift between the elements along the x-axis are respectively represented by d_x and β_x.

By extension, when the elements are placed in a plane, the array factor for the planar array is seen in equation 5.4.

$$AF(\theta,\phi) = \sum_{m,n} I_{m,n} e^{j(m-1)(kd_x sin(\theta)cos(\phi)+\beta_x)} e^{j(n-1)(kd_y sin(\theta)sin(\phi)+\beta_y)} \tag{5.4}$$

Now, $I_{m,n}$ is the feeding or excitation matrix. While d_x and d_y define the grid, β_x and β_y define the phase shift that control the beam scanning for θ and ϕ angles.

With those formulas the known as Array Analysis is developed. From the known variables as the element radiation pattern, distance between elements, and the currents fed to them, it can be computed to obtain the resulting array radiation pattern. Besides, it is the Array Synthesis, in

which the objective radiation pattern specified runs as a known variable to finally obtain the currents to feed the elements.

There are different techniques for array synthesis as Dolph-Chebyshev, Taylor, etc. Those techniques can theoretically obtain arbitrary specifications by root perturbations and several iterations.

As the radiation pattern is related to the Fourier Transform of the currents of the aperture distribution, given a desired radiation pattern, the aperture distribution should be obtainable by a Fourier Transform. And then, by discretization of the continuous solution, the feed and position of elements should be determined.

For developing those kind of array synthesis techniques, it would be necessary to have freedom in the element position which is only the case for punctual elements. The final element feed can be very difficult to implement. It is necessary to study it in a deeper way and develop a computational software to achieve the expected results. And furthermore, the array synthesis is presented for the design of an array at a determined single frequency, whereas the design in a broadband scenario is not consistent with a fixed electrical distance.

Array synthesis is not the best way for the objective design of actual arrays in this chapter. Firstly, the elements in the array have some physical restrictions as they are not point elements and have to be placed geometrically in places that the fit in, and where the mutual coupling between them is not too high. Secondly, the theory behind array synthesis is developed for a single frequency, so for the other frequencies of the band, the array is not as designed and does not fulfill the requirements. At the end, the most famous way of implementing array synthesis is by canonical feeding that are perturbed to approach the required radiation pattern. For those reasons, the array synthesis theory is not used in the current chapter.

Antenna or array Directivity is an important quantitative description of how much an antenna concentrates the energy in one direction respect to radiation in the others. Directivity of an antenna is defined from IEEE Standard Definitions of Terms for Antennas as the ratio of the radiation intensity in a given direction from the antenna to the average radiation

intensity over all directions. It can be seen in equation 5.5. The average radiation intensity is equal to the total power radiated by the antenna divided by 4π. In other simple words, the directivity of an antenna is equal to the ratio of the radiation intensity in a specific direction over that of an isotropic source, that can be expressed in dBi as are decibel relative to isotropic level. [2, 14]

$$D = \frac{U_m}{U_{ave}} = \frac{U_m}{P/4\pi} \tag{5.5}$$

As $P = U_m \Omega_A$, the exact result for the directivity value can be determine as follows in equation 5.6.

$$D = 4\pi/\Omega_A \tag{5.6}$$

where Ω_A is the beam solid angle and can be computed as

$$\Omega_A = \int\int |F(\theta, \phi)|^2 \mathrm{d}\Omega \tag{5.7}$$

where F is the normalized field pattern and $\mathrm{d}\Omega = sin(\theta)\mathrm{d}\theta\mathrm{d}\phi$

There are different approximation to the exact result. One of them is the linear approximation for broadside uniformly excited, equally spaced linear arrays for the linear section of the curve.

$$D \approx 2\frac{L}{\lambda} = 2N\frac{d}{\lambda} \tag{5.8}$$

As can be seen in figure 5.2, the directivity curves increase within each wavelength and fall when ther is a step between integer number of wavelegths. This effect is due to the grating lobes emerging in the visible region. The single results for elements spaced a multiple of half-wavelength apart obtain directivity value equal to the number of elements D=N in natural units, value of convergence for increasing distance.

Sometimes, at least for starting an array design, a single frequency fixed distance theoretical calculation can be done to achieve the number

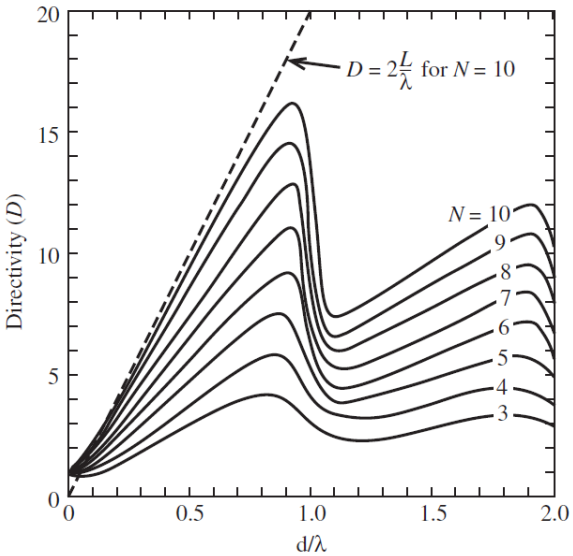

Figure 5.2: Directivity as a function of element spacing for a broadside array of isotropic elements for several element numbers N. Comparison between exact result and linear approximation. Picture extracted from [2].

of elements resulting in a desired value of directivity in the array factor. It is not an exact result, as the design should be broadband and the electrical distance between element is not a single value for every frequency. Resulting in different array factors for each frequency, as the distance is related to the wavelength. Apriori, to avoid multilobulation it is recommended not to used very large distance between element, specially much larger than lambda. But in the global scenario, it does not matter if there are lobes in the array factor back radiation zone, as the element should be cancelling that radiation by multiplying of both patterns, the element pattern and the array factor. Finally, it is about to find a trade off for every frequency in the bandwidth, to achieve the required directivity value without important lobulations.

For starting, a fast calculation can be done. If a gain of 8dBi for the element is assumed, then, a directivity of 8dB in the array factor would be necessary to obtain 16 dBi in the complete array. Assuming an array at a single frequency, in which the elements are spaced $d = n\lambda/2$.

As the directivity in natural units is equal to N number of elements for $d = n\lambda/2$, then, 8dB in the array factor can be theoretically obtained with 7 elements, as

$$10^{(8dB/10)} = 6.3096 => 7elements$$
$$10log_{10}(7elements) = 8.4510dB$$

This calculation can be assumed as a first approximation for the number of elements because, according to Eq.5.2, the array factor directivity for a 7 elements array is 8.45dB for $d = \lambda$ and $d = n\lambda/2$, while for values between them, the obtained result values are higher.

Regarding the current distribution, it is important to notice that the implicit generator of the radiated field and radiation pattern are the currents presented in the elements and at the end presented in the whole space occupied by the array arrangement. The most widely used current distribution is the homogeneous developed by an equispaced element array with uniform feed, i.e. same amplitude feed in every element. The homogeneous current distribution advantages are such as ease of implementation, it is generally known as obtain the maximum value of directivity and the narrowest beamwidth, although it is not optimum in terms of sidelobe level (SLL), so it can be considered as a disadvantage.

By modifying the current distribution, the side lobe level suppression can be enhanced, at the cost of losing some directivity and widening the beam. For doing such a task, there are two different approaches. The first and easiest one to do it with an equispaced array is modifying the element feed relative amplitude, in that case with a non uniform feed, the secondary lobes in the array factor are reduced. As different feeds for that purpose, some canonical feed amplitude distributions are deeply studied as triangular, binomial, or Dolph–Chebyshev, in which their characteristic are already known. However, the elements can be fed with whatever feed distribution can be imagined, even with non canonical amplitude distributions, but a study for the final behavior should be accomplished in those cases.

The second approach to obtain a non uniform current distribution is the one that occurs when the elements in the array are non equally

spaced. This can happen deliberately or due to some physical restriction in the design. When the elements in the array are not equally spaced the amplitude in the overall current distribution is usually increased in some areas with respect to others, which hence obtains another current distribution different to the uniform. Furthermore, in a non equispaced array, the element can be fed with uniform or non uniform amplitudes, which makes the task of studying the whole current distribution even harder. As those cases have not been analytically studied clearly before, it is very difficult to guess the final result in those arrays. For that reason, a simulation in which those properties are included would be very recommended.

The modification that can be made in the current distribution with a non uniform one, can be meant to achieve better values in SLL when needed at a cost of reducing the maximum gain of the array. Although, this approach in the array is in the ψ domain, meaning that it could reduce the value of the secondary lobes in the array factor, but the method is not valid when trying to reduce the repetition grating lobes as they are the principal lobe as well. As the First Side Lobe Level is not a crucial problem in the presented arrays of the chapter, homogeneous distribution with uniform feed is used in this chapter due to its benefits.

Notice, even when the array is uniformly fed and their elements are equally spaced, due to the fact that the actual elements in practice are not punctual, or their element current distributions are not completely homogeneously distributed, assuming the the actual array current distribution is fully flat and homogeneous to apply some approximations can lead to some small mistakes. For that reason, a full simulation for the arrays is always prefer to obtain more realistic results.

5.2.1 Software Tool Implemented in Matlab

For the development of this chapter, a software tool has been developed in Matlab. The presented code implies an improvement with more realistic simulations than classic approximation and lower computational cost than full-wave simulations. This development achieves some contributions that are explained below.

Generally, when a full-wave simulation of the array is too resources-

consuming to be done, for analyzing base station arrays, the array factor is applied to isolated elements and the solution is only obtained in the vertical plane, the plane containing the distribution of elements of the array, as for example can be seen in [15]. In these cases, the obtained solution is a generic approximation for the vertical plane, while in the horizontal plane it is assumed that the same diagram of the element will be obtained unmodified. However, the proposed software works with all points in space and, therefore, a complete 3D distribution is obtained. In addition a more complete array solution, from which the horizontal, vertical, or those desired cutting planes can then be obtained is also provided. The mentioned complete distribution results can be seen in figure 5.3.

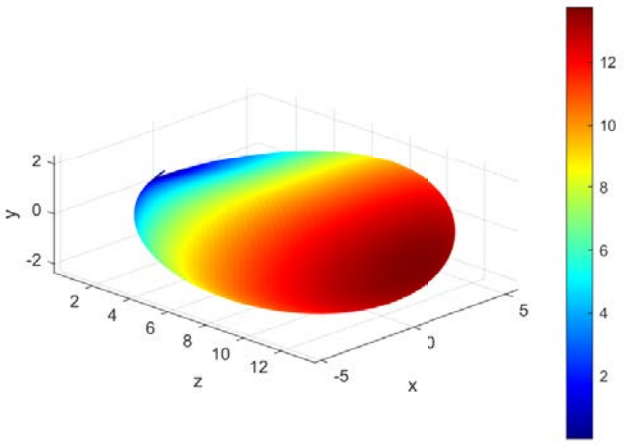

Figure 5.3: Example of a complete 3D result obtaining the antenna array gain (dBi) for every space point using the presented software. The figure represents the result for a 3 elements array.

Following with the classical base station array design, till now linear arrays were generally presented. In the developed code, planar arrays can also be studied, simply by defining a matrix or mesh grid, and placing the desired elements as pixels on the plane. Therefore, in addition, the elements do not have to be equally spaced as normally happens in classic arrays. In the presented code implementation, elements can be

placed with different distances between them or with different desired patterns, and the program will generate a grid containing the elements spaced as desired. In practice this benefits the fact that in linear arrays the elements can be separated from each other with different distance values, and in planar arrays the elements do not have to be placed in a square grid, being able to form different patterns.

An approximation that is usually assumed when working with arrays is that every element in the array is the same, as they are all equal. However, in general, this is not completely true, because although in the cases in which the elements individually studied are physically equal, the position in which they are in the array affects and modifies their radiation pattern and therefore, the radiation pattern for each of the elements integrating the array are not equal. This is included in the presented program, since the field sum of the different elements or groups of elements can be computed, such as the elements on the edges or the sides other than the central elements of the array. Even for extreme cases in which an array is composed by physically different elements or with different designs, their radiation pattern can be imported to compute the final result.

In addition to the elements being able to allocate different positions, the software also includes the possibility of feeding them with different currents. Current distribution can be defined as uniform, or non uniform, either it is canonically defined or a new distribution personally defined by the user.

In cell phone base stations, a limited vertical plane downtilt control is usually included with a range of 10 degrees with the purpose of moving the beam down for θ values between 0° and 10°, with a fixed ϕ being defined by the orientation of the array, vertical in common cases. In the proposed code, the computational ability to steer the beam has also been included for both degrees of freedom, θ and ϕ angles. The code shows independency and freedom when has to move the radiation beam in all directions of the space, theoretically the full front semisphere although in practice is less than that. This tool is necessary and very useful for planar arrays to be able to perform beamsteering and apply it to Massive MIMO applications.

Regarding the directivity obtained in the array, different approxima-

tions are often used, which are usually more appropriate when certain conditions are met, which is not always the case. For that reason, in this implementation the complete calculation of the directivity of a 3D radiation pattern has also been included, so that with the computing of the integral the most realistic value possible is obtained.

Typically, when reading and studying about arrays, the theory focuses on a single frequency design, which could be used without problems for narrow band arrays. However, when the array is intended to work in a wide band, once a physical distance between elements has been set, it can be observed how the electrical distance is different for each frequency of the band and therefore the array behavior will be different. To observe the broadband behavior of the arrays, instead of developing a narrow-band design at a single frequency, designs have been made considering the broadband behavior by using representative frequency points, that is, in the 1427 to 2690 MHz band, frequency points as 1.5 GHz, 2 GHz and 2.6 GHz have been chosen to study the performance in the low, central and high frequency sections of the band.

In the following lines, the operating program is explained for a better understanding with a simplified example.

For a planar array composed of three columns, by analyzing the elements and their individual radiation patterns, they can be grouped in three kinds of elements regarding their radiation pattern according to their position in the array columns (Left, Central and Right). As it is already known, the radiation pattern of an element is related to their environment and neighbourhood. Note that assuming infinite vertical array approach, border elements discrepancies in the vertical direction are omitted in this example, but they can be included as individual element contributions. From equations 5.1 and 5.2 the following equation 5.9 can be obtained for this example, in which each element is grouped with its alikes, resulting in three array factors, one per column. The result of the equation is the complete radiation pattern, that is composed by the contribution of the product of each different element and their group array factor added to the contribution of every other different groups of elements (in the example with column groups) or elements.

$$\begin{aligned} G_{Array}(\theta,\phi) = G_{ElementL}(\theta,\phi)AF_L(\theta,\phi)+ \\ G_{ElementC}(\theta,\phi)AF_C(\theta,\phi)+ \\ G_{ElementR}(\theta,\phi)AF_R(\theta,\phi) \end{aligned} \tag{5.9}$$

Each of the defined Array Factors has to be computed. For that task, the equation 5.10 is presented.

$$AF(\theta,\phi) = \sum_{m,n} I_{m,n} e^{j(m-1)(kd_x sin(\theta)cos(\phi)+\beta_x)} e^{j(n-1)(kd_y sin(\theta)sin(\phi)+\beta_y)} \tag{5.10}$$

Now, $I_{m,n}$ is the excitation matrix for the array. While d_x and d_y define the grid, β_x and β_y define the phase shift that control the beam scanning for θ and ϕ angles. For more clarification, figure 5.4 presents an example of the feeding matrix for three columns array where the elements are alternately placed as a chessboard pattern. In the figure each uniformly fed element and its weight is represented with 1, at the same time the 0s performs spaces in the grid definition. Note that the figure represents the complete feeding matrix, while it has to be particularized for each array factor of the example, i.e. for the left column array factor (AF_L), its excitation matrix ($I_{m,n}L$) keeps active the left column elements, while other elements have to be deactivated by placing a zero in their positions.

Once the array radiation pattern shape is achieved, a denormalization needs to be executed to avoid non accurate results in the magnitude obtaining the actual and desired directivity for the studied array. For developing that task, the precise directivity has to be computed with the directivity exact formula presented in equation 5.11, where F is the normalized field pattern.

$$D = \frac{4\pi}{\int\int |F(\theta,\phi)|^2 sin(\theta) \mathrm{d}\theta \mathrm{d}\phi} \tag{5.11}$$

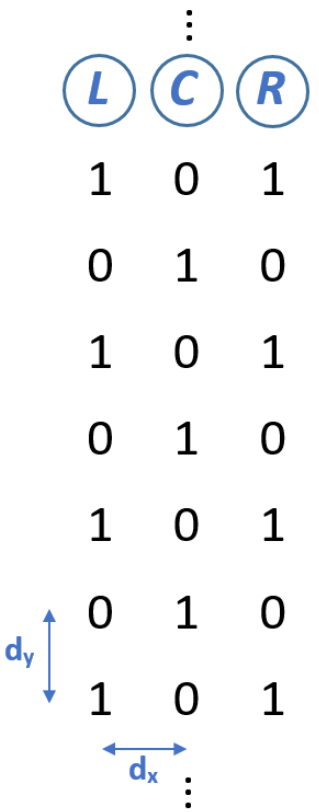

Figure 5.4: Simplified example of an array feeding matrix. The example shows uniformly fed elements placed in a chessboard pattern. Elements and their weights are represented with 1s, while 0s are spaces in the grid. The grid dimension is defined by d_x and d_y. The array is composed by three columns of elements: Left, Center and Right.

With the computed directivity the denormalization can be easily accomplished to the whole radiation pattern by removing the maximum value and adding the computed directivity in dB units.

After that, the final result is achieved. Then, the cuts for the interest planes are defined to show them in a user friendly environment.

In the presented example, only three element radiation patterns need to be accomplished in the full-wave simulator, and the result is as realistic as the complete array full-wave simulation without the full computational cost. In contrast to the unrealistic result that is obtained when the array factor is directly applied to an isolated element radiation pattern.

5.3 Single Band Array

For the beginning of this section, a comparison between different array approaches is developed. This is a small example to validate the designed software and compare its results with the different options. Figure 5.5 shows the obtained results for a three element array at 1.5 GHz with a distance between elements of 110 mm ($\lambda_{2.7GHz}$).

The first approach is to apply the Array Factor to the radiation pattern for an isolated element. This is the most standardized used, once the element is designed alone its radiation pattern is combined with the corresponding array factor. The results are not the best, because the effects caused by the proximity of other elements are ignored. Hence, the resulting diagram is overestimated, as can be seen in figure 5.5 with blue line.

Second approach is applying the same Array Factor to the simulated radiation pattern for an element with its neighbours. At least three elements are included in the full-wave simulator but only the central one is fed and exported for combining it with the array factor. This is equivalent to the infinite array concept, where every element is considered to be surrounded by neighbours to the infinite, so the concept of array factor is fully operative. Although, in real live the infinite array is truncated to the actual number of elements, and consequently, the radiation

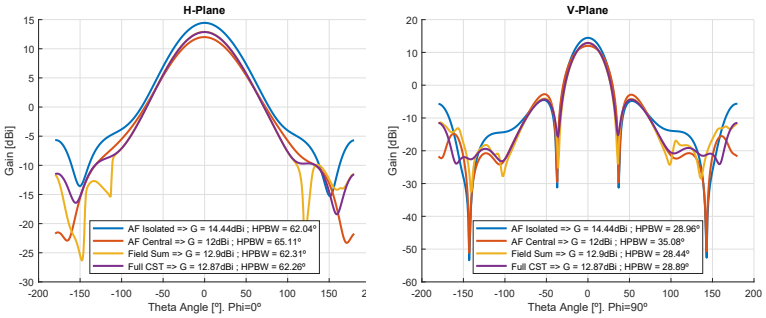

Figure 5.5: Different techniques array results for a three elements array. The presented software is compared with the full wave simulation and approximations as Array Factor and Infinite Array.

provided by the elements at the end difers to the central ones, leading to a different between this approach and the actual array behaviour. The difference between this approximation and the actual behaviour is minimized as the number of elements increase. The result can be observed in red line in figure 5.5.

In the presented software both kinds of elements are used. Only the radiation pattern that are different are computed in the full-wave simulator. For these linear arrays, two different elements are exported: the central elements that are affected by neighbours and are considered as in an infinite array, and the element located at the border. Then, the software, making use of the explained principles as field sum, obtains a much more realistic results with less computation load than the complete full array full-wave simulation.

Figure 5.5 shows the presented software result in yellow, and the complete full array full-wave simulation in purple. It can be observed how they are overlapped in the complete front semisphere, with small differences on the back, for that reasons, the obtained values of gain and beamwidth are almost the same.

From this first study, by using the three element full wave simulation, the resulting array can be obtained for seven or any number of elements without increasing the computational complexity.

A 7-element array has been chosen because is enough to achieve the

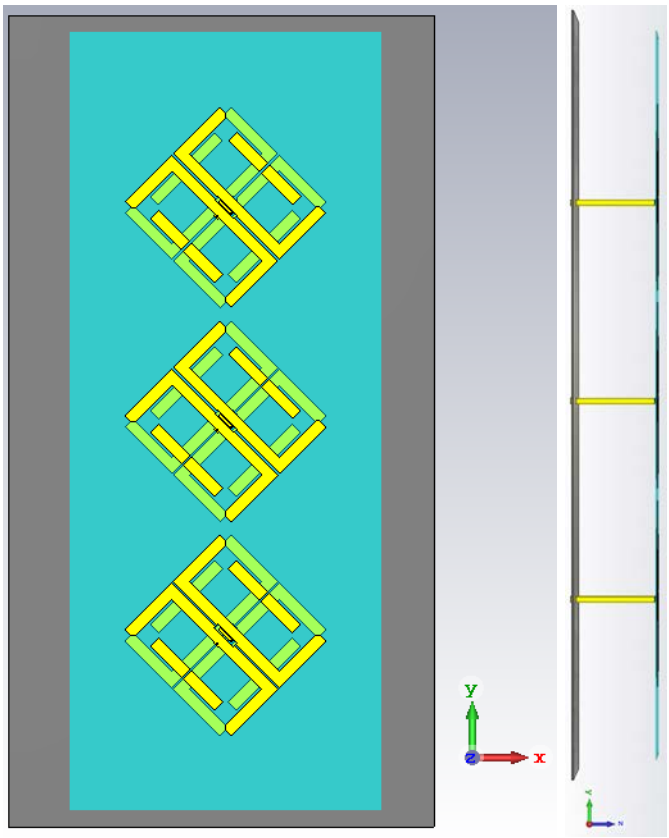

Figure 5.6: Single Band Array for ExtUWB. Fragment composed by 3 elements.

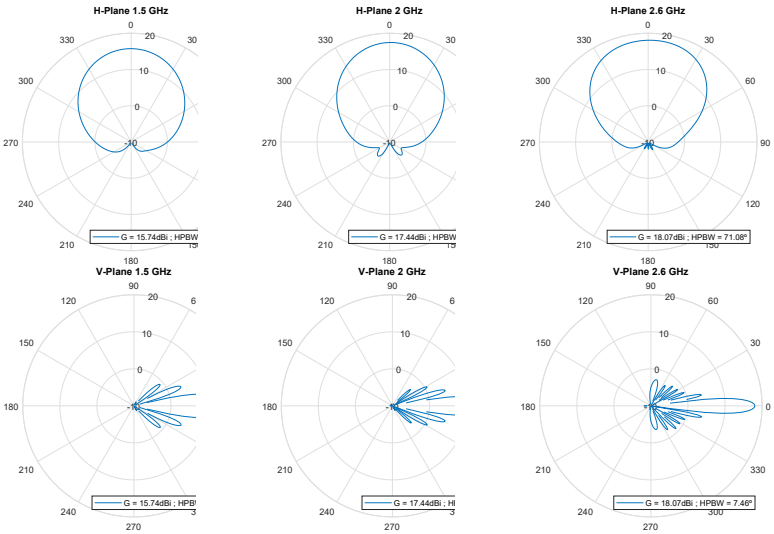

Figure 5.7: Results for the ExtUWB Array composed by seven elements.

array requirement in term of gain, while the size is restrained enough to fit the size requirements.

For a seven elements array, spaced a distance of 110 mm between them, which is equivalent to λ at 2.7GHz, the obtained results can be observed in figure 5.7. The horizontal beamwidth is kept near the original values with 64.7 ± 6.4 degrees, while due to array properties the vertical beamwidth is converted to 10.5 ± 3 degrees, which results in a gain of 16.9 ± 1.1 dBi.

In the same way, a low band frequency array is developed. With seven elements and a distance center to center between them of 280 mm, equivalent to $0.9\lambda_{960MHz}$, the array results are shown in figure 5.8. The values for the horizontal beamwidth in the band is 70.8 ± 0.3 degrees, and the resulting gain in the array is 16.5 ± 0.5 dBi.

The presented individual arrays for single band, are both good in the results, with the radiation properties covering the requirements, and restrained physical dimensions of 770x140x38 mm for ExtUWB array and 1960x280x130 mm for LBF array.

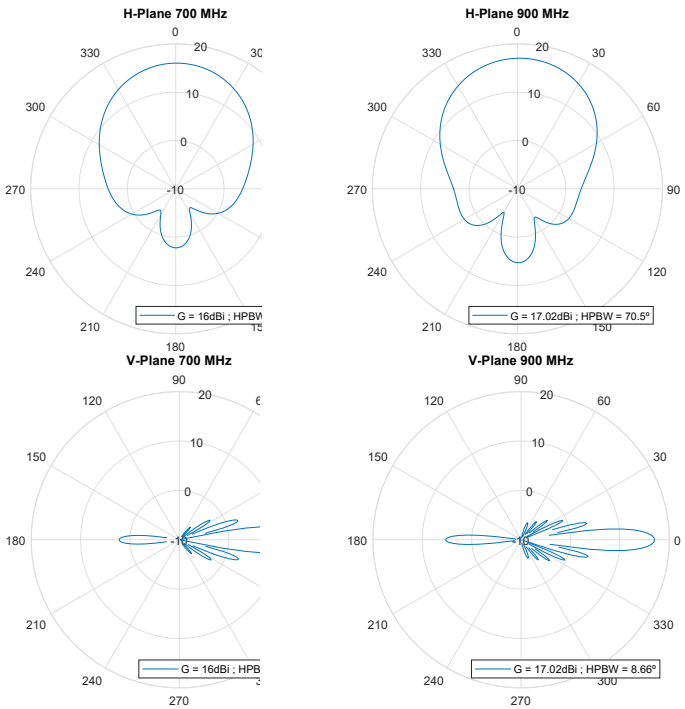

Figure 5.8: Results for the LBF Array composed by seven elements.

5.4 Dual Band Array

The objective of this section is to cover both bands with their respective arrays in the same space. For that reason, the integrated setup arrangements presented in Chapter 4 are been used.

As presented previously, the design configuration is physically limited by its architecture. The distance between low band frequency elements, stablished as 240 mm ($0.77\lambda_{960MHz}$), and the architecture itself, results in a distance between ExtUWB elements of 140 mm ($1.25\lambda_{2.7GHz}$). Figure 5.9 shows the inclusion of a new ExtUWB element (A) in the space located between two lateral elements (L), giving as a result the allocation of elements in a chess board pattern of d=70mm. The configuration for this base station antenna achieves three columns for ExtUWB and one LBF column, i.e. 6 ExtUWB arrays and 1 LBF array, or 2 LBF ports and 12 ExtUWB ports.

The linear arrays are being configured by combining groups of seven elements in vertical groups or positions, which results in one array for Low Band Frequency and six for ExtUWB, two central, two lateral on the left and two lateral on the right.

The different array results are shown in figures 5.10 to 5.12. For simplification and symmetry, one central array, one lateral array, and the LBF array are shown, as the other ones can be obtained by symmetry operations. As expected from previous chapter, the LBF array obtain good results for gain and beamwidth because the presence of other elements does not influence its significantly. Moreover, the arrays working in the ExtUWB obtain a non-perfect performance in the horizontal beamwidth due to the influence and occlusion caused by LBF elements located on top of them. However, the arrays themselves work good in terms of gain, and the First Side Lobe Level is right without significant secondary lobes in the interest front sector.

As an extension of this architecture, a double column for LBF base station can be achieved. If the single column is replicated and placed side-by-side to each other, a new double column base station is obtained. Figure 5.13 shows the resulting architecture, in which, a new ExtUWB

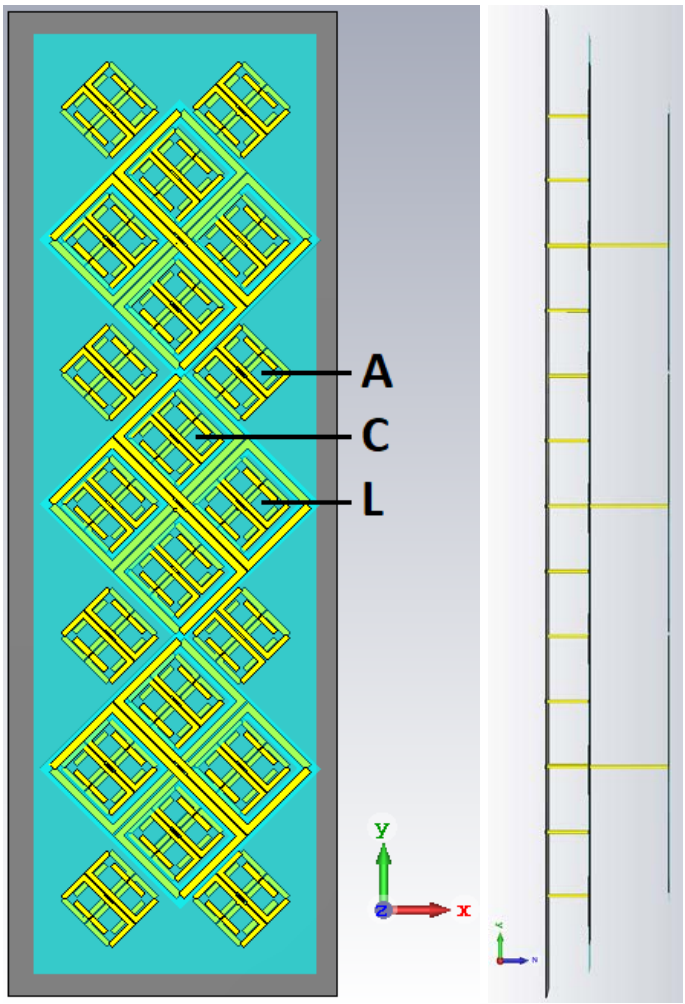

Figure 5.9: Fragment of the architecture for One Column BTS composed by LBF elements and ExtUWB elements.

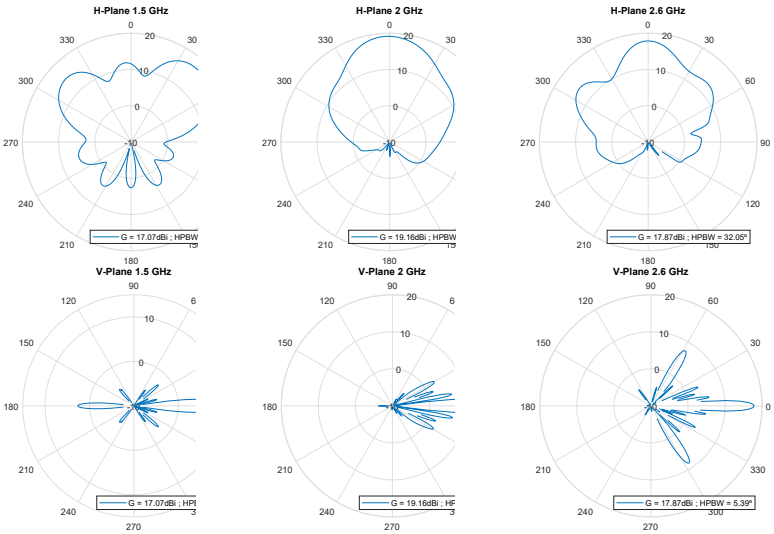

Figure 5.10: One Column BTS in Classic Configuration. Central Element Array.

column is placed between them, making use of the unused space formed between columns. That element column placed between the two LBF columns can be called Bridge (B). That configuration obtains 2 LBF arrays and 14 ExtUWB ones, i.e. 4 LBF ports and 28 ExtUWB ports.

The results for the double column implementation are shown in figures 5.14 to 5.18, in which the radiation pattern for the Lateral External, Lateral Internal, Central, Bridge arrays, and LBF one are presented. While the behaviour of ExtUWB arrays is similar to presented before, the LBF arrays present a small deformation in the horizontal plane for the lowest frequency due to the new proximity of the second LBF array.

Although the final results in the ExtUWB are not optimal, this section has presented a new architecture in which six high frequency arrays are integrated per one LBF array, in comparison with the two per one widely used in the state of art and commercial products. Furthermore, the presented arrays make use of a new element covering the extended band that hinders the complete array, instead of the classic band. Besides, the next section presents a new novel application for these arrays different than the presented classical lineal arrays.

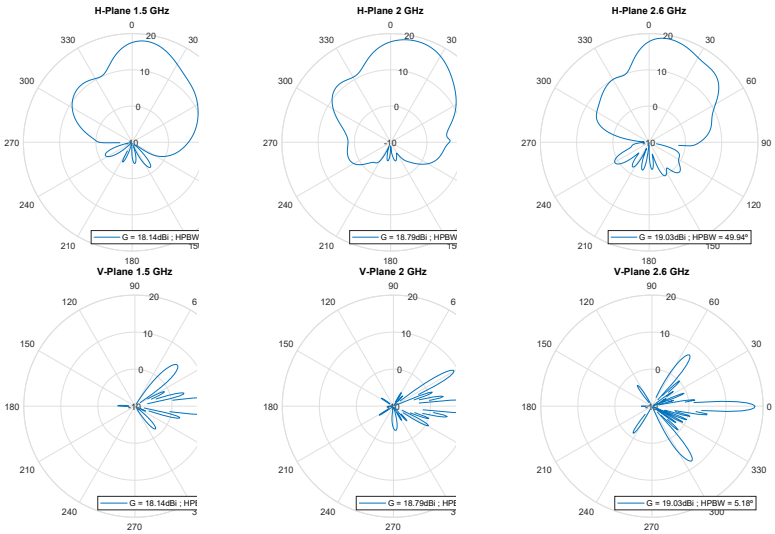

Figure 5.11: One Column BTS in Classic Configuration. Lateral Element Array.

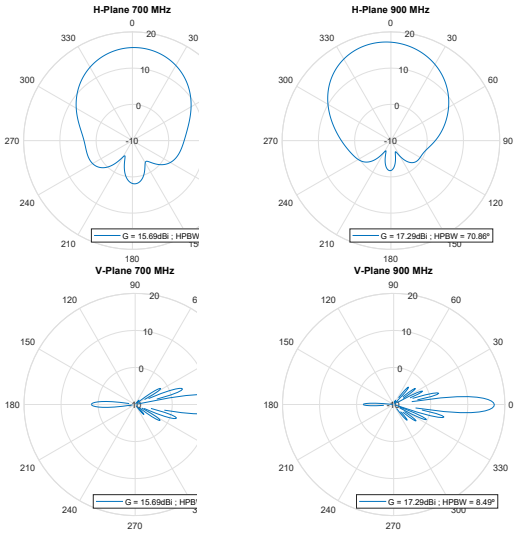

Figure 5.12: One Column BTS in Classic Configuration. Low Band Element Array.

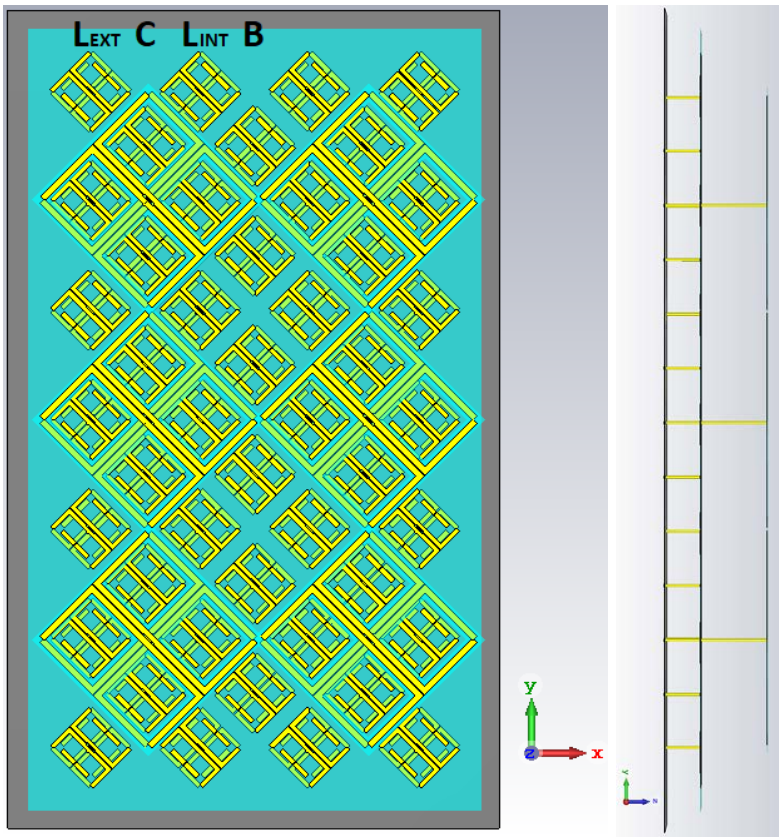

Figure 5.13: Fragment of the architecture for Two Column BTS in which another array (B) is included in the middle.

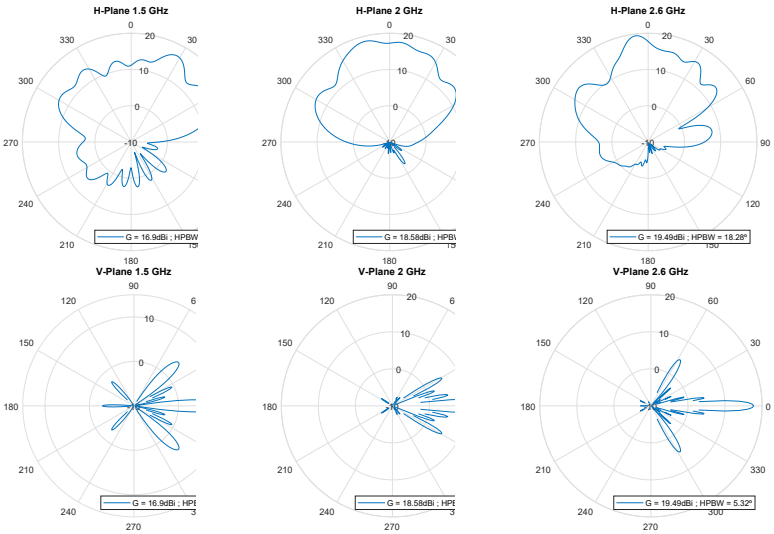

Figure 5.14: Two Column BTS in Classic Configuration. Central Element Array.

5.5 Dual Band Massive MIMO Beam-Steereable Array

For a different and novel performance in the ExtUWB, the elements can be grouped in different ways, with a result of beam steering in both theta and phi angles and Massive MIMO performance.

On the first proposal, one LBF array is combined with MMIMO in ExtUWB. Figure 5.19 shows ExtUWB half length column working together, when 21 elements are fed, achieving two MMIMO with a gain of 18.5 $\pm$ 2.0 dBi, combined with one classical LBF array. Figure 5.20 shows one column when every of the 44 elements is fed for MMIMO. With this architecture, one MMIMO with gain of 21.5 $\pm$ 2.1 dBi is combined with one classical LBF array. This architecture is contained in a box 1960 mm length, 280 mm width and 130 mm depth.

When using a double column scenario for achieving two LBF arrays, the MMIMO arrays can be configured in a more flexible way. Firstly, two or four MMIMO composed by 44 or 21 elements respectively as

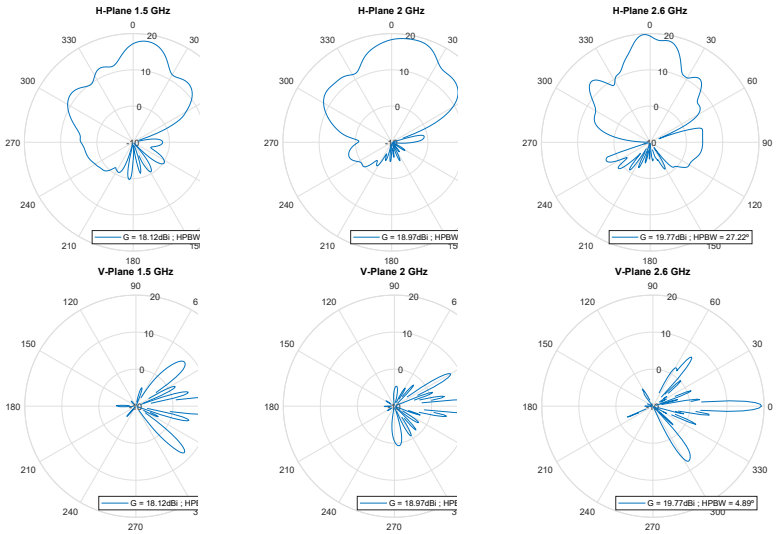

Figure 5.15: Two Column BTS in Classic Configuration. Lateral Internal Element Array.

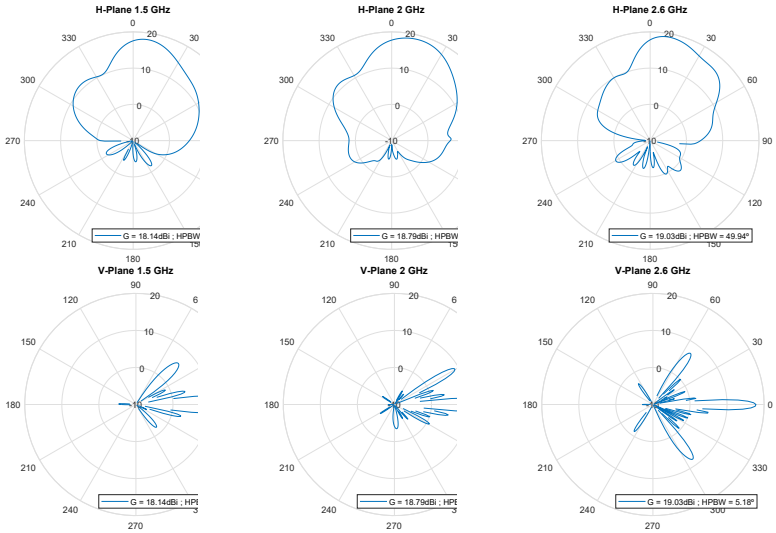

Figure 5.16: Two Column BTS in Classic Configuration. Lateral External Element Array.

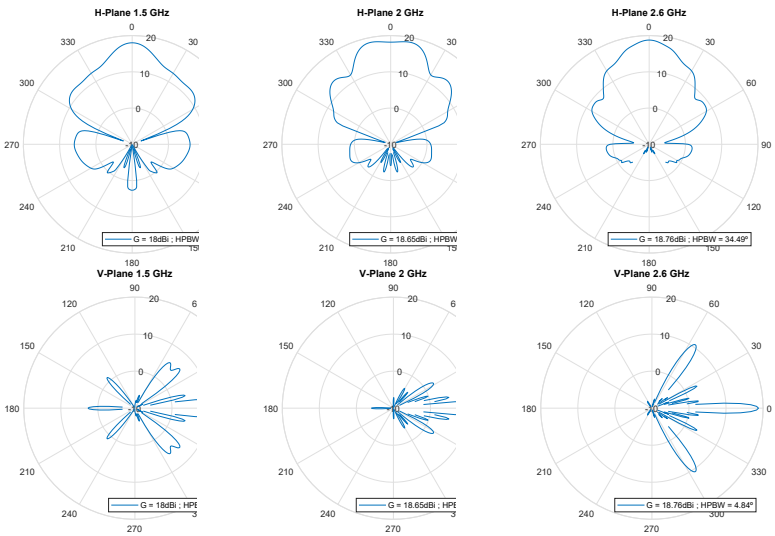

Figure 5.17: Two Column BTS in Classic Configuration. Bridge Element Array.

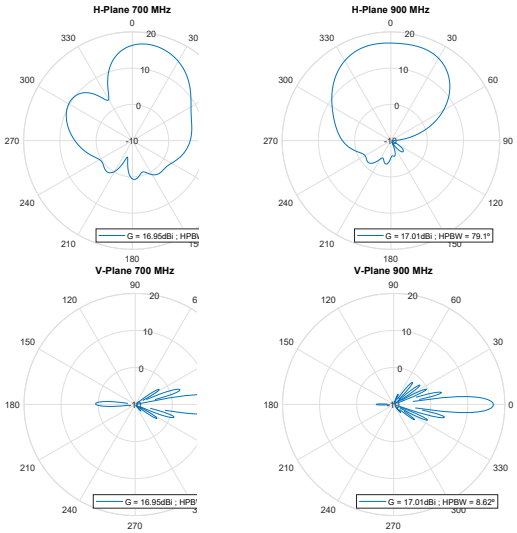

Figure 5.18: Two Column BTS in Classic Configuration. Low Band Element Array.

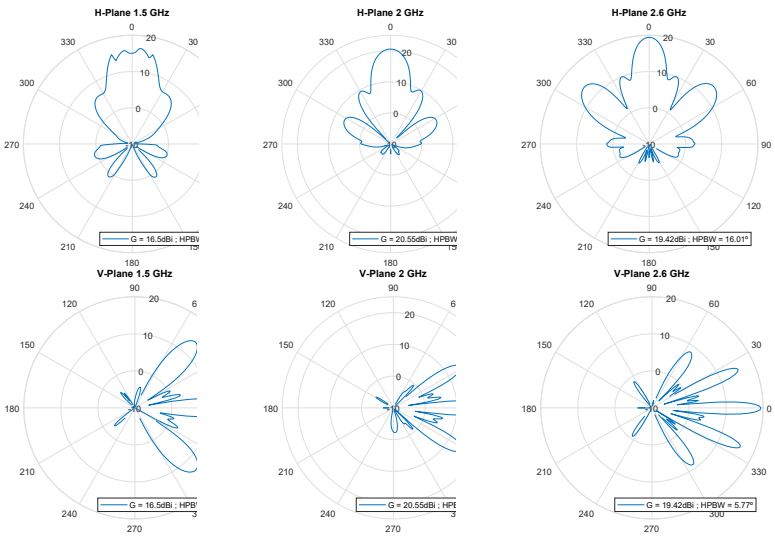

Figure 5.19: Massive MIMO Radiation Pattern composed by One column half length 21 ExtUWB elements.

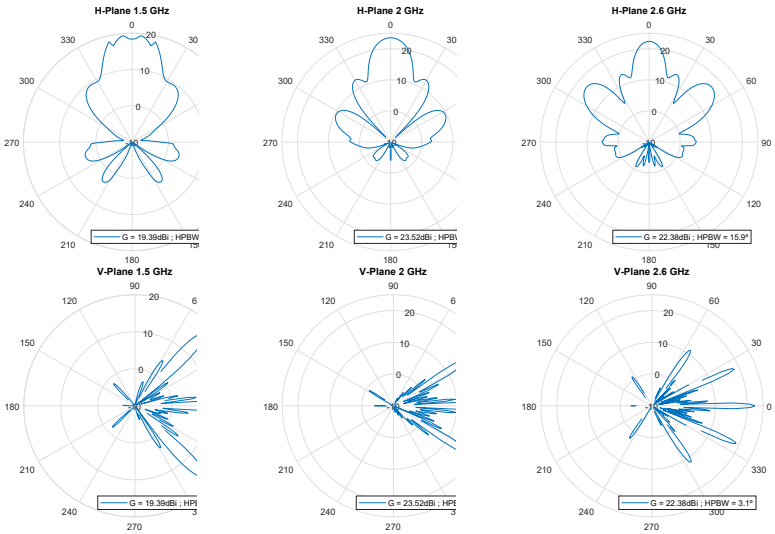

Figure 5.20: Massive MIMO Radiation Pattern composed by One column 44 ExtUWB elements.

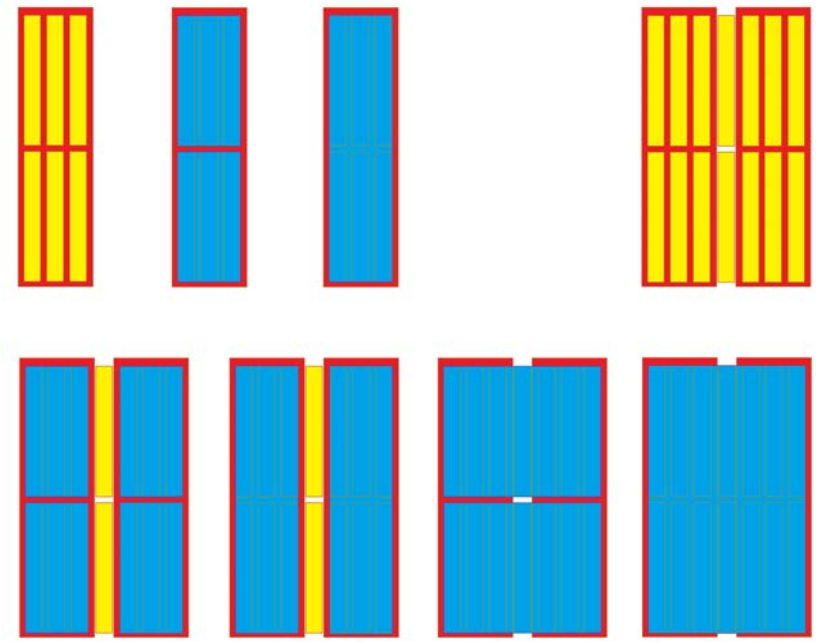

Figure 5.21: Different configurations. Low Band Frequency Arrays represented in red. High Frequency Band ExtUWB Classical Lineal Arrays represented in yellow. Massive MIMO Planar Arrays in ExtUWB represented in blue.

presented before, can be found with two LBF arrays, and the two Bridge arrays located in the middle. Figure 5.21 shows different examples of the configurable flexible architecture.

Specifically in the double column scenario, the MMIMO horizontal pattern can be enhanced by combining the whole rows. Figure 5.22 shows the results when the ExtUWB elements are fed together in double width and half length/height with a total of 49 ExtUWB elements, achieving two MMIMO arrays with gain 20.9 $\pm$ 1 dBi, combined with two LBF classic arrays. If the whole arrangement is fed together with the 102 elements in the same MMIMO ExtUWB array, the results shown in figure 5.23 are obtain, with a gain of 23.8 $\pm$ 1 dBi, combined with two LBF classic arrays.

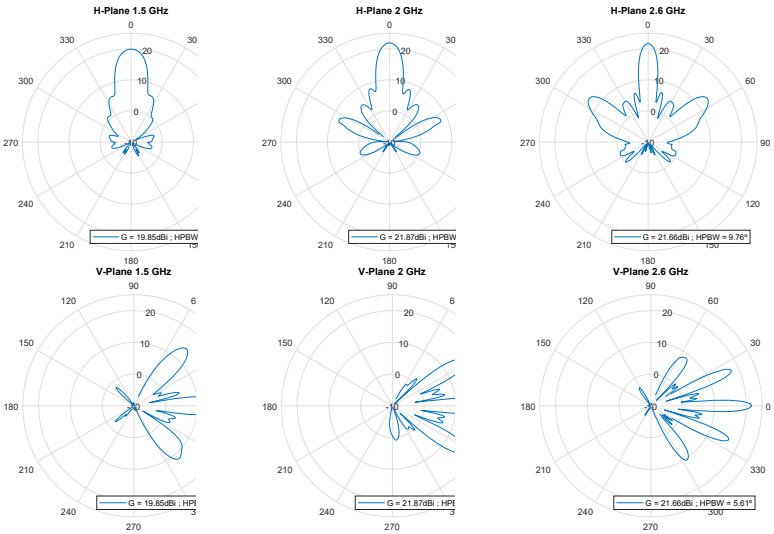

Figure 5.22: Massive MIMO Radiation Pattern composed by Two column half length 49 ExtUWB elements.

As seen in figure 5.21, this architecture is very flexible, capable of combining different elements as could be requested to achieve a vast combination of solutions with beam steering MMIMO in ExtUWB, and classical arrays for ExtUWB and LBF.

One of the different test done, regarding high frequency elements placed on the bottom, they can be printed in small square substrate pieces or together in the same substrate, as can be seen in figure 5.24. There is not any effect that has to be accomplished and both approaches have the same behaviour.

In the figure 5.25 a different simplification is presented. In this case, the 102 ExtUWB elements are working together to provide beamsteereable MMIMO, but without the presence of LBF elements in a higher top layer. This performance is better, both in terms of gain as in the beam shape and secondary lobes. It is improved in comparison with the previous case.

Figure 5.26 shows some examples in the beam steering or scanning. Whereas classic vertical arrays are required to achieve a vertical downtilt

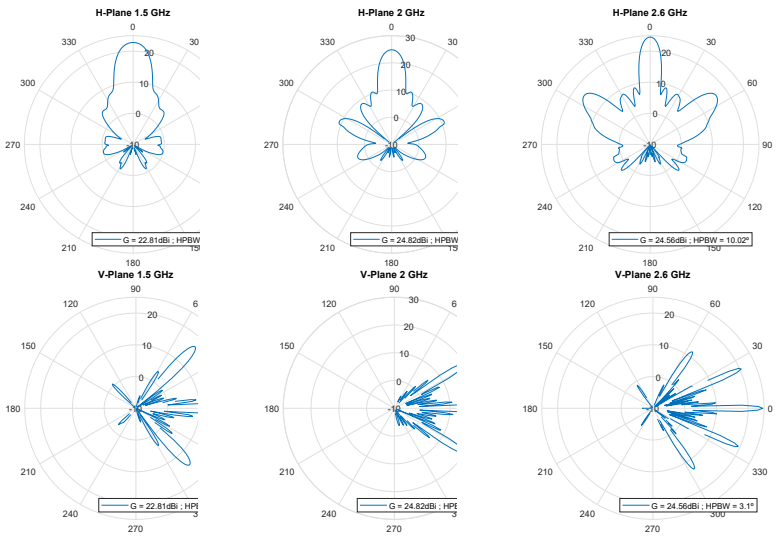

Figure 5.23: Massive MIMO Radiation Pattern composed by Full Two columns 102 ExtUWB elements.

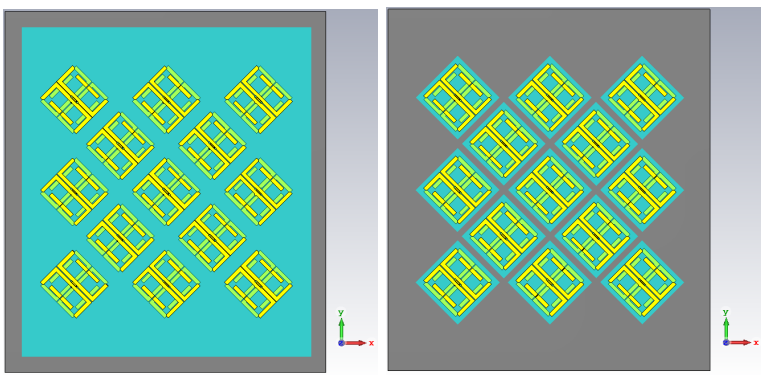

Figure 5.24: Fragment example for planar MMIMO with ExtUWB elements. Left picture shows the elements printed in the same substrate. Right picture shows the substrate cut in squares corresponding to each element.

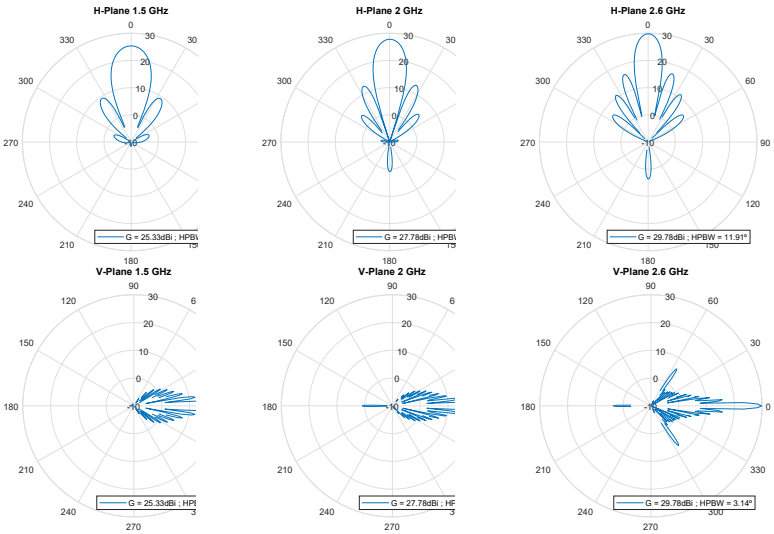

Figure 5.25: Radiation Pattern for Massive MIMO of 102 ExtUWB elements without the presence of LBF element in a top layer.

from 0 to -10 degrees, now, the presented antenna for MMIMO application can achieve beam steering in terms of both θ and ϕ for at least $\pm 30°$. In the figure can be observed how for horizontal tilt to the right of 30° or vertical down tilt of -30°, the gain achieves similar values as broadside direction without significant increase of secondary lobes.

Two different details can be observed with this proposal. Firstly, how removing the top element that occludes modify and affects. And secondly, the improvement in the planar array when most of the elements are equal, there is no differences related to the relative position to the LBF element, assuming now the elements surrounding are the same except the borders.

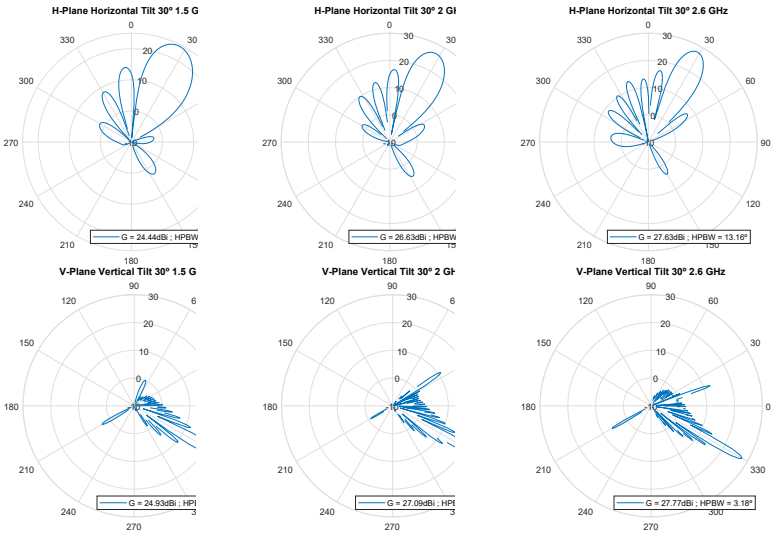

Figure 5.26: Radiation Pattern for Massive MIMO showing two examples of beam steering. Top pictures show horizontal tilt 30° to the right and bottom pictures shows vertical down tilt of -30°.

5.6 Arrays Combined with Commercial Elements

This section continues the work with arrays using the integration presented in Chapter 4, in which ExtUWB elements are combined with commercial elements for covering the LBF. As it is already mentioned, the results related to the commercial elements in low band can not be shown, but LBF arrays can be exposed by their array factors, while the ExtUWB array is presented. The objective is to present new options for linear classical arrays in which the new extended band is included.

Firstly, the integrated arrays for ExtUWB and Cross Dipoles is presented. The elements are placed as can be seen in figure 5.27, where the distance between LBF elements is 240 mm and the distance for the ExtUWB elements is a combination between 110 mm for consecutive elements and 130 mm where there is an intercalated LBF element between them.

Once simulated and included in the developed software, figure 5.28 shows the resulting radiation pattern for the ExtUWB, with results

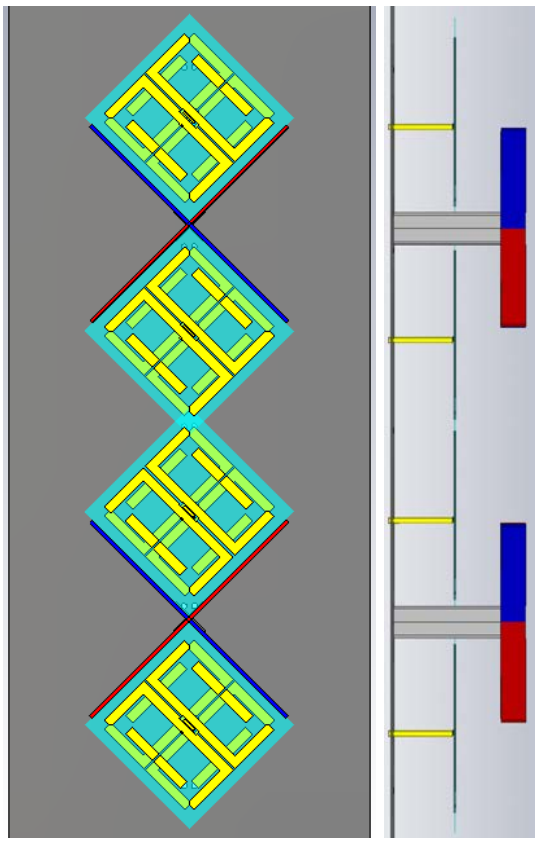

Figure 5.27: Fragment of the architecture for the arrays composed by Cross Dipoles in the Low Band Frequency and the ExtUWB elements.

showing a gain of 15 ± 0.6 dBi and a horizontal beamwidth of 67.6 ± 8.5 degrees .

For the Low Band the obtained Array Factor is shown in figure 5.29. Array Factor gain values is 9.3 ± 0.5 dB that added to the approximated 8 dBi that the element should have, a total array gain for the LBF can be at 17 dBi, with a horizontal beamwitdth that would be defined by the element.

Secondly, figure 5.30 shows the integrated array for ExtUWB and Bowl elements for LBF. As can be seen in the picture, there is a ExtUWB

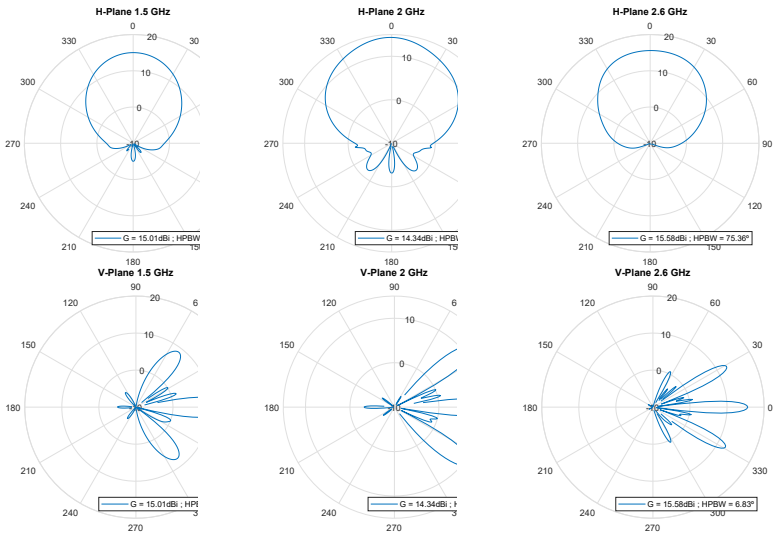

Figure 5.28: Radiation Pattern for the ExtUWB array included in the integration with Cross Dipoles.

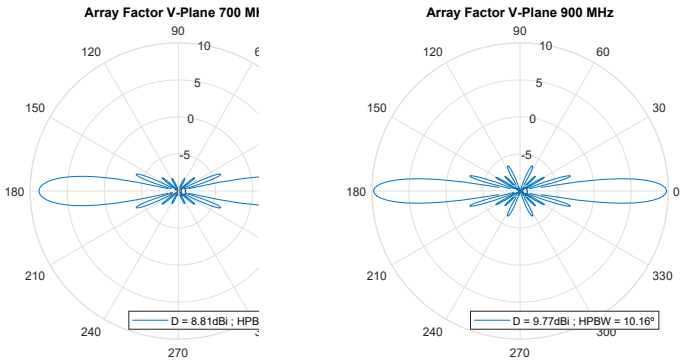

Figure 5.29: Cross Dipoles Array Factor for LF element.

element in the interior of every LBF element, and another ExtUWB element between them. Resulting in a distance of 260 mm for LBF array, and 130 mm for ExtUWB array.

The individual radiation pattern is simulated and included in the Matlab developed array software. Figure 5.31 shows the resulting radiation pattern for the ExtUWB, with results showing a gain of 15.5 $\pm$ 1.16 dBi and a horizontal beamwidth of 64.4 $\pm$ 5.1 degrees.

For the Low Band the obtained Array Factor is shown in figure 5.32. Array Factor gain values is 9.6 $\pm$ 0.5 dB that added to the approximated 8 dBi that the element should have, a total array gain for the LBF can be at 17.6 dBi, with a horizontal beamwitdth that would be defined by the element.

In this section, there has been presented good results for classical configuration BTS arrays. These BTS includes one array for LBF and two arrays in ExtUWB, although as before, they can be doubled as a double column configuration if the size allows it. The results in ExtUWB are good, as both of them achieves the required gain while the radiation pattern obtain horizontal beamwidth of 67.6 $\pm$ 8.5 and 64.4 $\pm$ 5.1 degrees respectively. As explained before, the final results for LBF arrays are not shown here, but analysing the Array Factor can ensure that the results are promising with gain values as required.

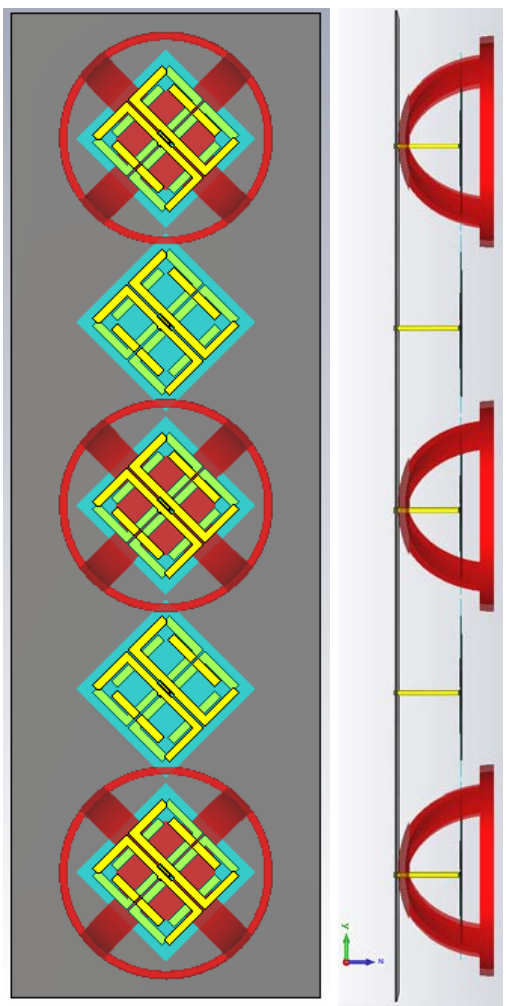

Figure 5.30: Fragment of the architecture for the arrays composed by Bowl shaped Dipoles in the Low Band Frequency and the ExtUWB elements.

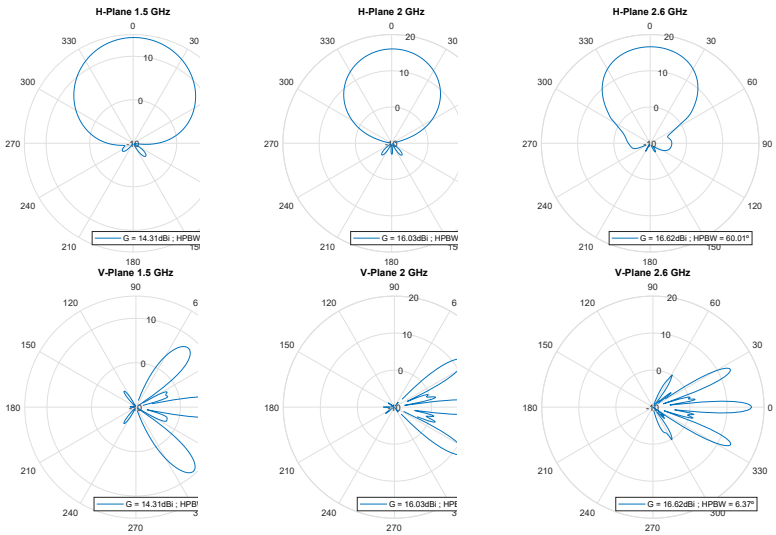

Figure 5.31: Radiation Pattern for the ExtUWB array included in the integration with Bowl shaped Dipoles.

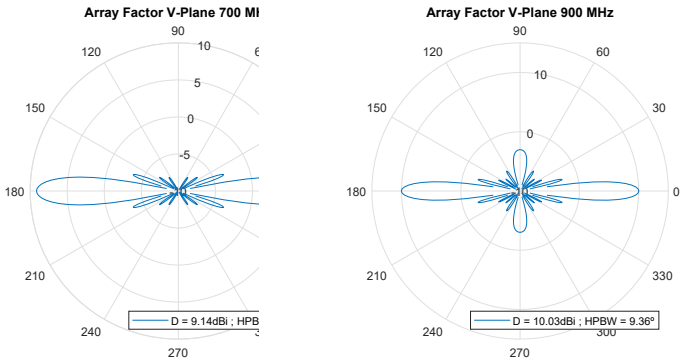

Figure 5.32: Bowl Array Factor for LF element.

5.7 Conclusions

In this chapter some arrays have been designed working in the new extended band with the purpose of being used as base stations in the new generation of mobile communication systems.

A new software tool based on array theory has been presented for the array designs. The purpose of the software is to obtain accurate array simulations with low computational cost, avoiding the high computational cost of full-wave simulations in the complete arrays. The computational program is flexible and scalable, in which different architectures, distances, feeding, etc, can be introduced to obtain realistic complete 3D space results for arrays radiation pattern.

This chapter has presented a single band linear array working in the 1.42 - 2.69 GHz band with the ExtUWB elements designed in Chapter 2. Dual band integrated arrays are presented for covering both bands, 690-960 MHz band and 1.42-2.69 GHz band. With that contribution, classic base station arrays are covered now with the extension of the new bands. Moreover, in the integration with commercial elements in the low band frequency, both bands has been covered in a classical base station configuration. Achieving results that fulfil the requirements, minimum gain of 15 dBi and horizontal beamwidth of $65 \pm 10^{\circ}$ for the ExtUWB.

A new topology solution is presented, in which by using planar array properties is possible to achieve beamsteering in both θ and ϕ direction for the ExtUWB, which is a novelty that can be used for future MMIMO applications. It is worth mentioning that the presented topology is multipurpose and scalable, it can be used as classical BTS or even with Massive MIMO in L-band (ExtUWB), which is a novelty far beyond the presented nowadays in the market and in the state of the art.

The results presented in this chapter lead to obtaining some products that are itemized in the following lines.

- Classical configuration base station dual band linear arrays with the extended band with the proportion of 6 arrays for ExtUWB per 1 Low Band Frequency array. Or 10 ExtUWB + 2LBF. Although the beamwidth results are not optimal.

- Classical configuration base station dual band linear arrays with the extended band by using commercial Low Band Frequency elements. In this case the proportion is 2 ExtUWB arrays per 1 LBF array.
- Multiconfigurable Massive MIMO array for ExtUWB with one or two LBF arrays, in the same size as state of the art for classical base station capsules.
- ExtUWB Massive MIMO planar array without including LBF radiating elements, which lead to more freedom and flexibility for the design.

Results for the different presented array configurations are summarized in the next tables, where their characteristics are compared with the requirements. Table 5.1 shows the results for the Single Band Arrays. Table 5.2 includes the resulting Dual Band Arrays with classical base station configuration, including both presented low band elements, designed in the document and commercial low band elements. Table 5.3 presents the results for the innovative ExtUWB Massive MIMO Beamsteerable arrays.

Table 5.1: Results of Single Band Antenna Arrays

Data	Requirements	ExtUWB 1427 - 2690 MHz	LF 690 - 960 MHz
Gain [dBi]	15 - 18	16.9 ± 1.1	16.5 ± 0.5
HHPBW [°]	65 ± 10	64.7 ± 6.4	70.8 ± 0.3
FirstUSLLSupp [dB]	10	12.6	13.3
Size [mm]	2000x500x350	770x140x38	1960x280x130
Ports	-	2	2

Table 5.2: Results of Dual Band Antenna Arrays Classic Configuration Comparison

Data	Requirements	1 Column sized Array	
		690 - 960 MHz	1427 - 2690 MHz
Gain [dBi]	15 - 18	16.5 ± 0.8	18.1 ± 1
HHPBW [°]	65 ± 10	72.1 ± 1.3	40.1 ± 8.9
FirstUSLLS [dB]	10	14.6	12.1
Size [mm]	2000x500x350	1960x280x130	
Ports	-	2 LF + 12 ExtUWB	
Data	Requirements	2 Columns sized Array	
		690 - 960 MHz	1427 - 2690 MHz
Gain [dBi]	15 - 18	17 ± 0.03	18.2 ± 1.3
HHPBW [°]	65 ± 10	63.5 ± 15.6	39.2 ± 20.9
FirstUSLLS [dB]	10	13.6	13.2
Size [mm]	2000x500x350	1960x560x130	
Ports	-	4 LF + 28 ExtUWB	
Data	Requirements	Cross Dipole	Bowl Shaped
		1427 - 2690 MHz	1427 - 2690 MHz
Gain [dBi]	15 - 18	15 ± 0.6	15.5 ± 1.16
HHPBW [°]	65 ± 10	67.6 ± 8.5	64.4 ± 5.1
FirstUSLLS [dB]	10	14.7	15.1
Size [mm]	2000x500x350	1680xWxH	1820xWxH
Ports	-	2 LF + 4 ExtUWB	2 LF + 4 ExtUWB

Table 5.3: Results of Massive MIMO Antenna Arrays for ExtUWB

Data	1 Column Half Length	1 Column Full Length
Gain [dBi]	18.5 ± 2.0	21.5 ± 2.1
HHPBW [°]	21.2 ± 5.2	24.1 ± 8.2
VHPBW [°]	8.5 ± 2.8	4 ± 0.9
Size [mm]	980x280x130	1960x280x130

Data	2 Columns Half Length	2 Columns Full Length	Full Size w/o LBF elements
Gain [dBi]	20.9 ± 1	23.8 ± 1	27.6 ± 2.2
HHPBW [°]	14.1 ± 4.3	14.1 ± 4.1	15.9 ± 3.9
VHPBW [°]	7.5 ± 1.9	4 ± 0.9	3.6 ± 0.5
Size [mm]	980x560x130	1960x560x130	1960x560x38

5.8 References

[1] E. Björnson, "What is a transmit antenna? 5g commentary, technical insights." Apr. 2018. [Online]. Available: https://ma-mimo.ellintech.se/2018/04/30/what-is-a-transmit-antenna/

[2] W. L. Stutzman and G. A. Thiele, *Antenna theory and design.* John Wiley & Sons, 2012.

[3] P. Kildal, *Foundations of Antenna Engineering: A Unified Approach for Line-of-Sight and Multipath.* Artech House Publishers, 2015.

[4] A. El Zooghby, *Smart antenna engineering.* Artech, 2005.

[5] J. D. Kraus, *Antennas.* New York: McGraw-Hill Inc.,US; 2nd Revised edition, 1988.

[6] L. C. Godara, *Smart Antennas.* CRC Press, jan 2004.

[7] A. K. Pandey, "Phased array antenna with beamforming network for 5g mmwave communication system," in *2020 50th European Microwave Conference (EuMC).* Utrecht, Netherlands: IEEE, jan 2021, pp. 364–367.

[8] Y. Liu, Y. Jia, W. Zhang, Y. Wang, S. Gong, and G. Liao, "An integrated radiation and scattering performance design method of low-RCS patch antenna array with different antenna elements," *IEEE Transactions on Antennas and Propagation*, vol. 67, no. 9, pp. 6199–6204, 2019.

[9] K. Kobrin, Z. Li, V. Sledkov, and M. Manuilov, "A broadband dual-polarized planar dipole antenna array for sub-6 ghz base stations," in *2020 7th All-Russian Microwave Conference (RMC).* Moscow, Russia: IEEE, nov 2020, pp. 180–183.

[10] F. Jia, S. Liao, and Q. Xue, "A dual-band dual-polarized antenna array arrangement and its application for base station antennas," *IEEE Antennas and Wireless Propagation Letters*, vol. 19, no. 6, pp. 972–976, 2020.

[11] Q.-X. Chu, D.-Z. Zheng, and R. Wu, "Multi-array multi-band base-station antennas," in *2017 International Workshop on Antenna*

Technology: Small Antennas, Innovative Structures, and Applications (iWAT). Athens, Greece: IEEE, 2017, pp. 137–139.

[12] G. Gottardi, G. Oliveri, D. Cunial, and A. Massa, "Designing new generation antennas for 5g mimo systems - a new perspective in array synthesis," in *Proc. IEEE Int. Symp. Antennas and Propagation USNC/URSI National Radio Science Meeting*, 2018, pp. 2175–2176.

[13] N. Anselmi, G. Gottardi, P. Rocca, G. Oliveri, and A. Massa, "Unconventional m-MIMO phased array design for 5g wireless systems," in *Proc. IEEE Int. Symp. Phased Array System Technology (PAST)*, 2019, pp. 1–3.

[14] C. A. Balanis, *Antenna Theory: Analysis and Design*. John Wiley & Sons, 2005.

[15] P. Fernandez-Martinez, S. Martin-Anton, and D. Segovia-Vargas, "Dual-band array of cross-polarized vivaldi antennas for 5g applications," in *2020 14th European Conference on Antennas and Propagation (EuCAP)*. Copenhagen, Denmark: IEEE, mar 2020, pp. 1–5.

CHAPTER 6

SUMMARY AND CONCLUSIONS

This chapter summarizes the conclusions of the overall document about broadband antennas and arrays for the new generation of mobile communication base stations, and presents some new lines to continue with this work.

An element has been presented for covering the new 5G extended band in a compact way fulfilling the hard requirements. A reflector and ground plane in near field study has been developed making evident the differences existing with the far field reflector study. A low band frequency element has been designed and the dual-band integration has been presented, as well as the integration of different architecture elements. Finally, different array designs have been presented for the full antenna. Those arrays are configurable for being used as classical base stations, but also as a new innovative system of Massive MIMO with beamsteering properties that has not been presented for the L-band till now.

In conclusion, a big step in research has been done, which implies the development of ideas and technologies that will be very useful for the design of base station antennas for the new generations of mobile communication, as can be 5G and future ones.

This thesis includes all the definitions contained in the R&D&i acronym. The developed work covers the Research in the topic, Development of new products and prototypes, and the Innovation that is carried with new technologies and applications. According to that, the objective of the thesis has been a success.

Chapter 2 has presented a broadband antenna to work in the sub 6-GHz frequency band for 3G to 5G standards. The antenna has been designed and fabricated in a cost-effective and affordable way presenting a compact and fully planar topology. The main idea behind the goal is the inclusion of active embedded dipoles in the antipodal part of the antenna itself. Compactness and dual polarized performance have been achieved for working in the whole frequency bandwidth between 1.427 and 2.69 GHz (ExtUWB). The performance of the antenna has been shown as good in terms of matching (below -14 dB), isolation (larger than 28 dB), and radiation pattern for a dual-polarization performance of $\pm 45^{\circ}$.

Studies of near field reflectors and ground plane shapes have been presented in Chapter 3. The influence of reflector shapes in the radiation pattern and the element matching has been shown for very broadband antennas.

For the elements that tend to lobulate at high frequency, it is necessary to use conformal profiles, as elliptical one, to shape the radiation pattern and have similar beamwidth behaviour in the wide frequency band while preserving a good matching for the antenna.

The presented dual polarization element is a compact design that prevents lobulation, making possible to use and fabricate a flat reflector with good performance. While single polarized elements can obtain good results with cylinder reflectors, dual polarized elements require to use a reflector shape which is symmetrical along the radiation axis to provide the same distance and power to feeder dipole arms. It can be a flat plane or a revolution shaped reflector.

According to the presented work, the key of this near field reflector search is to achieve the trade-off in which the reflector is spaced the specific distance in which the perturbation is positively affecting being

the return losses good enough to be worked with, and the aperture area is not too big that the beamwidth is narrower than needed with multilobes appearing, obtaining at the end a well matched antenna with stable beamwidth values along the frequency band.

In Chapter 4, the dual-band integration has been covered. An antenna element has been designed for the low frequency band (690 to 960 MHz), and then integrated with the ExtUWB elements to achieve the coverage in both bands within the same physical space. The new designed antenna for low frequency band presents some spaces that have been used as an advantage to allocate high frequency band elements.

Integration of ExtUWB elements with different elements that cover the low band frequencies has been presented obtaining good results. Those elements have different shapes due to the topologies and architectures that can be found in the market.

Chapter 5 presented some arrays working in the new extended band with the purpose of been used as base stations in the new generation of mobile communication systems.

Array designs were done with a new presented software that obtains accurate results with low computational cost. The program is flexible and new characteristics can be included to obtain any array 3D space result radiation pattern.

Single and Dual band arrays have been presented to cover the 690-960 MHz and 1.42-2.69 GHz bands. With that contribution, base station arrays are covered now with the extension of the new bands. The presented arrays with the integration with commercial elements in the LBF achieve results fulfilling the requirements of minimum gain of 15 dBi and horizontal beamwidth of $65 \pm 10°$.

A new topology solution has been presented, in which by using planar array properties it is possible to achieve beamsteering in both θ and ϕ direction for the ExtUWB, which is a novelty that can be used for future MMIMO applications. It is worth to mention that the presented topology is multipurpose and scalable, it can be used as classical BTS or even with Massive MIMO in L-band (ExtUWB), which is a novelty

far beyond the presented nowadays in the market and in the state of the art.

The thesis finished with the presentation of some obtained products and their results:

- Classical configuration base station dual band linear arrays with the extended band with the proportion of 6 arrays for ExtUWB per 1 Low Band Frequency array. Or 10 ExtUWB + 2LBF.
- Classical configuration base station dual band linear arrays with the extended band by using commercial Low Band Frequency elements. In this case the proportion is 2 ExtUWB arrays per 1 LBF array.
- Multiconfigurable Massive MIMO array for ExtUWB with one or two LBF arrays, in the same size as state of the art for classical base station capsules.
- ExtUWB Massive MIMO planar array without including LBF radiating elements, which lead to more freedom and flexibility for the design.

6.1 Future Lines

This thesis has started a new research topic in the research group in which has been developed. As it is a new line of work, new contributions could be done as the presented work can be improved and optimized while following the topic and obtain new contributions.

Feeding networks, which complexity is such that can lead to a new research focused on broadband matching and feeding networks. Feeding networks need to be specific for each kind of array, including the matching correction in each case, as well as the phase delay for each array element and their amplitude ponderation.

The elements for the extended ultrawide band, that can be improved according to the needs. For example, new elements even smaller in size could achieve the opportunity of placing them nearer in the array and develop an array with enhanced performance.

Low band frequency elements, it would be positive to design new architecture elements in which the low band elements do not shade on top of the highest frequency elements disturbing their performance. New elements placed nearer the ground plane or around the ExtUWB element, as the bowl-shaped dipole does, would produce an improvement in the radiation and matching of the other band elements.

Furthermore, it will be necessary to adapt the presented work to the needs that will be emerging in the market and the future requirements that will appear.

About the Author

SERGIO MARTIN-ANTON was born in Plasencia, Caceres, Spain, in 1992. He received the bachelor's degree in sound and image engineering for telecommunications from Extremadura University, in 2014, obtaining one of the best academic records, and the double master's degree in telecommunications engineering and multimedia and communications from the Universidad Carlos III de Madrid (UC3M), in 2016.

He is currently pursuing the Ph.D. degree with the Group of Radiofrequency, Electromagnetics, Microwaves and Antennas (GREMA), Universidad Carlos III de Madrid. In 2014, he was developing his bachelor final project at Kassel University, Germany, with an Erasmus Scholarship, where he learned and experienced with microwave circuits manufacture and measurement. He has authored several national and international articles as European Conference on Antennas and Propagation (EUCAP) or International Symposium on Antennas and Propagation and North American Radio Science Meeting (IEEE APS/URSI). His present research interest is focused on base station broadband antennas for new generations of mobile communication systems.

Mr. Martin-Anton's awards and honors also include the Erasmus Scholarship for his German stay and a grant for predoctoral contracts for University Teacher Training (FPU16/00459) by the Spanish Ministry of Education, Culture and Sport.